

UNIVERSITY OF CALIFORNIA, SAN DIEGO

**Positron Annihilation on Atoms and Molecules**

A dissertation submitted in partial satisfaction of the requirements for  
the degree of Doctor of Philosophy in Physics

by

Koji Iwata

Committee in charge:

Clifford M. Surko, Chair  
John M. Goodkind  
William E. Moerner  
Lu J. Sham  
John D. Simon

1997

Copyright  
Koji Iwata, 1997  
All rights reserved.

The dissertation of Koji Iwata is approved and it is acceptable in quality and form for publication on microfilm.

---

---

---

---

---

---

Chairman

University of California, San Diego

1997



# Contents

Signature Page . . . . .	iii
Table of Contents . . . . .	iv
List of Figures . . . . .	ix
List of Tables . . . . .	xi
Acknowledgments . . . . .	xiii
Vita, Publications and Fields of Study . . . . .	xv
Abstract . . . . .	xviii
<b>1 Introduction</b> . . . . .	<b>1</b>
1.1 Simple illustration of a positron interacting with a molecule . . . . .	1
1.2 Background in positron physics . . . . .	3
1.2.1 Prediction and discovery of the positron . . . . .	3
1.2.2 Positron sources . . . . .	4
1.3 Physics involved in the interaction of a positron with a molecule . . . . .	5
1.3.1 Long range; polarization and dipole-charge interactions . . . . .	6
1.3.2 Short-range interactions ( $r \sim a_0$ ) . . . . .	6
1.3.2.1 Potential from atomic nuclei . . . . .	6
1.3.2.2 Pauli exclusion principle . . . . .	7
1.3.2.3 Positronium atom formation . . . . .	7
1.3.2.4 Annihilation . . . . .	8
1.4 Interaction of positrons with solids, liquids, and gases . . . . .	9
1.4.1 Solids . . . . .	9
1.4.1.1 Positron moderators . . . . .	11
1.4.2 Liquids . . . . .	11
1.4.3 Gases . . . . .	11
1.5 Outline of dissertation . . . . .	12
<b>2 Overview of previous atomic and molecular physics studies using positrons</b> . . . . .	<b>13</b>
2.1 Dense-gas and low-pressure experiments . . . . .	14
2.1.1 Dense-gas experiments . . . . .	14
2.1.2 Low-pressure experiments . . . . .	15
2.2 Annihilation rates . . . . .	16

2.2.1	Anomalous high annihilation rates . . . . .	18
2.3	Momentum distribution measurements . . . . .	19
2.4	Ion mass spectrum measurements . . . . .	20
<b>3</b>	<b>Description of the experiments</b>	<b>23</b>
3.1	Source and moderator . . . . .	24
3.2	Beam line . . . . .	26
3.3	Positron trap . . . . .	26
3.4	Gas-handling system . . . . .	32
3.4.1	Gases . . . . .	32
3.4.2	Liquids and solids . . . . .	32
3.5	Annihilation rate measurements . . . . .	33
3.6	$\gamma$ -ray spectral measurements . . . . .	36
3.6.1	Experimental procedure . . . . .	36
3.6.2	Spectral analysis . . . . .	37
3.6.3	Calibration and detector response . . . . .	38
<b>4</b>	<b>Annihilation rates</b>	<b>41</b>
4.1	Theoretical considerations . . . . .	41
4.1.1	Long-lived resonances . . . . .	42
4.1.2	Large cross sections from the resonance collision . . . . .	44
4.2	Results . . . . .	44
4.2.1	Noble gases . . . . .	45
4.2.2	Inorganic molecules . . . . .	47
4.2.3	Alkanes and substituted alkanes . . . . .	49
4.2.4	Alkenes . . . . .	51
4.2.5	Oxygen-containing hydrocarbons . . . . .	52
4.2.6	Aromatics and saturated rings . . . . .	53
4.2.7	Deuterated hydrocarbons . . . . .	56
4.2.7.1	Deuterated alkanes . . . . .	57
4.2.7.2	Deuterated benzenes . . . . .	58
4.2.8	Partially fluorinated hydrocarbons . . . . .	59
4.3	Discussion . . . . .	62
4.3.1	Empirical scaling of annihilation rates . . . . .	62
4.3.2	Dependence of annihilation rates on positron temperature . . . . .	66
4.3.3	Recent theoretical work . . . . .	67
4.3.3.1	Semi-empirical approach . . . . .	67
4.3.3.2	Large scale calculations for molecules . . . . .	68
4.3.4	Other issues . . . . .	68
4.3.4.1	Noble gas atoms . . . . .	68
4.3.4.2	Reproducibility of measurements . . . . .	68
4.3.4.3	Delocalized $\pi$ bonds in benzene . . . . .	69

4.3.4.4	Determination of positron annihilation sites in a molecule . . . . .	69
4.3.5	Current state of annihilation rate studies . . . . .	69
4.4	Concluding remarks on annihilation rate measurements . . . . .	70
<b>5</b>	<b>Annihilation <math>\gamma</math>-ray spectra</b>	<b>71</b>
5.1	Introduction . . . . .	71
5.2	Momentum distribution measurements . . . . .	72
5.2.1	Annihilation $\gamma$ -ray angular correlation measurements . . .	74
5.2.2	Doppler-broadened $\gamma$ -ray spectral measurements . . . . .	75
5.3	Results . . . . .	76
5.3.1	Noble gases . . . . .	76
5.3.1.1	Helium . . . . .	78
5.3.1.2	Neon, argon, krypton, and xenon . . . . .	79
5.3.1.3	Previous measurements from other experiments	81
5.3.2	Inorganic molecules . . . . .	81
5.3.2.1	Hydrogen . . . . .	82
5.3.2.2	Other gases . . . . .	83
5.3.3	Alkanes . . . . .	84
5.3.4	Alkane, alkene, and alkyne . . . . .	88
5.3.5	Aromatics . . . . .	88
5.3.6	Fully halogenated carbons . . . . .	89
5.3.7	Partially fluorinated hydrocarbons . . . . .	90
5.3.8	Other organic molecules . . . . .	94
5.3.9	Annihilation on inner-shell electrons . . . . .	94
5.4	Spectral analysis beyond the 1-Gaussian approximation . . . . .	95
5.5	Discussion . . . . .	98
5.6	Concluding Remarks . . . . .	100
<b>6</b>	<b>Positron annihilation with inner-shell electrons in noble gas atoms</b>	<b>101</b>
6.1	Introduction . . . . .	101
6.2	Experiment . . . . .	102
6.3	Results . . . . .	102
6.4	Concluding remarks for inner-shell electron annihilation . . . . .	108
<b>7</b>	<b>Positron annihilation in the interstellar media</b>	<b>109</b>
7.1	Introduction . . . . .	109
7.2	Positrons in the interstellar media . . . . .	110
7.3	Interstellar molecules . . . . .	113
7.4	Astrophysical positron annihilation simulation . . . . .	114
7.4.1	Description of the experiment . . . . .	114
7.4.2	Experimental results . . . . .	114

7.5	Summary of positron annihilation in the interstellar media . . . .	116
<b>8</b>	<b>Conclusion</b>	<b>119</b>
8.1	Summary of this dissertation . . . . .	119
8.2	Future work . . . . .	120
8.3	Concluding remarks . . . . .	121
	<b>Appendices</b>	<b>122</b>
<b>A</b>	<b>Ion gauge sensitivity calibration for gases and molecular vapors</b>	<b>123</b>
<b>B</b>	<b>Table of physical parameters of atoms and molecules</b>	<b>127</b>
<b>C</b>	<b>Table of annihilation <math>\gamma</math>-ray spectra from atoms and molecules</b>	<b>133</b>
	<b>References</b>	<b>137</b>



# List of Figures

1.1	Schematic diagram a low-energy positron interacting with a molecule.	2
1.2	Schematic illustration of positronium atom formation.	7
1.3	Schematic diagram of positron trapping in a defect.	10
2.1	Apparatus for measuring annihilation time spectra in high-pressure experiments.	16
2.2	Schematic drawing of annihilation time spectrum in a high-pressure experiment.	17
2.3	Annihilation time spectrum for helium gas.	18
2.4	2D-ACAR spectra of noble gases.	20
3.1	Schematic overview of the experimental setup.	23
3.2	Schematic diagram of the source and cold-head assembly.	25
3.3	Schematic diagram of a Penning-Malmberg trap.	27
3.4	Schematic diagram of the positron trap electrode structure.	28
3.5	Gas pressure in the third stage of the positron trap during a pumpout cycle.	30
3.6	Schematic diagram of the positron trap.	31
3.7	A schematic diagram of a gas-handling system for test substances that exist in gas form at atmospheric pressure.	33
3.8	A schematic diagram of a gas-handling system for test substances, which are in liquid or solid form at atmospheric pressure.	34
3.9	Annihilation rate data for benzene- <i>d</i> .	35
3.10	$\gamma$ -ray spectrum of the 514.0-keV line from a $^{85}\text{Sr}$ source.	39
4.1	Experimental values of $Z_{\text{eff}}/Z$ plotted against $Z$	42
4.2	Theoretical and experimental values of $Z_{\text{eff}}$ for noble gases.	47
4.3	Values of $Z_{\text{eff}}$ and structures of alkenes with six carbons.	52
4.4	Values of $Z_{\text{eff}}$ and structures of cyclohexane and substituted benzenes.	55
4.5	Ratio of $Z_{\text{eff}}$ for deuterated alkanes to those for protonated alkanes.	58
4.6	Values of $Z_{\text{eff}}$ and structures of deuterated benzenes studied.	61
4.7	Empirical scaling of $Z_{\text{eff}}$ for non-polar molecules containing only single bond.	63

4.8	Empirical scaling of $Z_{\text{eff}}$ for oxygen-containing hydrocarbons and small molecules with a dipole moment and/or double bonds. . . .	64
4.9	Empirical scaling of $Z_{\text{eff}}$ for alkenes, ring hydrocarbons, and substituted benzenes. . . . .	65
4.10	Dependence of annihilation rates of noble gases on positron temperature. . . . .	66
5.1	Illustration of the momentum of an annihilating electron-positron pair and the resulting $\gamma$ -ray momenta. . . . .	73
5.2	Observed spectra from $\text{H}_2$ and Ne. . . . .	77
5.3	Annihilation $\gamma$ -ray spectrum from helium atoms. . . . .	79
5.4	Experimentally measured $\gamma$ -ray spectra from noble gases. . . . .	80
5.5	$\gamma$ -ray spectrum from positron annihilation on molecular hydrogen. . . . .	83
5.6	$\gamma$ -ray spectra for positrons annihilating with CO and $\text{CO}_2$ . . . . .	85
5.7	The Gaussian linewidth for alkane molecules. . . . .	87
5.8	$\gamma$ -ray spectrum from positron annihilation on fluoroethane. . . . .	91
5.9	Fraction of positrons annihilating on fluorine atoms in partially fluorinated hydrocarbons. . . . .	93
5.10	$\gamma$ -ray spectrum of $\text{H}_2$ . . . . .	96
5.11	$\gamma$ -ray spectrum of hexane. . . . .	97
6.1	The $\gamma$ -ray spectrum resulting from positrons annihilating on xenon atoms. . . . .	103
6.2	The $\gamma$ -ray spectrum resulting from positrons annihilating on krypton atoms. . . . .	104
6.3	The $\gamma$ -ray spectrum resulting from positrons annihilating on argon atoms. . . . .	105
7.1	Positron annihilation $\gamma$ -ray spectrum from the Galactic center. . . . .	111
7.2	Positron annihilation $\gamma$ -ray spectrum from the Galactic center using a Ge detector. . . . .	112
7.3	Molecular structures and $Z_{\text{eff}}$ of polycyclic aromatic hydrocarbons. . . . .	113
7.4	$\gamma$ -ray line for positrons annihilating on mixture of hydrogen and naphthalene molecules. . . . .	115

# List of Tables

3.1	Parameters of the neon and tungsten moderators, and the positron trap. . . . .	26
4.1	Values of $Z_{\text{eff}}$ for noble gases. . . . .	46
4.2	Measured values of $Z_{\text{eff}}$ for inorganic molecules. . . . .	48
4.3	Measured values of $Z_{\text{eff}}$ for alkanes and substituted alkanes. . . . .	50
4.4	Measured values of $Z_{\text{eff}}$ for isomers of pentane. . . . .	51
4.5	Measured values of $Z_{\text{eff}}$ for alkenes. . . . .	51
4.6	Measured values of $Z_{\text{eff}}$ for alcohols, carboxylic acids, and ketones. . . . .	52
4.7	Measured values of $Z_{\text{eff}}$ for ring molecules and aromatics. . . . .	54
4.8	Measured values of $Z_{\text{eff}}$ for other large organic molecules. . . . .	56
4.9	Measured values of $Z_{\text{eff}}$ for protonated and deuterated alkanes. . . . .	57
4.10	Measured values of $Z_{\text{eff}}$ for deuterated benzenes. . . . .	59
4.11	Measured values of $Z_{\text{eff}}$ for partially fluorinated hydrocarbons. . . . .	60
5.1	The $\gamma$ -ray linewidths for noble gases. . . . .	78
5.2	The $\gamma$ -ray linewidths for $\text{H}_2$ . . . . .	82
5.3	The $\gamma$ -ray linewidths for inorganic molecules. . . . .	82
5.4	The $\gamma$ -ray linewidths for hydrocarbons. . . . .	86
5.5	The $\gamma$ -ray linewidths for fully halogenated carbons. . . . .	89
5.6	The $\gamma$ -ray linewidths for partially fluorinated hydrocarbons. . . . .	90
5.7	The $\gamma$ -ray linewidths for other organic molecules. . . . .	94
5.8	Values of $\chi_r^2$ from fits to various models. . . . .	95
6.1	The annihilation $\gamma$ -ray line shapes for argon, krypton, and xenon in the static Hartree-Fock approximation. . . . .	106
7.1	Results of astrophysical positron annihilation simulation. . . . .	115
A.1	Relative sensitivities of ion gauge response. . . . .	124
B.1	Physical parameters of molecules studied. . . . .	128
C.1	$\gamma$ -ray line-shape parameters from fits to two Gaussians for all atoms and molecules. . . . .	135



# Acknowledgments

This dissertation could not have been completed without the help of numerous people. I will mention people who helped me most significantly through the last 6 years of my graduate work.

First of all, I am very grateful to my thesis adviser, Prof. Cliff Surko. Even though I was not always the best student, he has guided me through the process of my graduate work patiently, helping me realize my potential to be a good scientist. I have learned greatly from his insight and dedication to the advancement of science. His high standards for publications and presentation, as well as his active critiquing of his students' work has helped us tremendously. My ability to communicate in a scientific environment has certainly benefited from his help. Since he was so critical in preparation of manuscripts for publications, he sometimes corrected his own modifications back to what they were in the previous version. It was an encouraging sign, however, since his behavior indicated that the manuscript was finally converging to the final form after numerous modifications. He likes many commas in manuscripts, and I thank him for all the commas he has given me.

I am indebted to our super postdoc, Rod Greaves, who has been in the lab with me for 6 years, and patiently guided me through my thesis research on a daily basis. His dedication to our work and his ability to run experiments as well as his general scientific insight are noteworthy. I was also impressed with his ability to sneakily get rid of extra commas inserted in manuscripts by Cliff. He will be leaving the group at the end of the year for a new position, and I wish him the very best for his future.

I thank our senior technician in the group, Gene Jerzewski, for his expert technical support for the experiments. His mastery of electronics, personal computers, and every aspect of technical matters has been an absolutely indispensable asset to the lab. He has taught me Zen and the art of electronic maintenance through flyfishing. My productivity was also greatly enhanced by our daily ritual of walking to the Grove Caffe for cups of coffee.

Others in the research group in last 6 years, Chris Kurz, Arthur La Porta, Mark Tinkle, Steve Gilbert, Steve Yamamoto, Chris Lund, Bill Baxter, Keith Eaton, and S. Z. Tang have also given me support for my work.

Our secretary, Judy Winstead, is gratefully acknowledged for her assistance and speedy proof reading of manuscripts including this dissertation.

Scientific interactions outside of our research group took place mainly at conferences because nobody else at UCSD works in my specific research field. I have had many delightful experiences meeting world class scientists at these conferences, and I appreciate them for treating me with respect. We had a pleasure of collaborating with Gleb Gribakin in University of South New Wales in Sydney, Australia, and Peter Van Reeth and John Humberston in University College London, UK. I appreciate them for their theoretical input in the project.

Personally, I thank all my peers and friends for giving me emotional support. Especially, my surfer buddies, Alex Burke, Bernie Freisler, and Neil Dilley, have stuck to the principle of the friends-don't-let-friends-surf-alone policy, and in turn surfing has enhanced my creativity at work. I thank my mentor in Japan, Kimiaki Nakata, for encouraging me to study in the US. Toward the end of the graduate work, Amy Chua Yew Yew has provided me with superb emotional support, and I acknowledge her for proof reading this dissertation.

Finally, my parents are acknowledged for their continuing support for my study and my father for teaching me a work ethic by an example.

Financial support of this thesis work was provided by the Office of Naval Research and the National Science Foundation.

# Vita

January 30, 1968	Born, Tokyo, Japan.
1990	B.S., Astronomy and Physics, University of Arizona.
1990–1991	Teaching Assistant, University of Arizona.
1990–1991	Research Assistant, National Optical Astronomy Observatories.
1991–1997	Research Assistant, University of California, San Diego
1993	M.S., Physics, University of California, San Diego.
1997	Ph.D., Physics, University of California, San Diego.

# Publications

## JOURNAL ARTICLES

1. Koji Iwata, G. F. Gribakin, R. G. Greaves, and C. M. Surko, “Positron annihilation with inner-shell electrons in noble gas atoms,” *Physical Review Letters* **79**, 39-42 (1997).
2. Koji Iwata, R. G. Greaves, and C. M. Surko, “ $\gamma$ -ray spectra from positron annihilation on atoms and molecules,” *Physical Review A* **55** 3586-3604 (1997).
3. K. Iwata, R. G. Greaves, and C. M. Surko, “Positron annihilation in a simulated interstellar medium,” *Canadian Journal of Physics* **51**, 407-410 (1996).
4. P. Van Reeth, J. W. Humberston, Koji Iwata, R. G. Greaves, and C. M. Surko, “Annihilation in low-energy positron-helium scattering,” *Journal of Physics B (Letters)* **29**, L465-471 (1996).
5. K. Iwata, R. G. Greaves, T. J. Murphy, M. D. Tinkle, and C. M. Surko, “Measurement of positron annihilation rates on organic molecules,” *Physical Review A* **51**, 473-487 (1995).
6. K. Iwata, R. G. Greaves, and C. M. Surko, “Annihilation rates of positrons on aromatic molecules,” *Hyperfine Interactions* **89**, 271-278 (1994).

## PAPERS AT CONFERENCES AND WORKSHOPS

1. C. M. Surko, Koji Iwata, R. G. Greaves, C. Kurz, and S. J. Gilbert, “Atomic and molecular physics using positrons in a Penning trap,” to be published in the Proceedings of the XX International Conference on the Physics of Electronic and Atomic Collisions (World Scientific, 1998).

2. Koji Iwata, R. G. Greaves, C. Kurz, S. J. Gilbert, and C. M. Surko, "Studies of positron-matter interactions using stored positrons in an electrostatic trap," to be published in *Material Science Forum*, Proceedings of the Eleventh International Conference on Positron Annihilation, Kansas City, Missouri, May 1997, edited by Y.C. Jean, M. Eldrup, D.M. Schrader, and R.N. West.
3. D. M. Rabin, D. Jaksha, C. Plymate, J. Wagner, and K. Iwata, "Plage magnetic field strengths from near-infrared spectra," in *Solar Polarimetry; Proceedings of the Eleventh National Solar Observatory/ Sacramento Peak Summer Workshop (1990)*, edited by L. J. November, pp. 361-369 (1991).

#### INVITED TALKS

1. Koji Iwata, "A new look at positron annihilation in atoms and molecules," Workshop on Low-Energy Positron and Positronium Physics (a satellite conference of the International Conference on the Physics of Electronic and Atomic Collisions), Nottingham, UK (1997).
2. Koji Iwata, "Localization of positrons in atoms and molecules," the 11th International Conference on Positron Annihilation, Kansas City, MS (1997).
3. K. Iwata, "Chemical trends in positron attachment to molecules," 211th American Chemical Society National Meeting, New Orleans, LA (1996).
4. K. Iwata, "Positron molecule interactions," Positron workshop (a satellite conference of the International Conference on the Physics of Electronic and Atomic Collisions), Vancouver, Canada (1995).

#### CONFERENCE ABSTRACTS

1. Koji Iwata, G. F. Gribakin, R. G. Greaves, and C. M. Surko, "Positron annihilation with inner-shell electrons in atoms," *Bulletin of the American Physical Society* **42**, 957 (1997).
2. K. Iwata, R. G. Greaves, C. Kurz, and C. M. Surko, "Positron annihilation studies in a Penning trap: partially fluorinated hydrocarbons," *Bulletin of the American Physical Society* **41**, 1141 (1996).
3. C. M. Surko, K. Iwata, and R. G. Greaves, "Measurements of atomic and molecular positron-annihilation rates using trapped positrons," *Bulletin of the American Physical Society* **40**, 1340 (1995).
4. K. Iwata, R. G. Greaves, and C. M. Surko, "Gamma-ray spectra from positron-atom and positron-molecule interactions," *Bulletin of the American Physical Society* **40**, 1340 (1995).



5. T. J. Murphy, C. M. Surko, and K. Iwata, "Annihilation of positrons on organic molecules," *Bulletin of the American Physical Society* **37**, 1131 (1992).

## Fields of Study

Major Field: Physics

Studies in Atomic and Molecular Physics  
Professor Clifford M. Surko

Studies in Positron Physics  
Professor Clifford M. Surko

## ABSTRACT OF THE DISSERTATION

# Positron Annihilation on Atoms and Molecules

by

Koji Iwata

Doctor of Philosophy in Physics

University of California, San Diego, 1997

Professor Clifford M. Surko, Chair

Positron annihilation on a wide variety of atoms and molecules is studied. Room-temperature positrons confined in a Penning trap are allowed to interact with molecules in the form of low-pressure gases, so that the interaction is restricted to binary encounters between a positron and a molecule. Data are presented for the annihilation rates and  $\gamma$ -ray spectra resulting from positrons annihilating in such interactions. The variety of substances includes noble gases, simple inorganic molecules, hydrocarbons, substituted hydrocarbons, fully and partially fluorinated hydrocarbons, deuterated hydrocarbons, and aromatics. Anomalously large annihilation rates are observed for large organic molecules, and the annihilation rates scale with the ionization potentials of molecules. To date these anomalously large annihilation rates and the observed scaling have not been understood. The  $\gamma$ -ray spectra are Doppler broadened due to the momentum distribution of the annihilating electron-positron pairs. Consequently, these spectra provide information about the electron and positron wavefunctions. The measurements are used to determine the probability of positrons annihilating at specific locations in the atom or the molecule. In the case of partially fluorinated hydrocarbons, we have been able to determine the relative probability of annihilation on fluorine atoms and on C-H bonds. For noble gas atoms, the inner-shell electron annihilation was identified for the first time in gaseous media. The large annihilation rates for hydrocarbons have astrophysical implications, and a study of positron annihilation in a simulated interstellar medium is also presented. New insights which these studies provide in understanding the interaction of low-energy positrons with atoms and molecules are discussed.

# Chapter 1

## Introduction

A positron, the anti-particle of an electron, is the most accessible form of antimatter. Since its discovery [4], the properties of the positron have been studied extensively. At a first glance, the studies of a positron interacting with an atom or molecule would seem to be difficult, since the positron might be expected to annihilate with an electron rapidly. However, this annihilation time is much longer than the collisional slowing process in media, and so studies of slow positrons in matter are possible. This dissertation deals with the interactions of low-energy positrons with isolated atoms or molecules.

In this chapter, background information about positrons and positron-matter interactions is presented. The processes relevant to the research topic of this dissertation are illustrated briefly in Sec. 1.1. A history of the prediction and discovery of positrons is given in Sec. 1.2. Then the positron-atom and positron-molecule interactions are described in Sec. 1.3, including the comparison with the analogous electron-atom and electron-molecule interactions. The physics of positrons interacting with matter in different states (solid, liquid, and gas) is discussed in Sec. 1.4. Finally, the outline of the dissertation is described in Sec. 1.5.

### 1.1 Simple illustration of a positron interacting with a molecule

A low-energy positron interacting with a molecule<sup>1</sup> is illustrated in Fig. 1.1. By low energy, we mean specifically below the positronium formation threshold energy. The positrons used in the experiments described here are stored and cooled to room temperature in a Penning trap. A test substance is introduced into the Penning trap in vapor form, and a positron experiences collisions with the test molecules. These two particles generally fly apart after a collision. However, a

---

<sup>1</sup>A “molecule” here means an atom or a molecule. “Molecule” is used interchangeably with “atom and/or molecule” throughout the dissertation.

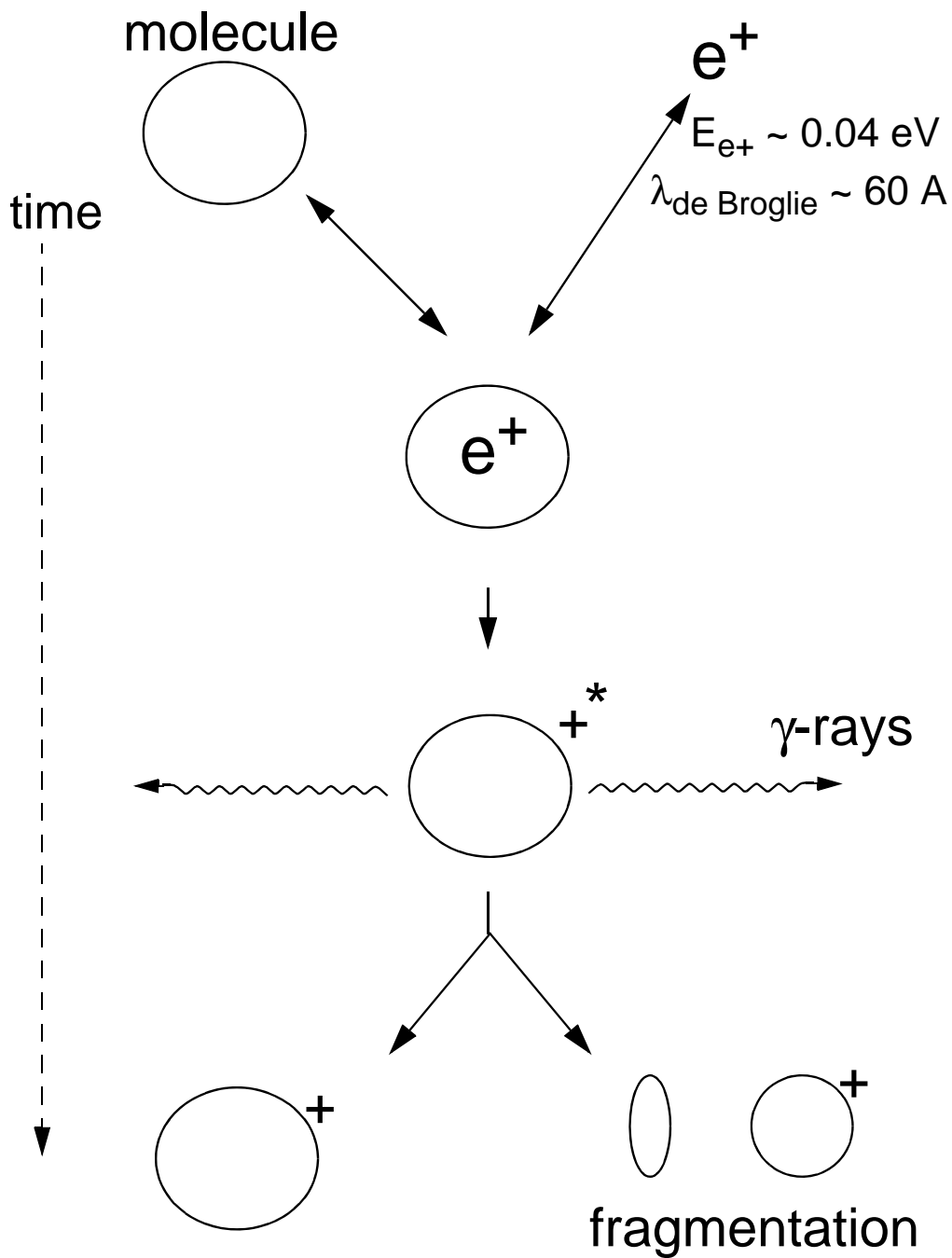


Figure 1.1: Schematic diagram a low-energy positron interacting with a molecule.

small fraction of collisions results in the annihilation of the positron with one of the bound electrons in the molecule, emitting two quanta of  $\gamma$  rays and leaving

a positive ion in an excited state. The excited positive ion can fragment. For higher energy positrons, positronium atoms, a bound state of a positron and an electron, can be formed by the collision process. However, at room temperature (i.e., the typical positron energy discussed here), the formation of positronium atoms is energetically prohibited for the types of molecules under study.

One type of measurement we are capable of making is annihilation rates measurements, which is described in Ch. 4. These measurements provide information about the annihilation cross sections of molecules, and as discovered earlier, the annihilation rates for large organic molecules are several orders of magnitude larger than those expected from simple elastic collisions [60, 134]. This enhancement may be explained by the existence of long-lived positron-molecule complex, but the nature of these complexes is still not understood.

Another type of experiment is spectral measurements of 511-keV annihilation  $\gamma$  rays, and these are described in Ch. 5. The annihilation  $\gamma$ -ray line is generally Doppler broadened due to the momenta of the annihilating pairs. These momenta are dominated by the momenta of the bound electrons, since the zero point momenta of these electrons are larger than those of thermal positrons. Thus, we can obtain information about the states of the annihilating electrons.

We can also measure the ion mass spectra resulting from the annihilation using a time-of-flight (TOF) mass spectroscopy technique, as discussed in Refs. [63, 109].

## 1.2 Background in positron physics

Since the discovery of a positron, the field of positron physics has become quite diverse. As the positron is the most readily available anti-particle on earth, studies of the interaction of positrons with matter have attracted a significant interest. Current research includes the analysis of surfaces using positrons [99], studies of quantum electrodynamics using positronium atoms [118], and the possible production of anti-hydrogen [19, 50]. Since the field of positron physics is too diverse to cover in this dissertation, the materials presented here are the subjects relating to positron-molecule interactions. In other literature, positronium research is reviewed nicely by Rich [118] including the history of the discovery of the positron. Positron interaction in gases is reviewed by Massey [89], while earlier experimental techniques are discussed in detail by Griffith and Heyland [55]. Research efforts in positron interactions with condensed matter, which have been pursued very actively, are reviewed in Refs. [99, 115, 124].

### 1.2.1 Prediction and discovery of the positron

The positron was first predicted by Dirac in 1930 [37]. He applied relativistic quantum theory to an electron moving in an external magnetic field and was successful in predicting the spin properties of the electron. However, his theory

involved one serious “difficulty,” his theory contained a solution with a negative energy in addition to the positive energy solution that corresponds to the electron. He then argued that, if there was a negative energy state, the electron with positive energy can decay into the negative energy state with the emission of  $2mc^2$  radiation, and concluded that “an electron with negative energy moves in an external field as though it carries a positive charge.” He had predicted annihilation of an electron-positron pair. However, the only positively charged particle known at that time was a proton, and he assumed that the particle was a proton, even though the difference in the mass of an electron and a proton was puzzling. The annihilation rate of an electron and a positron (or the negative energy state) was calculated by Dirac [36] and Oppenheimer [106]. In these calculations, the positron mass was assumed to be the same as that of an electron. It is interesting to note that, in Dirac’s work [36] he mentioned regarding the mass of this other particle, “This means, of course, a serious deficiency in our work and prevents one from attaching much physical importance to the result.” (In fact, his assumption of the same mass for an electron and a positron was right, and the assumption that the negative energy state being the proton was wrong.) The annihilation rate for a positron in a gas of electrons with density,  $n_s$ , of spin opposite to that of the positron, in the non-relativistic limit, is

$$\Gamma_s = 4\pi r_0^2 c n_s, \quad (1.1)$$

where  $r_0$  is the classical radius of the electron and  $c$  is the speed of light. For an uncorrelated electron gas of density  $n_e$ ,  $n_s = n_e/4$ , so that the spin-averaged rate of annihilation for free electrons is

$$\Gamma_e = \pi r_0^2 c n_s. \quad (1.2)$$

The first discovery of a positron came when Anderson was measuring traces of cosmic rays in cloud chambers [4,5]. He discovered evidence of particles with positive charge. Up to this time, the only known positive particles were protons and  $\alpha$  particles. This new particle penetrated a 6 mm lead plate and made a path much longer than that expected for a proton. To explain this observation, Anderson concluded that the particle had to be less massive than a proton – most likely the mass of an electron. Anderson called this new particle the positive electron or a positron.

The discovery of a positron was particularly significant in that it was the first form of an anti-matter. The unique properties of positrons can be exploited for the study of antimatter-matter interactions.

### 1.2.2 Positron sources

A positron source with high intensity and known energy distribution is desirable. Currently, two different types of positron sources are employed, linear accelerator

(LINAC) based sources and radioactive isotopes that undergo  $\beta^+$  (i.e., positron) decay.

A LINAC source consists of a high-energy electron beam and a positron converter. The high-energy electron beam ( $\sim 100$  MeV) is slowed down in a material, causing the emission of Bremsstrahlung  $\gamma$  rays. The high-energy  $\gamma$  rays create electron-positron pairs, and the positrons can be extracted. The intensity of the positron beam produced is proportional to the intensity of the incoming high-energy electrons. The intensity of the positrons produced also increases very rapidly with the energy of the electron source in the range of energies 20-150 MeV [61]. An advantage of LINAC based sources is their high intensity ( $> 10^9$  slow positrons/s). Another advantage is that they can be operated in pulsed mode, so that experiments can be performed confining the detection time to that of the positron pulse, thereby improving the signal-to-noise ratio. A disadvantage is the cost of LINAC's, and the facility tends to be relatively large.

There are several radioactive isotopes commonly used as positron sources. High activity and long lifetimes are important criteria for use in studies of positron-matter interactions. Commercially available sources that satisfy these criteria include  $^{22}\text{Na}$ ,  $^{58}\text{Co}$ , and  $^{68}\text{Ge}$ . We utilize a  $^{22}\text{Na}$  source, which has the half-life of  $\tau_{1/2} = 2.6$  years and is commercially available in sealed sources at activities up to 150 mCi. Advantages of radioisotope sources are their availability and compactness, while a disadvantage is the relatively low intensity compared to LINAC sources. One way to overcome this disadvantage of radioisotope sources, is use of  $^{64}\text{Cu}$ . Using  $^{64}\text{Cu}$ , an intense ( $\sim 10^{12}$  high-energy positron/s) short-lived ( $\tau_{1/2} = 12.8$  hours) source has been generated in a high-flux nuclear reactor [86]. However, this source also has a similar disadvantage to LINAC sources, namely the need for a large facility (in this case a nuclear reactor) on site.

### 1.3 Physics involved in the interaction of a positron with a molecule

The basic physics involved in a positron interacting with an isolated neutral atom or molecule is described in this section. This discussion focuses in particular on low positron energies, where the time scale of a positron approaching a molecule is much larger than the electron-cloud relaxation time. The interaction has some similarities to the case of an electron interacting with a molecule, and comparisons and contrasts between these two different systems are given.

### 1.3.1 Long range; polarization and dipole-charge interactions

At distance  $r$  much larger than the molecular size ( $r \gg a_0$ , where  $a_0$  is the Bohr radius), the interaction of a positron with a molecule is dominated by the induced dipole-charge and permanent dipole-charge interactions for nonpolar and polar molecules, respectively. When a charged particle approaches a nonpolar molecule, the electron cloud in the molecule is polarized, giving the induced electric dipole moment  $\vec{\mu}_\alpha = \alpha \vec{E}$ , where  $\alpha$  is the polarization constant of the molecule and  $\vec{E}$  is the field inducing the moment. The field at the origin, due to a positron located at  $\vec{r}$ , has the form  $\vec{E} = -(e/r^2)\hat{r}$ , where  $e$  is the electric charge, and  $\hat{r}$  is a unit vector in the direction of  $\vec{r}$ . The induced dipole moment in the presence of a positron therefore is

$$\vec{\mu}_\alpha = -\frac{\alpha e}{r^2} \hat{r}. \quad (1.3)$$

The force between the molecule and the positron due to the induced dipole-charge interaction is

$$F_\alpha = \frac{2\alpha e^2}{r^5}. \quad (1.4)$$

This polarization induced dipole moment-charge interaction is attractive for either an electron or a positron interacting with a neutral molecule.

For the case of molecules with a permanent dipole moment  $\vec{\mu}_p$ , the force on the positron exerted by this dipole is

$$F_p = \frac{2e\mu_p}{r^3}. \quad (1.5)$$

One can notice that the  $r$  dependence for nonpolar molecules is  $1/r^5$  [Eq. (1.4)], while that for polar molecules is  $1/r^3$  [Eq. (1.5)]. Thus, the long-range interaction for polar molecules is much stronger than that for nonpolar molecules.

### 1.3.2 Short-range interactions ( $r \sim a_0$ )

At shorter distances ( $r \sim a_0$ ), the interactions are more complicated. The polarization no longer has the simple multipole expansion form given in Eq. (1.4). In addition, the potential of the atomic nuclei, the Pauli exclusion principle, positronium atom formation, and annihilation of a positron with an atomic/molecular electron must be considered.

#### 1.3.2.1 Potential from atomic nuclei

Once a positron approaches a molecule and penetrates the electron shielding cloud, it will experience Coulomb repulsion from the atomic nuclei, which are positively charged, while the screening from the molecular electrons continues to reduce the repulsion of the positron. This is in contrast to the case of an electron interacting with a molecule, where the Coulomb interaction with the atomic nuclei is attractive.



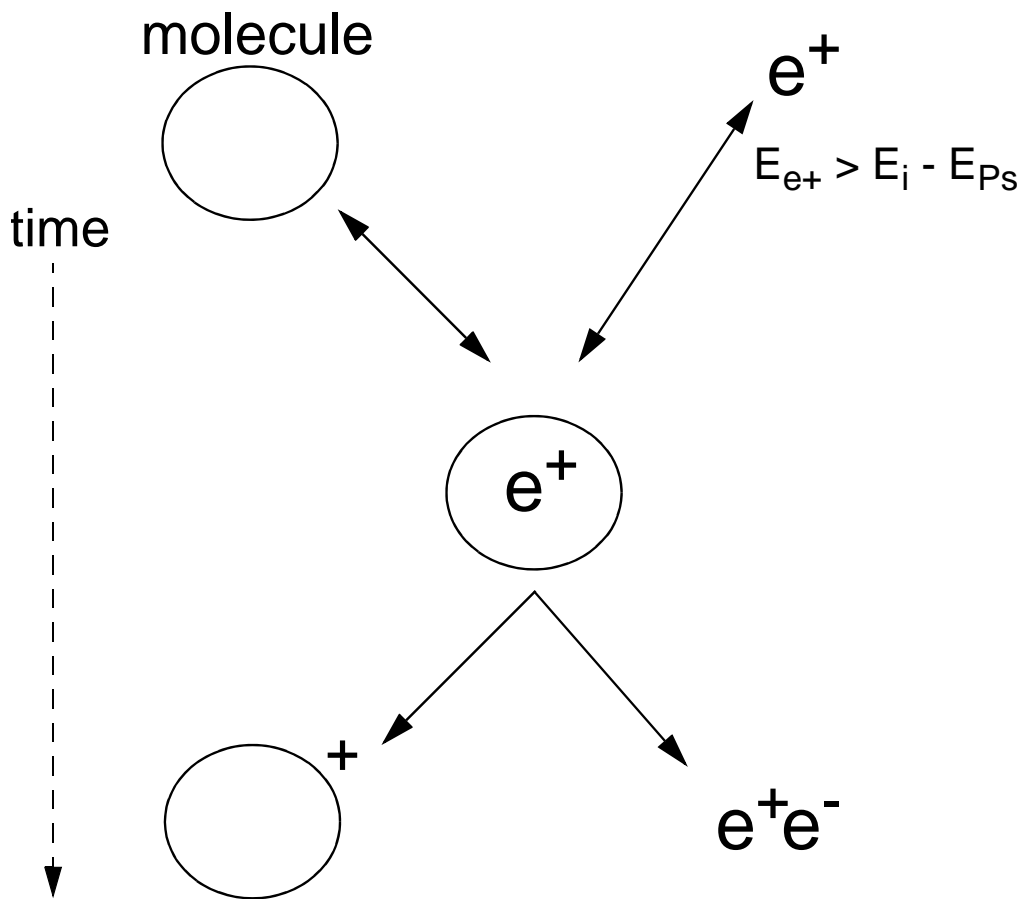


Figure 1.2: Schematic illustration of positronium atom formation.

### 1.3.2.2 Pauli exclusion principle

For an electron interacting with a molecule, the Pauli exclusion principle needs to be considered, since the scattering electron is an identical particle with the bound electrons in the molecule. For a positron interacting with a molecule, the scattering positron is not influenced by the Pauli exclusion principle with the bound electrons.

### 1.3.2.3 Positronium atom formation

A positron can form a bound state with an electron, which is called a positronium atom, often denoted by the symbol Ps. The process is schematically illustrated in Fig. 1.2. The positronium atom was first discovered by Deutsch [34]. Studies of positronium atoms are an active area of research and have been reviewed by Rich [118]. Even though studies of positronium atoms are not a

subject of this dissertation, the formation of positronium atoms is important in the positron trapping scheme used here, and positronium may well possibly be crucial for understanding the annihilation processes since the formation of “pseudo-positronium atoms” are suspected for responsible for the anomalously high annihilation rates observed (Ch. 4). Therefore, the properties of positronium atoms are briefly reviewed here.

The binding energy of a positronium atom,  $E_{\text{Ps}}$  is 6.8 eV, which is about half that of the hydrogen atom, since the reduced mass of the system is  $\frac{1}{2}m$ . There are two different total spin states, and they differ greatly in mean lifetime. The singlet  $S$  state decays by the emission of two  $\gamma$  rays. The ground singlet state (so called para-Ps) annihilates in the time of  $\tau_p = 1.25 \times 10^{-10}$  s. On the other hand, for the triplet  $S$  state (ortho-Ps) 2- $\gamma$  annihilation is forbidden by conservation of the spin angular momentum, and in this case, the annihilation occurs with emission of 3  $\gamma$  rays with the time scale of  $\tau_o = 1.41 \times 10^{-7}$  s. In the center-of-mass frame, both 2- and 3- $\gamma$  annihilation must carry away  $2mc^2$ . In the rest frame of the annihilating particles, for 2- $\gamma$  annihilation, each  $\gamma$  ray carries 511.0 keV energy, while in the case of 3- $\gamma$  annihilation, the energies of these three  $\gamma$  rays are continuously distributed up to 511.0 keV [89].

The ortho-Ps annihilation time is 3 orders of magnitude larger than that for para-Ps. The spin averaged annihilation time of positronium atom is

$$\tau_0 = 5.0 \times 10^{-10} \text{ s}. \quad (1.6)$$

It turns out that this annihilation time  $\tau_0$  is a reasonably good estimate of annihilation times in condensed matter.

In order for a positron to capture an electron from a gas molecule in the (usual) case where  $E_i > E_{\text{Ps}}$ , the incident positron must possess an initial kinetic energy,  $E_k$ , of at least

$$E_k = E_i - E_{\text{Ps}}, \quad (1.7)$$

where  $E_i$  is the ionization energy of the molecule.

#### 1.3.2.4 Annihilation

A free positron annihilates with an electron in a molecule with emission of 2 quanta of  $\gamma$  rays. This is a unique process in positron-molecule interactions. The annihilation signal can give information about the interaction, which is not available in electron-molecule interactions, and it is the main detection method used in this dissertation.

One quantity that can be measured is the annihilation rates of positrons for molecules, which is described in Ch. 4. The annihilation rate for a molecule is proportional to the overlap of the wave functions of the positron with the molecular electrons. Therefore, the measurement of annihilation rates gives information about the close-range interaction of the positron with the molecular electrons.

Another quantity that can be measured is the Doppler broadening of the 511-keV  $\gamma$ -ray line from positron annihilation on a molecule. The line is broadened due to the momentum distribution of the annihilating electron-positron pairs. For the case of room-temperature positrons discussed here, the momentum of the pair is dominated by the momentum of the annihilating electron. This  $\gamma$ -ray spectral measurement gives information about the site of annihilation in the molecule. This type of measurement is the topic of Ch. 5 and 6.

## 1.4 Interaction of positrons with solids, liquids, and gases

Positrons interact differently with solid, liquid, and gaseous media, as do electrons, and the interactions of positrons with these different media are briefly reviewed in this section. This dissertation focuses on the interaction of positrons with gaseous media. Due to their inherent simplicity, knowledge of these positron interactions with gases, can aid in the understanding of positron-solid and -liquid interactions.

Positrons possess high kinetic energies ( $\sim 1$  MeV) when they are created either by the  $\beta^+$  decay of radioactive nuclei or by the pair production from high-energy  $\gamma$  rays. Once the high energy positrons encounter matter, they quickly slow down through inelastic processes such as ionization and electronic excitation of the media, eventually reaching thermal equilibrium with the matter, since the energy-loss cross sections are much larger than the annihilation cross section. For positrons with energies above the positronium formation threshold, positronium formation, ionization, and electronic excitation are the dominant effects. This picture of the slowing down of positrons is valid for solid, liquid, or gas medium. However, the physics involved after thermalization can be very different in these three media. The interaction of thermalized positrons with matter is the subject of this dissertation.

At high energies, the main interaction is the ionization of the atoms in the media, and the cross section for this process is similar for electrons and positrons. However, at low energies positrons behave very differently from electrons, since, as discussed above, the differences in the interactions of positron and electrons with molecules play bigger roles.

### 1.4.1 Solids

Studies of positrons interacting with solids are an intense field of research; see for example the review papers by Schultz and Lynn [124], by Puska and Nieminen [115], and by Mills [99].

A brief history of an energetic positron is as follows. After its introduction into the solid, the positron loses energy by ionization (or creation of electron-

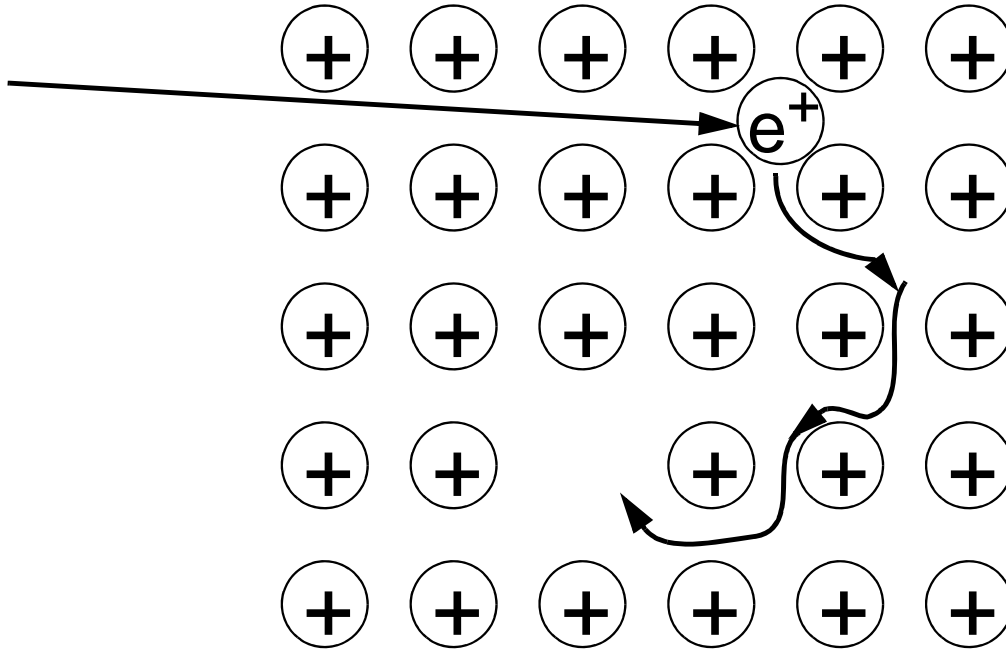


Figure 1.3: Schematic diagram of positron trapping in a defect.

hole pairs) and at lower energies by positron-phonon interactions. The positron eventually comes to thermal equilibrium with the environment, and then diffuses due to positron-phonon collisions. During this diffusion process the positron can interact with defects in the solid, resulting in the trapping of the positron in localized states. Eventually, the positron annihilates with an electron, resulting in the emission of  $\gamma$  rays.

One important facet of earlier studies of positron solid-state interactions was on the mapping of Fermi surfaces in metals [12]. Measurement of momentum distribution of conducting electrons in metals using positrons provided an accurate measure of the detailed shape of the Fermi surface.

The trapping of positrons in defects is also an area in which there has been much activity [124]. The mechanism of positron trapping in a defect is illustrated schematically in Fig. 1.3. A thermalized positron diffuses freely in the field created by the lattice ion cores. The positron is attracted to a defect, since the ion is missing at the defect and the repulsive potential is absent. The positron forms a localized state at the defect, and the annihilation signal provides information about the nature of this localized state and the defect itself.

#### 1.4.1.1 Positron moderators

One interesting and important aspect of positron-solid interactions is the interaction of positrons with the solid surface. Thermalized positrons in solids can diffuse to the surface. In some materials, the work function of a positron on the surface is negative, and a fraction of positrons can be re-emitted from the surface with electron-Volt energies. This positron “moderation” in fact was first discovered by Cherry [21] and confirmed later by Costello *et al.* [27]. An example of applications of this process is the positron re-emission microscopy, which maps the work function of positrons on the surface [62]. The efficiency of positron moderation is a few percents at the most, with the loss due predominantly to annihilation in the solid. However, compared with the energy selection from a continuous spectrum of a  $\beta^+$  decay, which range up to energies of hundreds of kilo-electron Volts, (which was mainly used before the invention of the moderator) positron moderators are several orders of magnitude more efficient in producing slow positrons. Current positron-matter interaction research relies heavily on this positron moderation process to obtain the slow positron beams, and this effect is crucial to the work described here.

The efficiency of moderators has seen steady increase from the efficiency value of  $\epsilon = 3 \times 10^{-8}$  for Cherry’s work [21], where the  $\epsilon$  is defined as the ratio of positrons extracted in a beam to the number being produced by the radioisotope. Single crystals of various metals, such as tungsten [47], nickel [150], and copper [98], have slow positron efficiencies as large as  $\epsilon \sim 10^{-4}$ . It has been observed that rare gas solids can moderate positrons with an order of magnitude more efficiently than single crystal metals [100], and currently we are using a solid neon moderator ( $\epsilon = 2.5 \times 10^{-2}$ ) [49]. Production of solid rare gas moderators involves making provision for a cold surface, where the rare gas can be deposited as a solid.

#### 1.4.2 Liquids

The interaction of positrons with liquids is complicated by the fact that the atoms or molecules are not located at the fixed positions. One phenomenon unique to positron-liquid interactions is the existence of Ps atoms in self-trapped states [130]. Because of the strong exchange repulsion between the electron in the Ps and the nearby atoms with tightly bound electrons of parallel spin, it is energetically favorable for the Ps atom to be in a region of lower than average atom density. Once in this region in a liquid, the Ps can repel the nearby atoms, thereby creating a cavity or a bubble.

#### 1.4.3 Gases

Positron interactions with isolated atoms and molecules are relatively simple as compared to positron-condensed matter interactions, yet they exhibit rich

behavior. A number of the many-body effects that exist in condensed matter are not present, and the behavior is described by a positron scattering off a molecule. Many experimental and theoretical techniques developed for studies of electron-molecule interactions have been adopted for the studies of positron-molecule interactions. They include measurement of collision cross sections, including differential cross sections and measurement of positronium formation cross sections for various molecules [1].

One type of experiment, which is unique to positron-molecule interactions, is the annihilation of the positron with a molecular electron. In earlier annihilation studies on molecules, a radioisotope, such as  $^{22}\text{Na}$ , which decays via positron emission, was placed directly in a gas cell, and the measurements using this configuration are described in details in Ch. 2. For small atoms and molecules, the positron interactions are well understood by the scattering picture, including positron-electron correlations [6]. However, Paul and Pierre first observed unusually high annihilation rates for methane, ethane, propane, and butane [110], and Heyland *et al.* later confirmed these observations [60]. Surko *et al.* have observed even higher annihilation rates for larger alkanes using positrons stored in a Penning trap [134]. These anomalously high annihilation rates cannot be understood with the simple scattering picture, and the process responsible for these high rates is still not understood.

## 1.5 Outline of dissertation

This dissertation is organized in the following manner. Previous measurements on annihilation rates and momentum distributions in gases are summarized in Ch. 2. Our positron trap and experimental setup are described in Ch. 3. The most complete survey of annihilation rate studies for a variety of chemical species is presented in Ch. 4. The test substances includes noble gases, inorganic molecules, alkanes, substituted alkanes, and aromatics. The experimentally measured annihilation rates are compared with theoretical calculations and previous measurements. The studies of 511-keV annihilation  $\gamma$ -ray spectra in gases for a variety of chemical species are presented in Ch. 5. The substances under study are similar to those of Ch. 4. Results from Ch. 5 indicate that annihilation is dominated by valence electrons. However, a small fraction of inner-shell electron annihilation was detected, which is described in Ch. 6. An application of positron annihilation rate and  $\gamma$ -ray spectrum studies is the positron annihilation in astrophysical media, and this aspect of research is described in Ch. 7. Finally, the conclusions are presented in Ch. 8. Additional information is presented in 3 appendices; the experimentally measured ion gauge sensitivities (Appendix A), various physical parameters (Appendix B), and  $\gamma$ -ray line shapes (Appendix C) for atoms and molecules studied are tabulated.

## Chapter 2

# Overview of previous atomic and molecular physics studies using positrons

Experimental configurations of positron-molecule interaction studies can be roughly divided into high (gas) pressure and low pressure experiments. While they have both been used to obtain useful information on the two-body interactions between positrons and molecules, they employ different detecting methods and involve different complexities. These issues are discussed in Sec. 2.1.

Two types of physical quantities have been mainly measured, the annihilation rates (Sec. 2.2) and the momentum distributions of annihilating electron-positron pairs (Sec. 2.3). Recently, mass spectra of ions resulting from positron annihilation on molecules have been measured in low-pressure experiments (Sec. 2.4). The annihilation rate measurement is sensitive to the over-all interaction of positrons with molecules, while the momentum distribution measurement is sensitive to the quantum states of annihilating electrons. Historically the rates of positron annihilation on molecules,  $\Gamma$ , have been expressed in terms of normalized annihilation rates,  $Z_{\text{eff}}$ , by modifying the Dirac annihilation rate for free electrons [Eq. (1.2)] to include the effective number of electrons  $Z_{\text{eff}}$  in the molecule that contribute to the annihilation process. In particular,

$$\Gamma = \pi r_0^2 cn Z_{\text{eff}}, \quad (2.1)$$

where  $n$  is the number density of molecules. As discussed in Ch. 4, this is a crude parameterization. Even though the  $Z_{\text{eff}}$  is in the same order of magnitude with the number of electrons  $Z$  for small atoms and molecules, this assumption of effective number of electrons breaks down for large organic molecules, where these  $Z$  values are several orders of magnitude higher than  $Z$ , due to the formation of the long-lived positron-molecule states.

## 2.1 Dense-gas and low-pressure experiments

### 2.1.1 Dense-gas experiments

The first experiments on positron-molecule interactions were performed at relatively high pressures ( $P \geq 1$  atm). In this work, the experimental setup is relatively simple since the high-energy positrons from the source are directly injected into the gas cell. They also have the advantage that at high material densities, the annihilation occurs in a small volume near the source so that angular correlation of annihilation radiation (ACAR) method (discussed in Sec. 5.2.1) is applicable. However, since the moderation gas is the same as the test gas, the energies of positrons at moment of annihilation depend on moderation processes and may not be well characterized for some gases. The annihilation  $\gamma$ -ray signals come from the annihilation of positronium atoms and from free positron annihilation on molecules. These positronium signals must be taken into account, resulting in the considerable reduction in the signal-to-noise ratio of free positron annihilation. Another disadvantage is that, because of the gas pressures required for these experiments, the number of test molecules is limited to those with high vapor pressures at room temperature (e.g., atmospheric or higher pressure). The results of these experiments are reviewed [26, 60, 88], as are experimental techniques involved in these types of measurements elsewhere in detail [55, 89].

Positrons emitted from the source typically have energies of a few hundred keV. They lose energy rapidly through ionization and electronic excitation of gas molecules until their energy falls below the threshold energy for electronic excitation. For example, the ionization cross section,  $\sigma_i$ , at 100 eV is about  $10^{-16}$  cm<sup>2</sup>, while the annihilation cross section is

$$\sigma_a = \frac{\Gamma}{nv} = \frac{\pi r_0^2 c Z_{\text{eff}}}{v}. \quad (2.2)$$

At 100 eV,  $\sigma_a \sim 10^{-23} Z_{\text{eff}}^2$  cm<sup>2</sup>. For these energies,  $\sigma_a \ll \sigma_i$ . Therefore, the positrons slow down without significant loss from annihilation at these energy ranges. Further moderation of positrons occurs through elastic collisions in the case of noble gases, and mainly through inelastic vibrational and rotational excitation collisions in the case of polyatomic molecules. In elastic collisions, a positron loses at most a fraction  $2m/M$  of its initial energy per collision, where  $m$  and  $M$  are the masses of the positron and the gas atom, respectively. As a result, about  $M/2m$  large-angle elastic collisions are required for thermalization, leading to the definition of an effective thermalization cross-section for elastic collisions,

$$\sigma_t^{\text{el}} = \frac{2m\sigma_m}{M}, \quad (2.3)$$

where  $\sigma_m$  is the elastic momentum-transfer cross-section, which is on the order of atomic dimensions. For polyatomic molecules, vibrational and rotational excita-



tions provide a more efficient thermalization mechanism, and the cross-sections,  $\sigma_t^{\text{inel}}$ , are typically around  $10^{-16} \text{ cm}^2$  [116]. In order to study the interaction of thermalized positrons with molecules, we must have

$$\frac{\sigma_t}{\sigma_a} \gg 1. \quad (2.4)$$

For noble gases,

$$\frac{\sigma_t^{\text{el}}}{\sigma_a} \sim \frac{10^3}{MZ_{\text{eff}}}, \quad (2.5)$$

where  $M$  is in atomic mass units, while for polyatomic molecules,

$$\frac{\sigma_t^{\text{inel}}}{\sigma_a} \sim \frac{10^5}{Z_{\text{eff}}}. \quad (2.6)$$

Thus, thermalization occurs before annihilation for small noble gases, such as helium and neon, and for polyatomic molecules with  $Z_{\text{eff}} \ll 10^5$ . However, these estimates indicate that positrons can annihilate before they reach thermal equilibrium for large noble gases and for some large organic molecules. In particular,  $Z_{\text{eff}}$  can be as large as  $10^2$  for large noble gases [25, 60, 101, 139, 146] and  $10^6$  for large organic molecules [60, 81, 102, 134]. A mixed-gas technique has been developed to address this thermalization problem [146].

### 2.1.2 Low-pressure experiments

In the last decade, positron trapping techniques have been developed by our group to overcome some of the disadvantages of the previous high-pressure measurements. In these trapping experiments, the positron energies are well-characterized since the moderation of high-energy positrons is achieved by media different from the test substances. In addition, the positron energy can be reduced below positronium formation threshold so that the signals from positronium annihilation can be eliminated.

The experimental setup is generally more complicated as compared to the high-pressure measurements. It involves a Penning trap, which is a trap using electrostatic potentials and a magnetic field for confining charged particles [87, 134, 148]. High-energy positrons produced by either radioactive isotopes or LINAC's are moderated to a few eV energy by a solid state moderator, such as tungsten or solid noble gas films. This slow beam of positrons (a few eV energy) is guided through a magnetic beam tube into a Penning trap. The positrons may be moderated further through various energy loss mechanisms, such as collisions with buffer gas. For the buffer gas system, these positrons reach thermal equilibrium. These stored positrons have desirable characteristics. In addition to their well-characterized energy, the number of positrons is large ( $> 10^6$ ) so that the resulting signal-to-noise ratio of annihilation measurements is large. Since the positrons can be stored for a long period of time, they can be used very

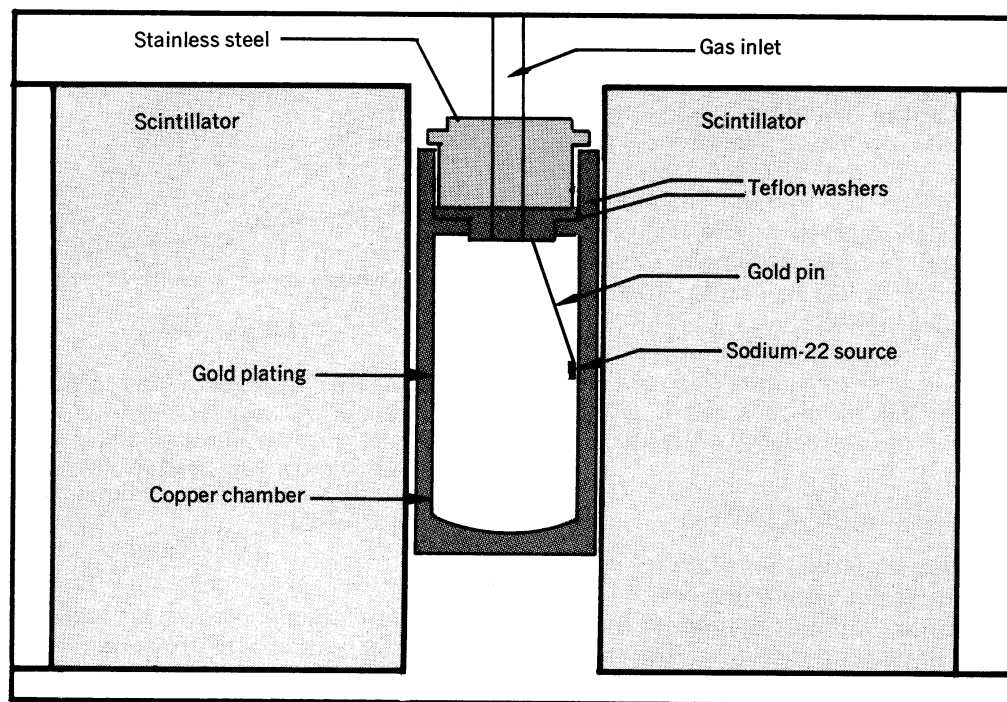


Figure 2.1: Apparatus for measuring annihilation time spectra used in Ref. [60]. The copper pressure vessel contains a  $^{22}\text{Na}$  source and gas at pressure up to 60 atmospheres. The two plastic scintillators provide “start” and “stop” pulses from which spectra are obtained with resolution of 1.5 ns.

efficiently. One unique feature of the low-pressure measurements is that mass spectrometry of ions resulting from positron annihilation is possible [63,109,148]. A detailed description of our positron trap is presented in Ch. 3.

## 2.2 Annihilation rates

Previous high-pressure gas experiments were performed in an apparatus similar to that shown in Fig. 2.1. This technique to measure annihilation rates uses a  $^{22}\text{Na}$  radioactive source, which emits a 1.28-MeV  $\gamma$  ray with a negligible delay after the emission of a positron. The positron annihilates in a pressurized gas chamber, and delayed coincidences are observed between signals recorded on scintillation counters from the 1.28-MeV  $\gamma$  ray and the annihilation  $\gamma$  rays. Thus, the time delay is a measure of the annihilation rate and is typically of the order of  $10^{-8}$  s in gases at atmospheric pressure.

Figure 2.2 shows an illustrated annihilation time spectrum. The prompt peak “A” is due to the fast decay of para-positronium atoms ( $\tau = 0.1$  ns). Curve I is due to free positrons annihilating with the molecule, while curve II is due to

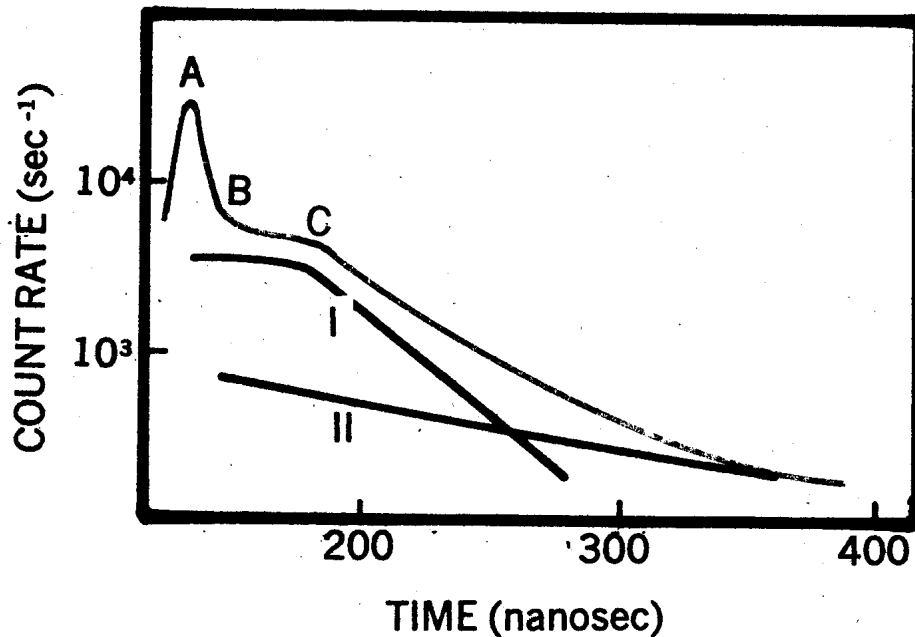


Figure 2.2: Schematic drawing of annihilation time spectrum (taken from Ref. [88]). The “prompt peak” is lettered “A,” and “BC” is the gradually changing “shoulder region.” Curve I is the contribution from free positron annihilation; curve II is the contribution from ortho-positronium annihilation.

the decay of ortho-positronium atoms ( $\tau = 137$  ns). The gradually changing shoulder region “BC” is due to changes in the free positron annihilation rates with energy. Generally, annihilation rates are smaller at higher energies, which occur while positrons are slowing down. The rate of positrons slowing down depends on the moderating gas, and the specific energy distribution during the slowing down of positrons is not well known. The straight section of curve I (time after “C”) is due to the thermalized free positrons annihilating with the gas molecules, and during this time, the annihilation rate can be measured. An example of data for helium is shown in Fig. 2.3.

This technique was first employed to confirm the existence of positronium atoms by Deutsch in 1951 [34]. The first studies of free positron annihilation soon followed [35]. The annihilation rates of most of the simple atoms and molecules that exist in the gas phase at standard temperature and pressure have been measured, and these measurements were summarized in Ref. [60]. The varieties of substances studied were widely extended by measurements performed at low pressure by Surko *et al.* [134] and Murphy and Surko [102]

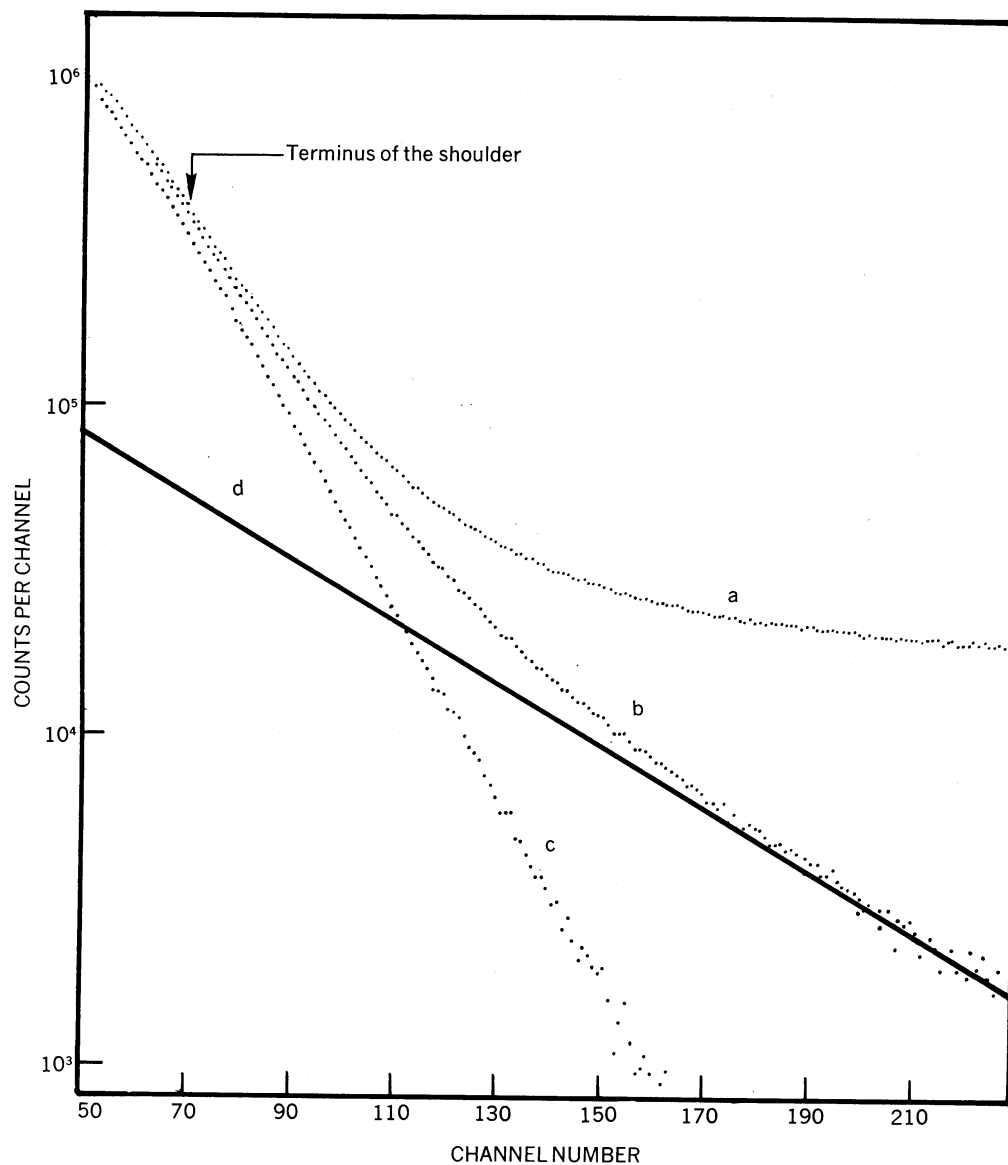


Figure 2.3: Annihilation spectrum observed with the apparatus of Fig. 2.1 for helium gas at a density of 43.6 Amagat (43.6 atm) at room temperature (taken from Ref. [88]). Each channel corresponds to 1.94 ns. Curve a is unprocessed data; curve b has the background subtracted; curve c is the free positron component, and curve d is the ortho-positronium component.

### 2.2.1 Anomalously high annihilation rates

One surprising result is the observation of anomalously large annihilation rates for large organic molecules. This phenomenon is still not understood. Deutsch

noticed very fast decay of free positrons on  $\text{CCl}_2\text{F}_2$  in 1951 [35]. He suspected that it was due to a large “positron attachment coefficient,” but the attachment mechanism was not discussed. Paul and Saint-Pierre performed systematic studies of this rapid annihilation of free positrons on some polyatomic gases, including alkanes that exist in gas form at atmospheric pressure, in 1963 [110]. They have suggested positron binding to molecules to explain the high annihilation rates. In order to explain the anomalously high annihilation rates, Heyland *et al.* later hypothesized clustering of molecules around the positron as well as the formation of positron-molecule bound states to explain this phenomenon, but their data and analysis could not distinguish between these two possible mechanisms [60]. In the case of xenon, Wright *et al.* then ruled out the possibility of clustering by measuring the annihilation rate for a wide range of pressures [146]. In 1988, Surko *et al.* measured even higher annihilation rates for larger organic molecules using stored positrons in a Penning-Malmberg trap, where the test substances were introduced as low-pressure gases [134]. They proposed the formation of long-lived positron-molecule compounds by the vibrational excitations of molecules based on the unimolecular reaction theory. An empirical scaling of  $\log_{10}(Z_{\text{eff}})$  with  $(E_i - E_{\text{Ps}})^{-1}$ , where  $E_i$  is the ionization energy of the molecule, was discovered by Murphy and Surko in 1991 [102]. To date, the physical process responsible for this scaling is not understood. Detailed discussions of these annihilation rates are presented in Ch. 4.

### 2.3 Momentum distribution measurements

In contrast to the large number of annihilation rate measurements in gases, momentum distribution measurements of annihilating pairs on isolated atoms or molecules have not been widely performed due to technical difficulties. There are two experimental techniques for measuring the momentum distribution of annihilating electron-positron pairs. One method of measuring momentum distributions is use of the ACAR technique. By measuring the angular correlation between two 511-keV  $\gamma$  rays, the momentum perpendicular to the  $\gamma$  rays can be measured. In gaseous media, an ACAR measurement suffers from low count rates because of limited flux of positrons and the relatively large volume of annihilation region. Two dimensional ACAR technique (2D ACAR) was used recently and was able to increase the count rates considerably as shown in Fig. 2.4 [26]. However, the signal-to-noise ratios of free positron annihilation signals were relatively poor, since the annihilation from positronium atoms had to be subtracted.

The other technique for measuring the momentum distributions is to measure the Doppler broadening of 511-keV annihilation  $\gamma$  rays. This method had previously been applied to a limited number [14, 136, 126]. Detailed discussions of momentum distribution measurements are presented in Ch. 5.

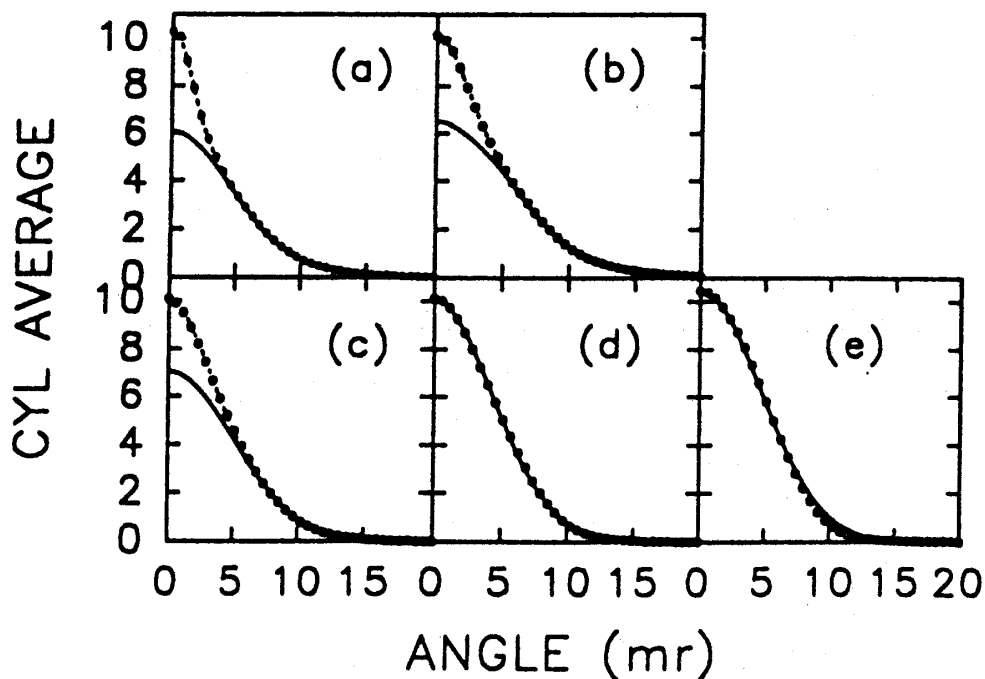


Figure 2.4: 2D-ACAR spectra of noble gases from Ref. [26]. (a) He. (b) Ne. (c) Ar. (d) Kr. (e) Xe. The narrow component is the free positronium annihilation signal, while the wider component is the signal from free positron annihilation on atoms.

## 2.4 Ion mass spectrum measurements

Positron and positronium chemistry, such as the formation of positronium hydride [121], has been studied previously [122]. A Penning-Malmberg trap can be a powerful tool to study this type of reaction. One type of study is the observation of positive ions.

Positron annihilation on atoms and molecules results in formation of positive ions. The mass spectroscopy of the resulting ions are possible. The techniques for ion mass spectroscopy are generally available only for low pressure experiments (Sec. 2.1.2) such as those possible in positron traps.

Positron annihilation and positronium formation are qualitatively different ways of producing positive ions, and they may have applications in chemical analysis. These methods may also be gentler ways of removing an electron from a fragile molecule than the conventional methods such as electron-impact ionization [63].

In 1989, Passner *et al.* first measured the ion mass spectrum following positron annihilation in a positron trap, using a time-of-flight (TOF) technique [109]. For alkane molecules, they observed a high probability of fragmentation following annihilation with room-temperature positrons. Later, these

observations were analyzed more carefully [45].

Hulett *et al.* developed an improved TOF mass spectrometer attached to a Penning trap and studied different aspects of the fragmentation of organic molecules [63, 147–149]. A highlight of their studies was the discovery of a large probability of producing unfragmented ions in the narrow energy range just above the positronium formation threshold [63]. Studies of various organic molecules revealed that the molecules with double and triple bonds tends to produce unfragmented ions. The mechanism of fragmentation has been investigated theoretically, and the theory is in general agreement with the experimental results [28].





## Chapter 3

# Description of the experiments

This chapter describes the apparatus and methods used to perform experiments on positron-molecule interactions. The schematic overview of the experimental setup is shown in Fig. 3.1. High-energy positrons emitted from a  $^{22}\text{Na}$  source are moderated to a few eV by the solid neon moderator (Sec. 3.1). These slow positrons are magnetically guided through the beam line (Sec. 3.2) into the positron trap (Sec. 3.3). The positron trap is a Penning-Malmberg trap designed to accumulate and store a large number of positrons. The confinement for these positrons is provided by the electrostatic and magnetic fields in axial

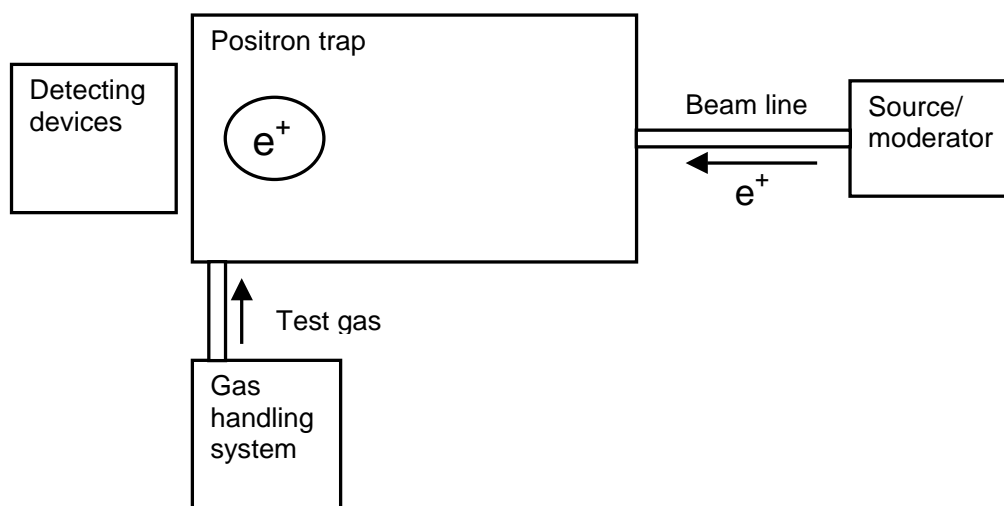


Figure 3.1: Schematic overview of the experimental setup. Positrons from the source chamber is guided through the beam line into the positron trap, which is a Penning-Malmberg trap for positron accumulation. The accumulated positrons, designated by “ $e^+$ ,” interact with the test gas introduced from the gas handling system. The annihilation signals and remaining positrons are recorded by the detecting devices.

and radial directions, respectively. The stored positrons interact with the test gas introduced through the gas handling system, where the test gas admission and pressure are regulated (Sec. 3.4). The signals from the positron annihilation in the trap are recorded with a Ge detector for  $\gamma$ -ray spectral measurements. For annihilation rate measurements the number of remaining positrons are measured by dumping these positrons on a plate at the end of the trap, where the accumulated charges or the  $\gamma$  rays resulting from positron annihilating on the plate are recorded.

### 3.1 Source and moderator

The positrons were obtained from a  $^{22}\text{Na}$  radioactive positron emitter, purchased from DuPont Pharma. This source has a relatively long lifetime of 2.6 y, and the strength at the time purchased was 150 mCi. It is sealed behind a 13  $\mu\text{m}$  tantalum window. The spectrum of positron energies is continuous up to 540 keV.

These high energy positrons were moderated by a single-crystal tungsten film in the earlier stages of the experiments and by solid neon film in the later stages. The tungsten moderator assembly was relatively simple and was used in a transmission geometry [47,85]. The neon moderator assembly is more complicated, but the moderation efficiency is about an order of magnitude larger than that of the tungsten.

The schematic diagram of the neon moderator system is shown in Fig. 3.2. The source is recessed into a parabolic copper cup mounted on an Elkonite rod, which is attached to the second stage of a two-stage closed-cycle refrigerator (APD model DE-204SLB). The Elkonite rod is electrically isolated from ground by a sapphire washer, to allow electrical biasing of the source. Indium gaskets are inserted between all surfaces in contact. The entire assembly is enclosed in a copper heat shield, which is attached to the first stage of the refrigerator. The heat shield extends 6 cm beyond the source to minimize the heat load on the source. The interior surface of this extension is coated with a layer of commercial spray-on colloidal graphite to minimize reflection of incoming infrared radiation from room-temperature surfaces.

The temperatures of the copper paraboloid and the second stage of the cold head are monitored by silicon diodes using a Lakeshore temperature controller, which controls the temperature over a wide range by means of heater coils attached to the second stage. The second-stage temperature is typically 6–6.5 K, while the source itself is about 1 K warmer.

The source/cold-head assembly is installed in an all-metal UHV system pumped by an ion pump. The base pressure of the system is  $2 \times 10^{-8}$  torr after bakeout at 150°C and rises to about  $5 \times 10^{-8}$  torr after neon has been frozen onto the source, presumably because of neon subliming from the warmer

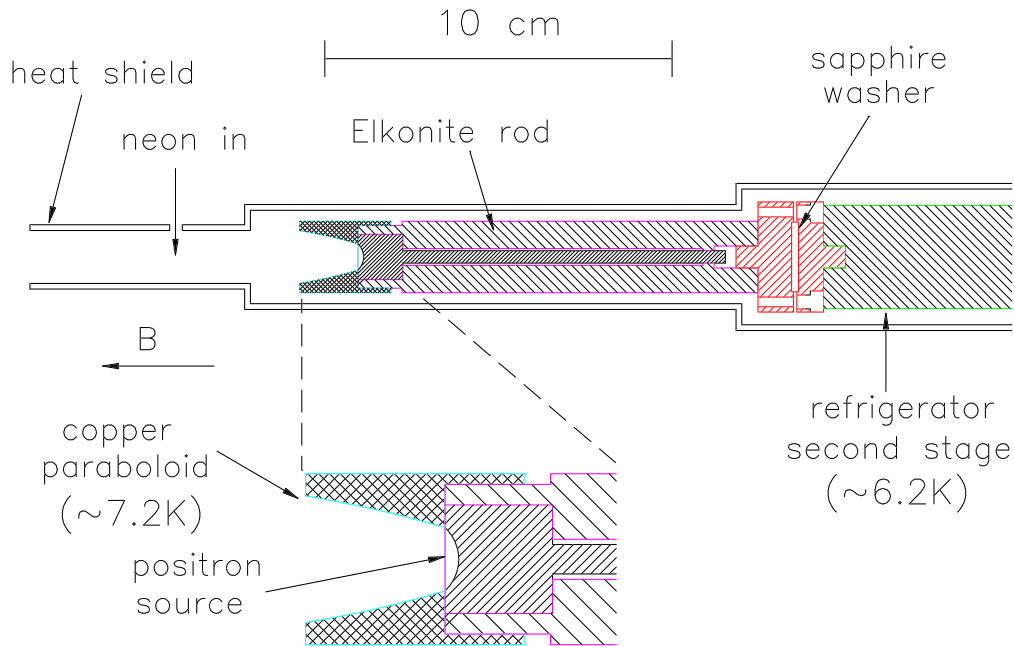


Figure 3.2: Schematic diagram of the source and cold-head assembly.

parts of the source/cold-head assembly.

Before a new moderator is grown, the source is slowly heated to 30 K, and the sublimated neon from the previous moderator is pumped out of the system using a turbo pump backed by an oil-free molecular drag pump. During the pumpout phase, the coldhead temperature is regulated so that the neon pressure does not rise above  $1 \times 10^{-2}$  torr.

The moderators are grown at a slightly elevated temperature (7.8–8.2 K). Neon is admitted at a pressure of  $1\text{--}3 \times 10^{-4}$  torr. This pressure is too high for operation of the ion pump, which is therefore shut off during this neon admission phase. As soon as the neon gas is switched off, the moderator is annealed by raising its temperature to 10 K for a few minutes.

The performances of our neon and tungsten moderators are summarized in Table 3.1. As can be seen in the table, the neon moderator significantly increased the moderation efficiency as compared to the tungsten moderator. Detailed description of the solid neon moderator apparatus and operation is given in Ref. [49].

Table 3.1: Parameters of the neon and tungsten moderators, and the positron trap.

Parameter	Neon moderator	Tungsten moderator
Source strength	65-mCi $^{22}\text{Na}$	65-mCi $^{22}\text{Na}$
Source efficiency	19%	19%
Fast $e^+$ flux	$4.6 \times 10^8 \text{ sec}^{-1}$	$4.6 \times 10^8 \text{ sec}^{-1}$
Moderated $e^+$ flux	$1.2 \times 10^7 \text{ sec}^{-1}$	$4.6 \times 10^5 \text{ sec}^{-1}$
Efficiency <sup>a</sup>	0.5%	$2 \times 10^{-4}$
Efficiency <sup>b</sup>	2.6%	$1 \times 10^{-3}$
Energy spread (FWHM)	$\sim 1.8 \text{ eV}$	$\sim 0.6 \text{ eV}$
Trapping rate	$3.9 \times 10^6 \text{ sec}^{-1}$	$1.8 \times 10^5 \text{ sec}^{-1}$
Trapping efficiency	$\sim 30\%$	$\sim 40\%$
Positron lifetime <sup>c</sup>	45 sec	45 sec
Positron lifetime <sup>d</sup>	1 hr	1 hr
Total trapped positrons	$1 \times 10^8$	$7.4 \times 10^6$

<sup>a</sup>Relative to source strength.

<sup>b</sup>Relative to emitted positrons.

<sup>c</sup>With buffer gas,  $p \sim 5 \times 10^{-7}$  torr.

<sup>d</sup>At base pressure,  $p \sim 5 \times 10^{-10}$  torr.

## 3.2 Beam line

The beam line consists of standard UHV components with stainless steel vacuum tubes. The tubes are surrounded by solenoid coil to exert confining magnetic field so that the positrons go through the tubes without hitting the wall. The field is generally about 100 G. The tube is bent so that the 1.27-MeV and 511-keV annihilation  $\gamma$  rays emitted from the  $^{22}\text{Na}$  source do not go into the detectors, which are located on the other side of the positron trap.

## 3.3 Positron trap

The low-energy positron beam is injected into the positron trap through the beam tube. The positron trap is a Penning-Malmberg trap specifically designed to accumulate and store positrons efficiently. Malmberg *et al.* modified a Penning trap to confine electron plasmas, and it was discovered that the device had a very long confinement time [87]. Taking advantage of this long confinement time, Surko *et al.* modified this trap to accumulate positrons efficiently [134],

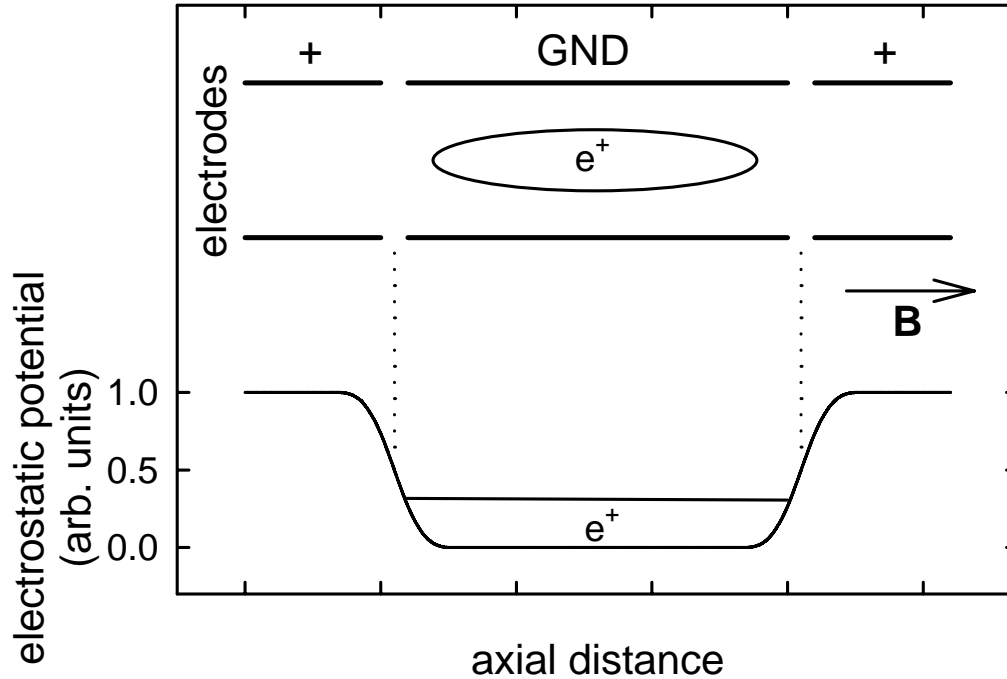


Figure 3.3: Schematic diagram of a Penning-Malmberg trap. A set of three cylindrical electrodes (above) provides a potential well (below) for charged particles.

resulting in the first creation in the laboratory of a positron plasma in 1989 [133].

The simplest form of a Penning-Malmberg trap is shown in Fig. 3.3. In a Penning-Malmberg trap, charged particles are confined magnetically and electrostatically in radial and axial directions, respectively. As can be seen in Fig. 3.3, the outside electrodes are biased positively, while the middle electrode is grounded. This creates a potential well for charged particles. In order to trap charged particles, two methods have been commonly used. One method is a fast-switching of the gate potential. This is effective when the beam is sent in pulses rather than as a continuous beam, such as when the positrons come from LINAC sources. The other method is to send a beam of particles with energy higher than the gate potential, and to arrange for an energy loss mechanism to reduce the energy of the particles below that of the gate potential so that they are trapped. The energy loss mechanism can be resistive damping [57] or inelastic collisions with buffer gas molecules [133]. Chaotic particle orbits have also been used to enhance trapping [42]. For positron trapping, the highest possible efficiency is desirable because of the limited flux of positrons. We employ a buffer gas for the energy loss mechanism, which has proven to be very efficient

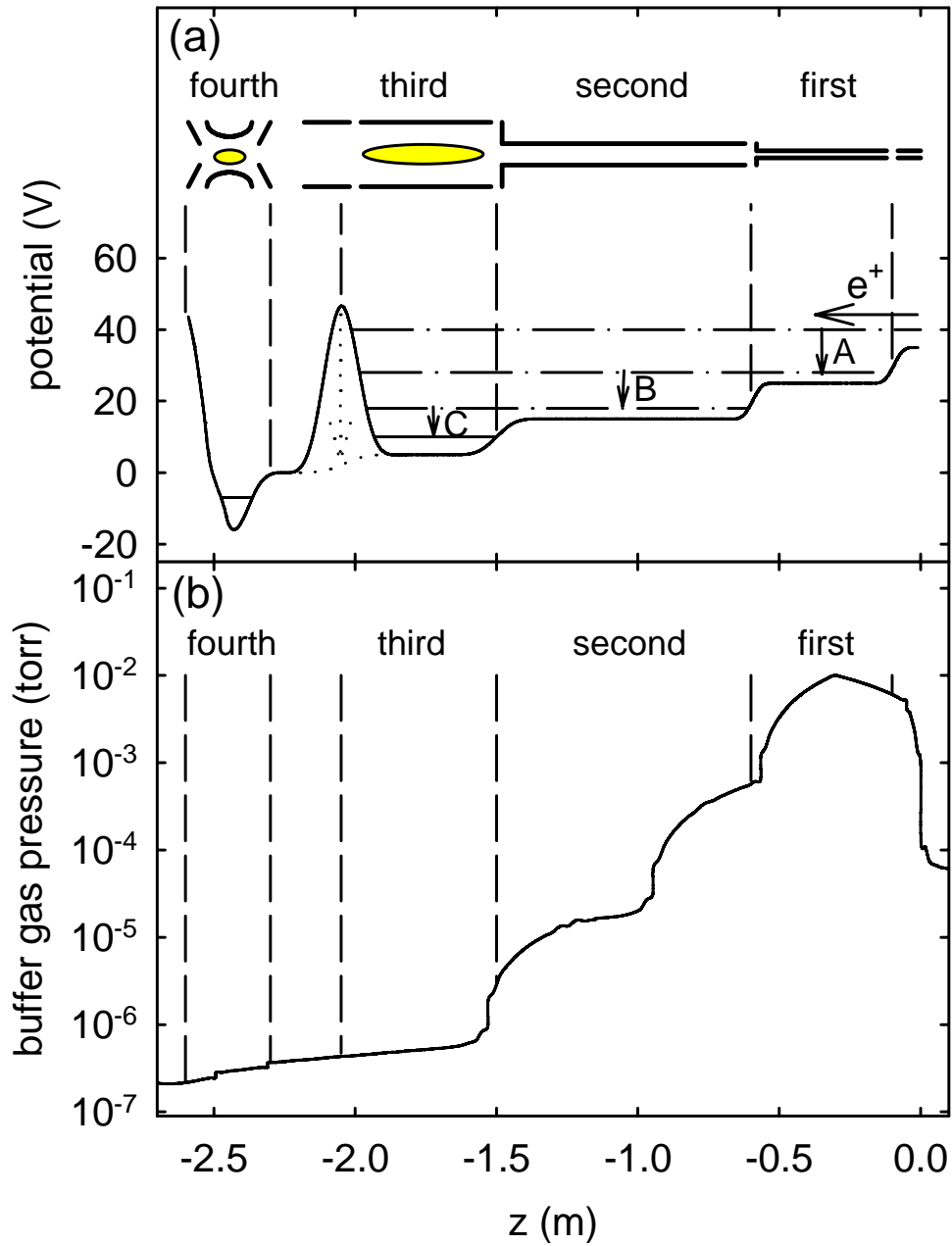


Figure 3.4: Schematic diagram of the positron trap electrode structure.

when used with a continuous positron source.

A schematic diagram of our four-stage positron trap is shown in Fig. 3.4(a) along with the confining potential well. The geometry of the electrodes is such

that the buffer gas pressure is high at the first stage of the trap, where the positrons have high probability of making inelastic collisions resulting in a high trapping efficiency. They continue to lose energy by inelastic collisions and eventually accumulate in the low pressure region, where annihilation on the buffer gas is relatively slow. The pressure of the buffer gas in the positron trap is plotted in Fig. 3.4(b) [48].

The potentials are adjusted so that, in the first stage, the main inelastic process is electronic excitation of  $N_2$  [shown A in Fig. 3.4(a)], which results in the positrons becoming trapped in the potential well. The positrons lose further kinetic energy through subsequent inelastic collisions (B and C in the figure) and become confined in the third stage. The fastest process is the electronic excitation of the  $N_2$  at about 8.8 eV. They reach thermal equilibrium with the buffer gas in the time scale of 1 s through vibrational and rotational excitations of  $N_2$ . The positron temperature in the third stage is measured to be  $\sim 300$  K using the “magnetic beach” energy analyzer [51]. The positrons stored in the third stage are shuttled to the fourth stage by lowering the potential barrier, as shown in the figure, since, in this stage, they are the closest to the detector and the buffer gas pressure is lower.

The potentials on each stage of the trap were adjusted to obtain optimal positron trapping [103]. This optimization was achieved by the computer assisted optimization software [51], and the efficiency of trapping [i.e., (number of trapped positrons) / (incident slow beam positrons)] is typically 30%.

Following positron loading, the nitrogen buffer gas can be pumped out. The time scale of buffer gas pumpout is about 8 s, as shown in Fig. 3.5. In this ultra-high vacuum environment ( $\sim 5 \times 10^{-10}$  torr), positron lifetime can be as long as 2 h (when a cold trap is filled with the liquid nitrogen). This long lifetime is especially important for the  $\gamma$ -ray spectrum measurements, as it minimizes the signal due to the annihilation on nitrogen gas.

A diagram of the positron trap including other hardware is shown Fig. 3.6. The cryogenic vacuum pumps are placed to provide appropriate differential pumping of the buffer gas, which is introduced at the first stage as indicated by the arrow in the figure. Originally, oil diffusion pumps were used for the positron trap, but it was discovered that the large oil molecules have extremely large annihilation rates, and so an oil-free vacuum system is required [134].

Magnetic field coils are used to supply approximately 600 G and 1000 G in the first and third stages of the trap, respectively. The positron filling of the trap is optimized by varying the currents in these magnetic field coils.

The confining electrodes are made of copper or aluminum, and they are gold coated to avoid corrosion. Test substances are introduced through a gas-handling

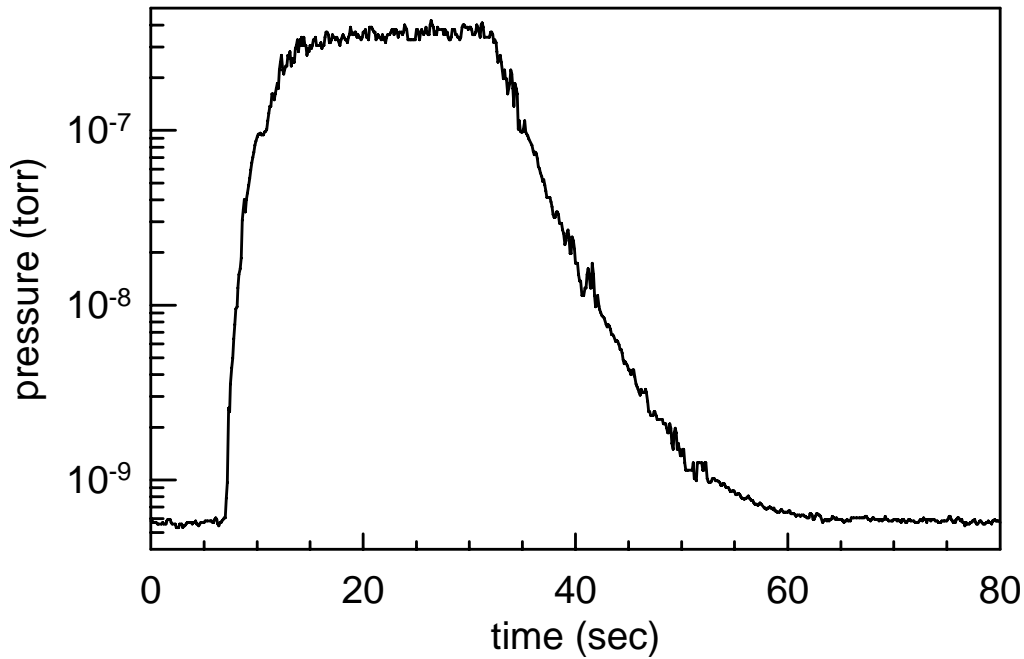


Figure 3.5: Gas pressure in the third stage of the positron trap during a pumpout cycle. The buffer gas feed is switched on at  $t = 7$  s, and switched off at  $t = 33$  s [131].

system with input located at the left end of the trap, as indicated in the arrow. This system is described in the next section. A cold trap is filled with liquid nitrogen when the test substance does not freeze at that temperature. These substances includes helium, neon, argon, krypton, hydrogen, nitrogen, oxygen, methane, and carbon tetrafluoride. The positron lifetime is typically about 1 h with liquid nitrogen in the cold trap. When a more condensable test substance is used, the cold trap is filled with a water-ethanol mixture chilled to about  $-10$  °C. The use of chilled water-ethanol mixture results in the positron lifetimes of about 5 m, which is still much longer than the typical annihilation time scale of 5 s for the  $\gamma$ -ray spectrum measurements.

The trapped positrons can be dumped onto an annihilation plate, and the charge accumulated on the plate can be measured using a charge sensitive amplifier. The number of dumped positrons can also be measured by detecting the 511-keV annihilation  $\gamma$  rays. We generally use a NaI(Tl) scintillator crystal in combination with a photomultiplier tube for this purpose. For the  $\gamma$ -ray spectrum measurements, an intrinsic Ge detector is used to measure the line shape of the 511-keV annihilation  $\gamma$  rays as a result of positron annihilation with the test gas in the fourth stage.



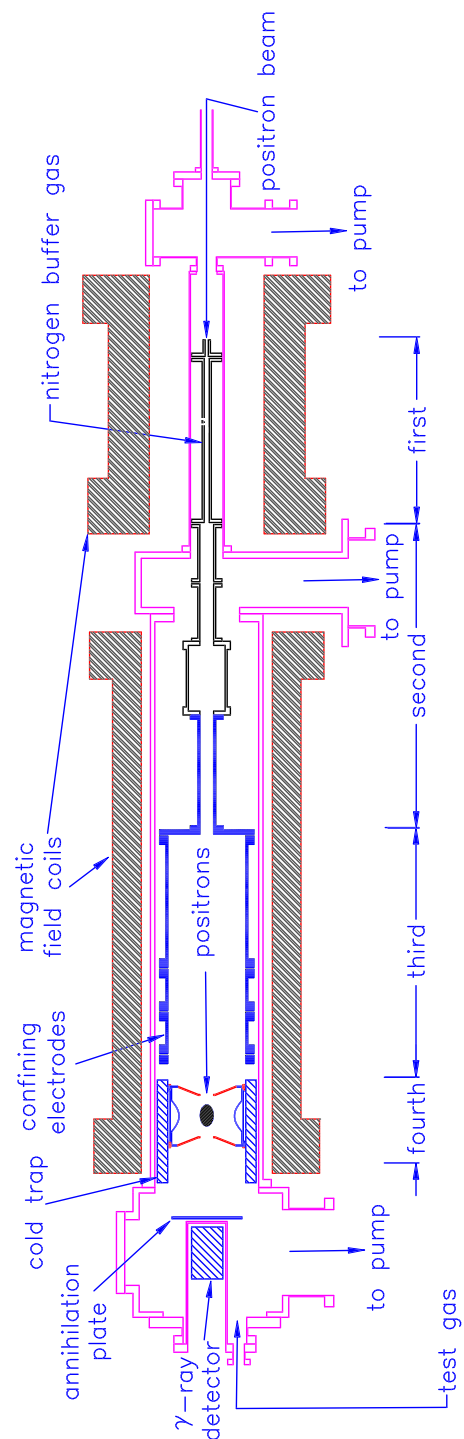


Figure 3.6: Schematic diagram of the positron trap.

## 3.4 Gas-handling system

As previously noted [55, 129], it is important to study high-purity test substances. The annihilation rates of large organic substances can be several orders of magnitude higher than those of small inorganic atoms and molecules. As a consequence, a very small amount of impurities can have very large effects on the experimental results. Thus, the careful handling of test substances and cleanliness of the system are essential. We used substances with the highest purity commercially available.

For the annihilation rate measurements, stability of the test gas pressure in the positron trap is also important, while fast switching of the test gas is important for the  $\gamma$ -ray spectral measurements to utilize available positrons efficiently.

We use different gas-handling systems for substances that exist as gases, liquids, or solids, which are described below.

### 3.4.1 Gases

A schematic diagram of a gas-handling system for gaseous substances at atmospheric pressure and room temperature is shown in Fig. 3.7. Test gas from a cylinder goes through a regulator, the piezo-electric valve, and a solenoid valve to the positron trap. The piezo-electric valve is controlled to adjust and stabilize the test gas pressure using a capacitance manometer pressure gauge reading. For  $\gamma$ -ray spectral measurements, the solenoid valve is used to switch on and off the test gas into the positron trap. In order to reduce the impurities in this gas-handling system, the entire gas line is baked to 100 °C under vacuum after a new test gas cylinder is installed. In addition, the gas line is flushed with the test gas at least three times before a measurement is taken.

### 3.4.2 Liquids and solids

The substances that exist as liquid or solid are introduced as low-pressure vapor gases into the positron trap. A schematic diagram of a gas-handling system for these substances is shown in Fig. 3.8. To ensure stable vapor pressure of a test substance, a test tube containing the substance is submerged in a tube containing a water-ethanol mixture. The temperature of this mixture is regulated with a thermoelectric unit. The pressure of the test gas going into the positron trap is regulated with a needle valve, which is adjusted to produce a suitable positron annihilation rate, in all cases larger than the rate on the background gas. For  $\gamma$ -ray spectral measurements, two solenoid valves are used to switch on and off the test gas. While the test gas is not going into the trap, it is pumped by a

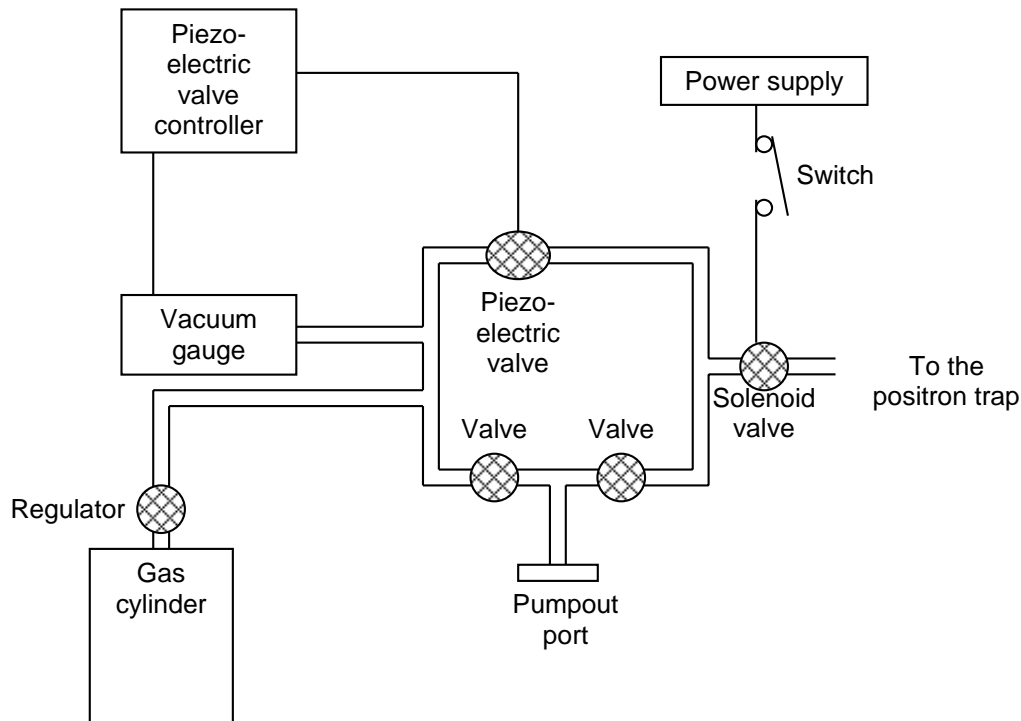


Figure 3.7: A schematic diagram of a gas-handling system for test substances that exist in gas form at atmospheric pressure.

vacuum pump to avoid the pressure build up in the line. The vacuum pump is an oil-free molecular drag pump backed by a diaphragm pump. In order to minimize the gas dissolved in the liquid substances, a process of freezing at liquid nitrogen temperature and thawing under vacuum is repeated three times prior to measurement. Solid test substances were placed under a vacuum for an hour prior to measurement in order to minimize the absorbed gases.

### 3.5 Annihilation rate measurements

Positron annihilation rates are presented in Ch. 4. These rates are measured using techniques similar to those described in Refs. [66, 67, 81, 101, 102, 133, 134].

As discussed in the previous section, various gases and vapors may be introduced directly into the fourth stage in order to study the annihilation of positrons on these substances. Molecules that exist as liquids or solids at room temperature are introduced in vapor form into the trap. The use of low-pressure gases helps to insure that one is studying a binary process involving one positron

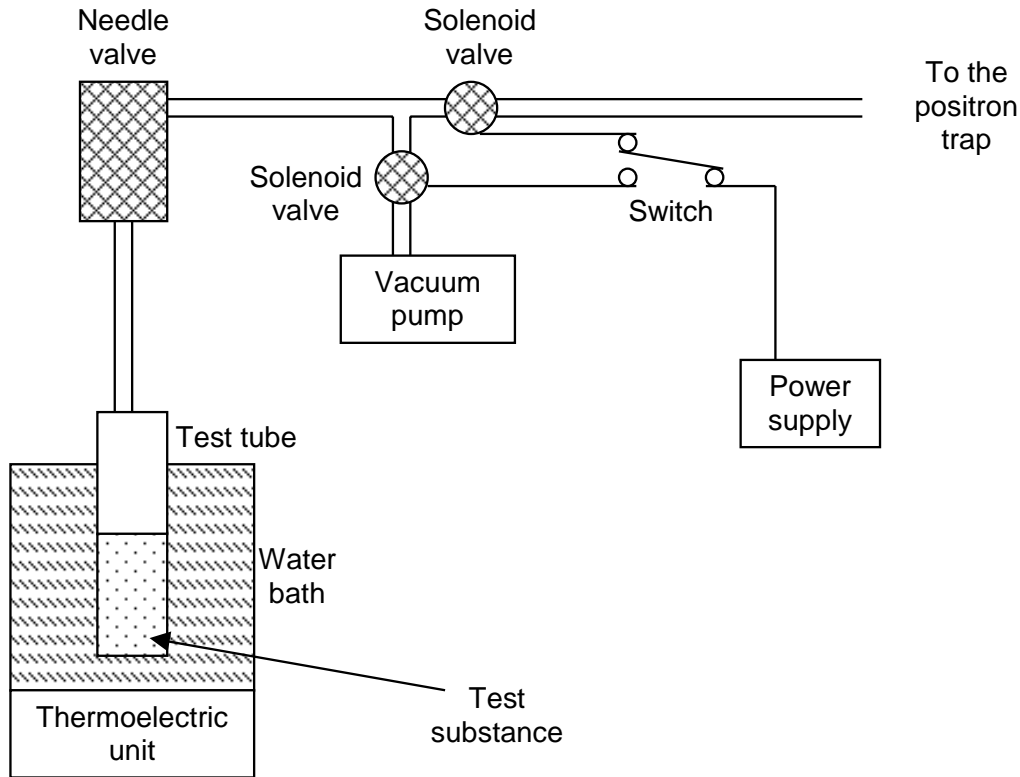


Figure 3.8: A schematic diagram of a gas-handling system for test substances, which are in liquid or solid form at atmospheric pressure.

and a single molecule. This avoids the potential complications due to the clustering of atoms or molecules at the site of the positron before annihilation takes place [95, 125]. Annihilation rates are determined by accumulating positrons for a fixed amount of time in the third stage (“filling”), waiting one second for the positrons to thermalize after they are shuttled to the fourth stage, and then waiting a variable amount of time while the positrons annihilate with the test gas (“storing”). After this storage time, the remaining positrons are dumped onto a metal annihilation plate, shown in Fig. 3.6, while the characteristic 511-keV annihilation radiation is measured using a NaI(Tl) scintillator. The light pulse amplitude from the scintillator is proportional to the number of positrons detected. A typical set of data is shown in Fig. 3.9(a), and the annihilation rate as a function of test gas pressure is shown in Fig. 3.9(b).

The linear dependence of the annihilation rate on test gas pressure, shown in Fig. 3.9(b), confirms that the process studied is a binary encounter between the positron and a molecule. In particular, for a binary process, the observed

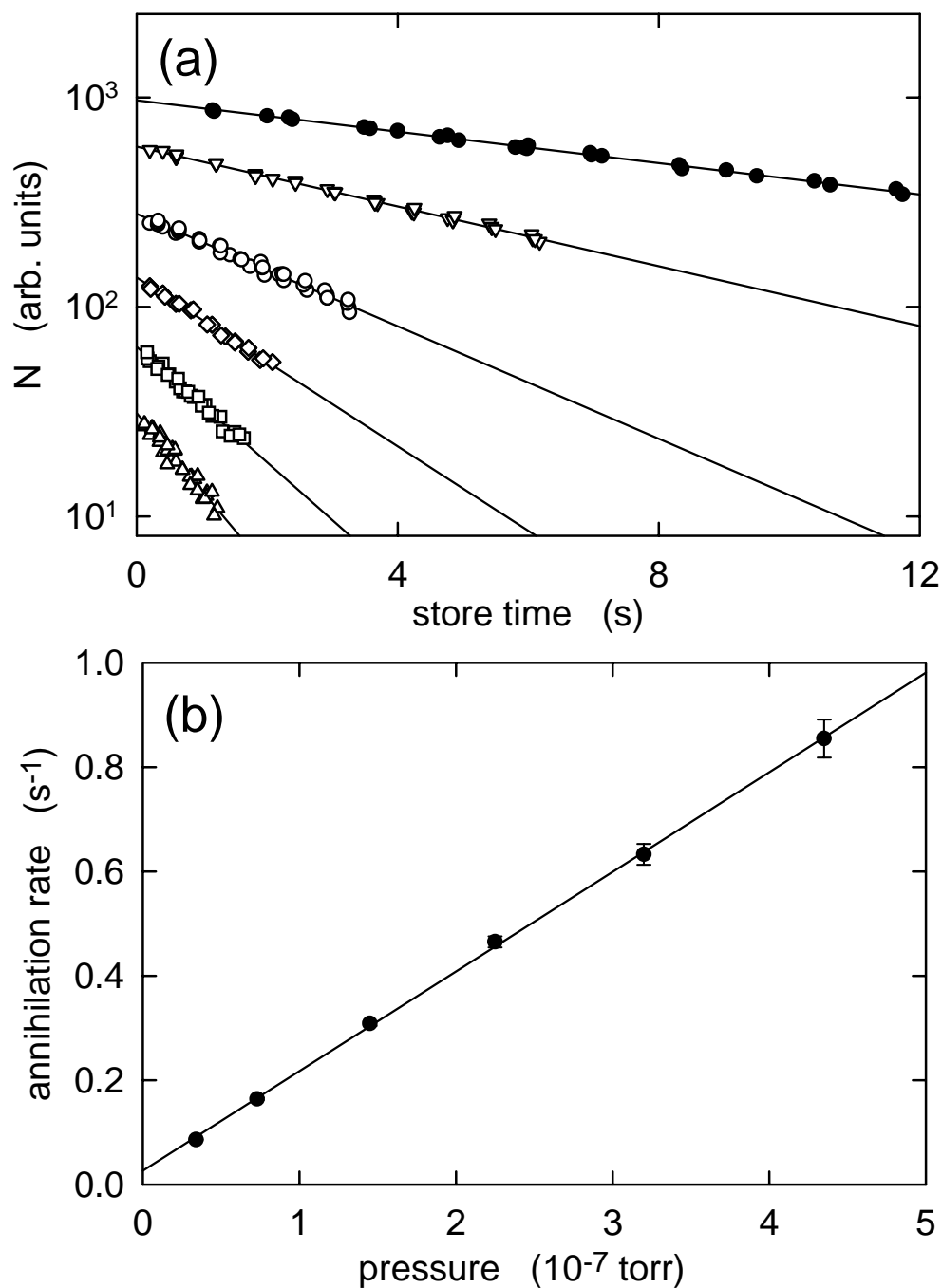


Figure 3.9: Data for the annihilation of positrons on benzene- $d$ . (a) Number of positrons remaining  $N$  as a function of time for various test gas pressures: ( $\bullet$ )  $3.4 \times 10^{-8}$ , ( $\nabla$ )  $7.3 \times 10^{-8}$ , ( $\circ$ )  $1.5 \times 10^{-7}$ , ( $\diamond$ )  $2.3 \times 10^{-7}$ , ( $\square$ )  $3.2 \times 10^{-7}$ , and ( $\triangle$ )  $4.4 \times 10^{-7}$  torr. (b) Annihilation rate as a function of test gas pressure, deduced from the data in (a).

annihilation rate is given by

$$\Gamma_{\Sigma} = \Gamma_0 + \Gamma_{N_2} + \Gamma_X, \quad (3.1)$$

where  $\Gamma_{N_2}$  and  $\Gamma_X = S_X P_X$  are the annihilation rates due to the nitrogen buffer gas and to the molecule under study. Here,  $P_X$  is the test gas pressure,  $S_X$  is a proportionality constant, and  $\Gamma_0$  is the annihilation rate on other large molecules present in the vacuum system. Using Eq. (2.1),  $\Gamma_X = \pi r_0^2 c n_X Z_{\text{eff}}$ , where  $n_X$  is the number density of the test molecule. In the regime studied, the ideal gas approximation is valid, and this density is related to the test gas pressure by  $n_X = P_X/(k_B T)$ , where  $k_B$  is the Boltzmann constant and  $T$  is the temperature of the test gas. Combining these equations,  $Z_{\text{eff}}$  of the test molecule can be expressed as

$$Z_{\text{eff}} = C S_X, \quad (3.2)$$

where  $C \equiv k_B T/(\pi r_0^2 c)$ . The value of this constant at  $T = 20^\circ\text{C}$  (293 K) is  $C = 4.058 \times 10^{-3}$  (s torr). Thus,  $Z_{\text{eff}}$  can be obtained from the slope in the observed annihilation rates versus pressure plot [e.g. Fig. 3.9(b)] using Eq. (3.2). The test gas pressure  $P_X$  is measured using a Bayard-Alpert ion gauge. The sensitivity of this type of gauge depends on the gas measured, and the calibration of this effect is described in Appendix A.

## 3.6 $\gamma$ -ray spectral measurements

### 3.6.1 Experimental procedure

The 511-keV  $\gamma$ -ray spectra resulting from positrons annihilating on a wide variety of atoms and molecules are presented in Ch. 5. The experiment is operated in a series of repeated cycles of positron filling and annihilation. In each cycle, positrons are accumulated for a fixed period of time (typically 5 s) in the presence of the  $N_2$  buffer gas. The buffer gas is then shut off, following a positron cooling time of 1 s. The buffer gas is then pumped out for 8 s. An intrinsic Ge detector is then gated on, and the test gas is introduced. Typically, the spectrum is accumulated on a multichannel analyzer (MCA) for 5 s in the presence of the test gas, and then the test gas is turned off. This cycle is repeated for about 12 h to accumulate a large number of counts. The total counts in the peak is typically  $\sim 10^6$ . The number of positrons in the trap and the pressures of the test gases are carefully adjusted to obtain the highest count rates consistent with avoiding  $\gamma$ -ray “pileup” in the detector, which can distort the shape of the spectrum.

### 3.6.2 Spectral analysis

We have found that a Gaussian line shape is a useful fitting function for both the detector calibration lines and the annihilation spectra observed from atoms and molecules. The fitting function used also contains a complementary error function component, which models Compton scattering in the detector crystal [72], and a constant background. It has the form:

$$f(E) = A_1 \exp \left[ - \left( \frac{E - E_0}{a \Delta E_{\text{fit}}} \right)^2 \right] + A_2 \operatorname{erfc} \left( \frac{E - E_0}{a \Delta E_{\text{fit}}} \right) + A_3, \quad (3.3)$$

where  $E$  is the  $\gamma$ -ray energy,  $\Delta E_{\text{fit}}$  is the full-width half maximum (FWHM) of the line,  $a = 1/(4 \ln 2)^{1/2}$ ,  $A_1$  and  $A_2$  are amplitudes,  $A_3$  is the background, and  $\operatorname{erfc}(x)$  is the complementary error function. The fit parameters are:  $A_1$ ,  $A_2$ ,  $A_3$ ,  $E_0$ , and  $\Delta E_{\text{fit}}$ . Representing the counts in each energy bin  $E_j$  by  $y_j$ , the quantity minimized is

$$\chi_r^2 = \frac{1}{N - k} \sum_{j=1}^N \left[ \frac{y_j - f(E_j)}{\sigma_j} \right]^2, \quad (3.4)$$

where  $\sigma_j = y_j^{1/2}$ ,  $N$  is the number of bins used in the fit, and  $k$  is the number of fitting parameters. The value of  $\chi_r^2$  is used as a measure of goodness of the fit and is expected to be of order unity for a fit to a good model. The fitting function given by Eq. (3.3) is a good approximation for the calibration  $\gamma$ -ray lines because the number of free electron-hole pairs produced by a monoenergetic  $\gamma$  ray in a germanium crystal has a Gaussian distribution. For calibration we used essentially monoenergetic  $\gamma$  rays emitted from a test source.

To first order, we have found that the annihilation lines can also be analyzed by fitting Eq. (3.3). While this is a convenient way of characterizing and comparing data, there is no *a priori* reason why the annihilation lines should have Gaussian line shapes. As discussed in Ch. 5, our data are now of sufficiently high quality to be able to resolve departures from Gaussian line shapes. The measured annihilation line is the convolution of the intrinsic annihilation line shape and the detector response. Under the assumption of Gaussian line shapes, the intrinsic FWHM,  $\Delta E$ , is given by

$$\Delta E = (\Delta E_{\text{fit}}^2 - \Delta E_{\text{det}}^2)^{1/2}, \quad (3.5)$$

where  $\Delta E_{\text{det}}$  is the detector linewidth and  $\Delta E_{\text{fit}}$  is the fitted linewidth from Eq. (3.3). The linewidths quoted in this dissertation are the values of  $\Delta E$  obtained in this way. In Sec. 5.4, we discuss other attempts (i.e., beyond the one-Gaussian approximation) to fit the measured spectra.

### 3.6.3 Calibration and detector response

The energy scale of the detector response was calibrated using 344.3-keV and 661.6-keV  $\gamma$ -ray lines from  $^{152}\text{Eu}$  and  $^{137}\text{Cs}$  test sources, respectively. The lines are fit with Eq. (3.3) to obtain the centroids and linewidths of the two peaks. The centroids are used to calibrate the energy scale of the spectra, while the widths of these two lines are interpolated to find the detector energy resolution at 511 keV. The resolution is typically 1.16 keV.

The detector line shape was also calibrated using a  $^{85}\text{Sr}$  calibration source, which has a  $\gamma$ -ray line at 514.02 keV, conveniently close to the 511-keV line. The spectrum measured with a 3- $\mu\text{Ci}$  source is shown in Fig. 3.10(a). The fit to Eq. (3.3) is shown in the figure as a solid line and yields  $\chi_r^2 = 1.3$ . The linewidth of the Gaussian,  $\Delta E_{\text{det}}$ , is typically  $1.16 \pm 0.01$  keV, which agrees with the interpolated value from 344.4-keV and 661.6-keV lines, where 0.01 keV is the drift in the detector linewidth during a measurement. The residuals from the fit are shown in Fig. 3.10(b). These data deviate slightly from the fit on the lower-energy side of the line. This low energy tail may be due to the trapping of electrons/holes in the defects of the Ge crystal [72]. Nonetheless, the residuals are generally quite small: less than 0.5% of the peak counts on the lower energy side and even smaller ( $\sim 0.1\%$ ) on the higher energy side. As described in Ch. 5, these residuals are also generally much smaller than the deviations from the Gaussian shape of the observed annihilation lines. In the following, we quote the linewidth of the Gaussian fit (typically 1.16 keV) as the width of the detector response. The detector energy response and line shape vary by a small amount from day to day (typically  $< 0.02$  keV), and a separate calibration spectrum was taken before and after each run.



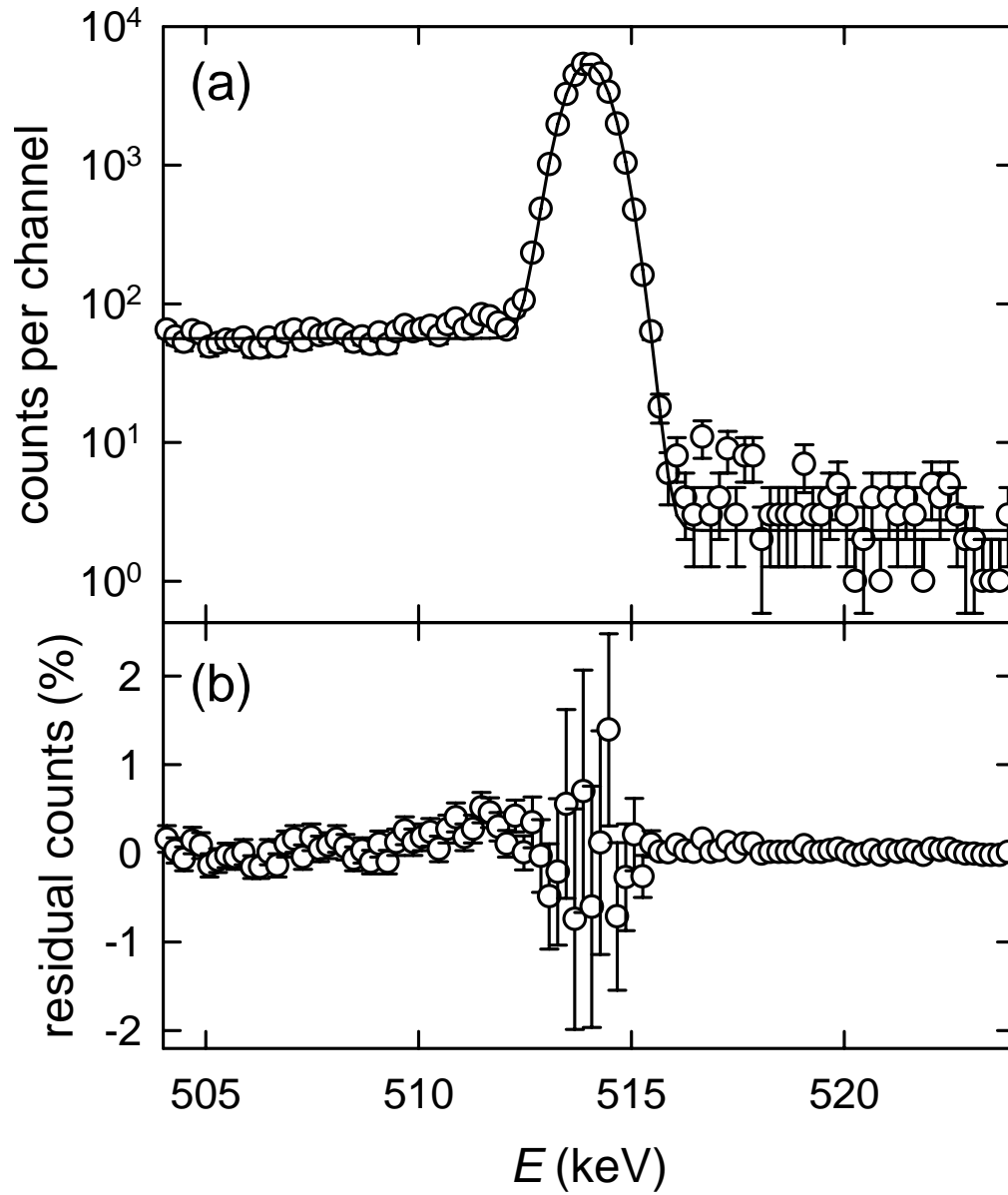


Figure 3.10: (a)  $\gamma$ -ray spectrum of the 514.0-keV line from a  $^{85}\text{Sr}$  source: ( $\circ$ ) observed spectra and (—) fit to the spectrum with a combination of a Gaussian and a step function [Eq. (3.3)]. The linewidth is 1.16 keV. (b) Residuals of the fit.



## Chapter 4

# Annihilation rates

A positron can annihilate with one of the bound electrons in a molecule. The annihilation rate is closely related to the interaction of the positron with the molecule at very short distances, since the rate is determined by the overlap of positron and electron wave functions. In this chapter, experimental results of annihilation rate measurements are presented along with previously measured and theoretically calculated values. Much of recent effort in this area was focused on possible explanations for the anomalously large annihilation rates observed for large molecules [134] and for the empirical scaling of annihilation rates with ionization and positronium binding energies (Sec. 4.3.1) [102]. Research on these issues is also presented. The majority of material covered in this chapter has been published elsewhere [66], and unpublished data are specifically noted.

### 4.1 Theoretical considerations

As described in Ch. 2, the positron annihilation rates on molecules are typically expressed in terms of  $Z_{\text{eff}}$ , defined as  $\Gamma = \pi r_0^2 cn Z_{\text{eff}}$  [Eq. (2.1)]. The annihilation of positrons on small atoms can be understood in terms of simple collisions [60,93]. Empirically, it is found that  $Z_{\text{eff}}$  for these molecules is of the order of, but somewhat larger than  $Z$ , the number of electrons in the molecule. In contrast, the annihilation rates for larger organic molecules are observed to be much higher than expected on the basis of simple models [60,102,110,134]. It is believed that this is due to the attachment of positrons to the molecule via long-lived positron-molecule resonances, but the detailed mechanism of attachment and subsequent positron annihilation are not understood [60,102,110,134]. Previous measurements [60,81,102,134] give various values of  $Z_{\text{eff}}/Z$  ranging from order unity to  $\sim 10^5$ , with anomalously high values for large organic molecules.

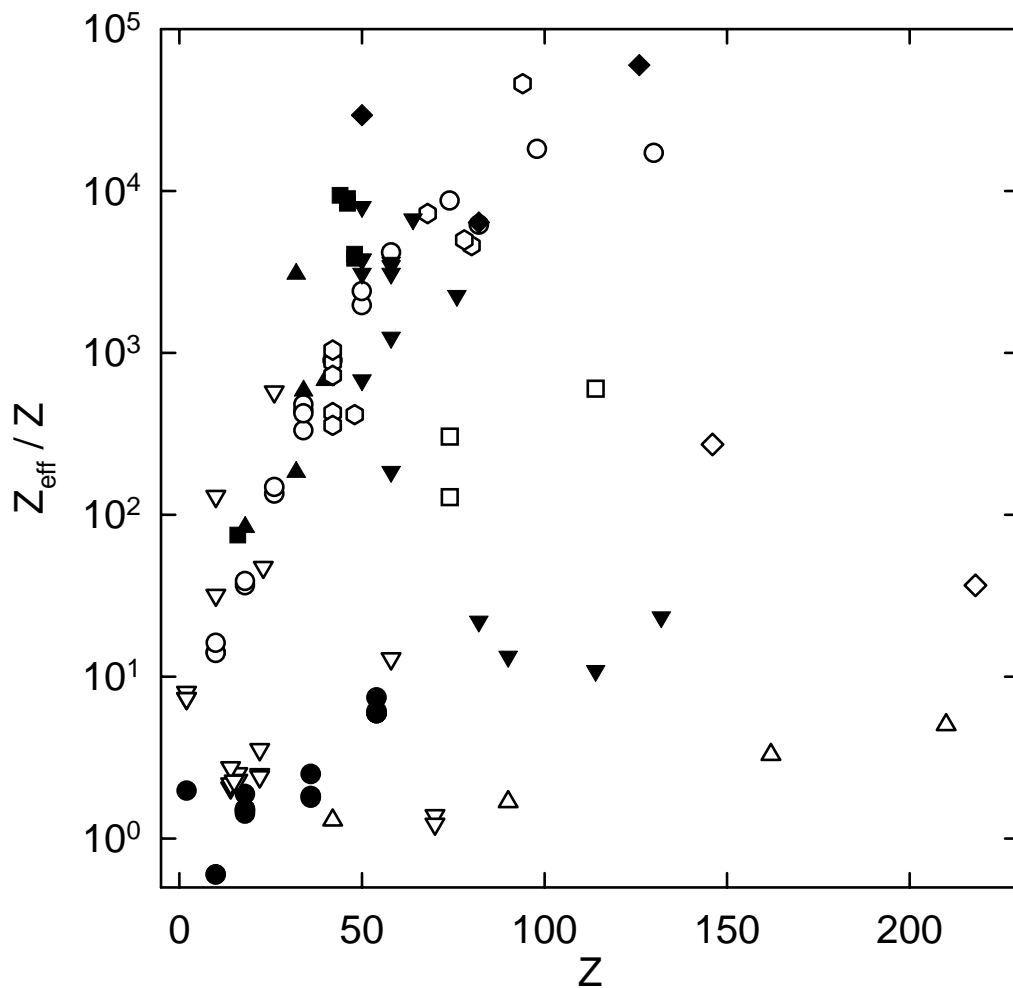


Figure 4.1: Experimental values of  $Z_{\text{eff}}/Z$  plotted against  $Z$ : (●) noble gases, ( $\nabla$ ) simple molecules, (○) alkanes, ( $\triangle$ ) perfluorinated alkanes, ( $\square$ ) perchlorinated alkanes, ( $\diamond$ ) perbrominated and periodated alkanes, (solid square) alkenes, (solid triangle up) oxygen-containing hydrocarbons, (open hexagon) ring hydrocarbons, (solid triangle down) substituted benzenes, and (solid diamond) large organic molecules.

Experimental values of  $Z_{\text{eff}}/Z$  for molecules are plotted against  $Z$  in Fig. 4.1, showing the strong dependence of  $Z_{\text{eff}}/Z$  on the size and chemical composition of the molecules.

#### 4.1.1 Long-lived resonances

The physical process resulting in the observed values of  $Z_{\text{eff}}$  might be understood qualitatively in the following way. The long-range interaction between

the positron and the molecule is attractive, due to the dipole resulting from the positron polarizing the electron cloud in the molecule. At low incident positron energy, this interaction will increase the collision cross-section,  $\sigma_c$ , above the value determined by the size of the molecule. The collision rate,  $\Gamma_c$ , can be expressed as  $\Gamma_c = n\sigma_c v$ , where  $v$  is the velocity of the positron. The velocity of the molecule is assumed to be negligible. When the positron-molecule interaction is a simple elastic collision, the time,  $\tau_c$ , spent by the positron in the molecular electron cloud is approximately  $\tau_c \sim d/v$ , where  $d$  is the molecular diameter. The probability of the positron annihilating during the collision may be expected to have the heuristic form  $(1 - e^{-\tau_c/\tau_0})$ , where  $1/\tau_0$  is the annihilation rate during the collision. A rough estimate for  $\tau_0$  is  $\tau_0 \sim 5 \times 10^{-10}$  s, which is the spin-averaged lifetime of a positronium atom [18]. With these assumptions, the annihilation rate for such an elastic collision,  $\Gamma^{\text{el}}$ , can be expressed as

$$\Gamma^{\text{el}} = n\sigma_c v(1 - e^{-\tau_c/\tau_0}). \quad (4.1)$$

Because  $\tau_c \ll \tau_0$ , this expression can be approximated as

$$\Gamma^{\text{el}} = n\sigma_c v \frac{\tau_c}{\tau_0}. \quad (4.2)$$

If, on the other hand, it is assumed that the positron forms a resonance with the molecule, the positron spends the resonance time,  $\tau_{\text{res}}$ , in the vicinity of the molecule. Electron-molecule resonances are known to occur with measured values of  $\tau_{\text{res}}$  as large as  $10^{-5}$  s [127], so  $\tau_{\text{res}} \ll \tau_0$  is not assumed here. By analogy with Eq. (4.1), the annihilation rate for resonance collisions,  $\Gamma^{\text{res}}$ , can be expressed as

$$\Gamma^{\text{res}} = n\sigma_{\text{res}} v(1 - e^{-\tau_{\text{res}}/\tau_0}), \quad (4.3)$$

where  $\sigma_{\text{res}}$  is the resonance formation cross-section. Comparing Eq. (4.2) and Eq. (4.3) with the definition of  $Z_{\text{eff}}$ , Eq. (2.1), it is found that

$$Z_{\text{eff}}^{\text{el}} = \frac{\sigma_c v}{\pi r_0^2 c} \frac{\tau_c}{\tau_0}, \quad (4.4)$$

for annihilation in elastic collisions, and

$$Z_{\text{eff}}^{\text{res}} = \frac{\sigma_{\text{res}} v}{\pi r_0^2 c} (1 - e^{-\tau_{\text{res}}/\tau_0}), \quad (4.5)$$

for annihilation in resonance collisions. For positrons at 300K, if we assume that  $\sigma_c$  is of the order of  $10^{-15}$  cm<sup>2</sup> and a simple elastic collision is considered, where  $\tau_c$  is of the order of  $10^{-14}$  s, then  $Z_{\text{eff}}^{\text{el}} \sim 10$  from Eq. (4.4). When the collision

involves attachment via long-lived positron-molecule resonances, Eq. (4.5) can be expressed as

$$Z_{\text{eff}}^{\text{res}} \sim 10^6 \left( \frac{\sigma_{\text{res}}}{10^{-15} \text{cm}^2} \right) (1 - e^{-\tau_{\text{res}}/\tau_0}). \quad (4.6)$$

Thus,  $Z_{\text{eff}}^{\text{res}}$  has its maximum value when  $\tau_{\text{res}} \geq \tau_0$ . If  $\sigma_{\text{res}}$  of the order of  $10^{-15} \text{cm}^2$  is assumed, then  $Z_{\text{eff}}^{\text{res}} \sim 10^6$  from Eq. (4.6). This range of  $Z_{\text{eff}}$ , from 10 to  $10^6$ , is what have been observed. For  $Z_{\text{eff}} \gg Z$ , the quantity  $Z_{\text{eff}}$  can no longer be interpreted as an effective number of electrons participating in the annihilation process. In this case,  $Z_{\text{eff}}$  should then be regarded as a normalized annihilation rate.

For the case of electron-molecule resonance collisions, values of  $\tau_{\text{res}}$  have been calculated successfully [22,23] by applying the Marcus-Rice equilibrium modification of the Rice-Ramsperger-Kassel theory (RRKM) [120], which was developed to describe unimolecular reactions.<sup>1</sup> The RRKM theory is a statistical theory which assumes a rapid statistical redistribution of energy among the various degrees of freedom of the molecule. The theory has been successfully applied to describe resonance collisions of electrons with selected molecules [22, 23], and could potentially provide quantitative insights into positron-molecule resonance lifetimes and annihilation rates.

### 4.1.2 Large cross sections from the resonance collision

Consideration must be given to the scattering of slow particles ( $kd \ll 1$ , where  $k$  is the wave number of the scattering particle and  $d$  is the size of the target molecule) in a field when the discrete spectrum of energy levels includes an  $s$  state whose energy is small compared with the value of the field  $U$  within its range of action  $d$ . This level is denoted by  $\epsilon$ :  $\epsilon > 0$  for a bound state and  $\epsilon < 0$  for an unbound (virtual) state. When the energy  $E_{e+}$  of the particle undergoing scattering is close to  $|\epsilon|$ , a considerable increase in the scattering cross section is observed [75, 129]. This enhancement of scattering cross sections is considered in Ref. [39] and discussed in Sec. 4.2.8.

## 4.2 Results

In this section, the values of  $Z_{\text{eff}}$ , measured in low-pressure gases using the positron trapping techniques described in Ch. 3, are compared with those of

---

<sup>1</sup>A unimolecular reaction is a reaction involving the isomerization or decomposition of a single isolated reactant molecule  $A$  through an activated complex  $A^\ddagger$  which involves no other molecule:  $A \rightarrow A^\ddagger \rightarrow \text{products}$ .

other experiments, where the measurements were made in dense gases. The experiments in dense gases [25,55,60,76,96,107,110,137,139,146] were performed at pressures  $\geq 10^2$  torr, while the low-pressure experiments [67,81,101,102,133,134] were performed at pressures  $\leq 10^{-5}$  torr. In general, the values of  $Z_{\text{eff}}$  in dense gases and those in low-pressure gas experiments agree to within 30%. Values of  $Z_{\text{eff}}/Z$ , which scale  $Z_{\text{eff}}$  by the number of electrons in the atom or molecule, are also tabulated, and they are summarized in Fig. 4.1. When plotted in this manner, the data show a large scatter. Plotting  $Z_{\text{eff}}$  as a function of molecular polarizability does not appreciably reduce this scatter, except for small molecules, where a dependence on molecular polarizability was previously noted [102]. (Values of molecular polarizability are tabulated in Appendix B along with other physical parameters.) In Sec. 4.3.1, another way of plotting the data, which appears to provide more insight into the physical mechanism underlying the annihilation process, is described.

The data recently published in Ref. [69] and unpublished data mainly in Tables 4.4, 4.9, and 4.11 were measured using an ion-gauge readout system with a different response from the previous measurements, and some of the values are different from the previous measurements. The values of  $Z_{\text{eff}}$  measured with this ion-gauge readout can be larger than the previous measurements by 50%. However, the same ion-gauge readout system is used for the data sets in Tables 4.4, 4.9, and 4.11, and the relative error should be within 10%. Ion-gauge sensitivity calibrations were not done for some of the molecules in the new data sets, and they are estimated from the values of similar molecules. The error associated with this estimation is not expected to exceed 30% and should not change the observed trends. These points are noted in the text and/or in the tables.

#### 4.2.1 Noble gases

Experimentally measured and theoretically calculated values of  $Z_{\text{eff}}$  for noble gases are listed in Table 4.1 and illustrated in Fig. 4.2. The theoretical calculation based on the Kohn variational model [140] for helium is in good agreement with the measurements. The polarized-orbital calculation for neon [91] also agrees reasonably well with the measurement. Our values for argon, krypton, and xenon are higher than those reported by other groups for measurements in dense gases. The ratios of the thermalization to the annihilation cross-sections calculated from Eq. (2.5) for argon, krypton, and xenon are 0.8, 0.1, and 0.02, respectively. These values suggest that positrons may not be thermalized before annihilation in heavier noble gases in the dense-gas experiments. A higher-

Table 4.1: Values of  $Z_{\text{eff}}$  for noble gases. References are given for previous measurements.

Molecule	Formula	$Z$	$Z_{\text{eff}}$ (Theory)	$Z_{\text{eff}}$	$Z_{\text{eff}}/Z$	Ref.
Helium	He	2	3.88 <sup>a</sup> , 3.84 <sup>b</sup>	3.94	2.0	[25]
Neon	Ne	10	6.97 <sup>c</sup>	5.99	0.6	[25]
Argon	Ar	18	28 <sup>d</sup>	33.8 <sup>†</sup>	1.9	[66]
				26.77	1.5	[25]
				27.3	1.5	[107]
				27.1	1.5	[96]
				25.5	1.4	[110]
Krypton	Kr	36	58 <sup>e</sup>	90.1 <sup>†</sup>	2.5	[66]
				65.7	1.8	[146]
				64.6	1.8	[25]
Xenon	Xe	54	217 <sup>e</sup>	401 <sup>†</sup>	7.4	[101]
				330	6.1	[139]
				320	5.9	[146]
				400-450 <sup>‡</sup>	7.4-8.3	[146]
				320	5.9	[60]
				320	5.9	[25]

<sup>†</sup>Measured in the positron trap, <sup>‡</sup>measured in a dense Xe-H<sub>2</sub> gas mixture, <sup>a</sup>Ref. [140], <sup>b</sup>Ref. [17], <sup>c</sup>Ref. [91], <sup>d</sup>Ref. [92], <sup>e</sup>Ref. [94].

temperature population of positrons would lead to a lower  $Z_{\text{eff}}$ , according to theoretical calculations [92, 94], and the trend of higher values of  $Z_{\text{eff}}$  measured in our positron trap is consistent with this.

In order to overcome the problem of slow thermalization of positrons in the larger noble gases, Wright *et al.* [146] developed a technique for measuring positron annihilation in dense-gas mixtures. In their experiments, a small admixture of H<sub>2</sub> is used to increase the thermalization rate of the positrons. The Xe-H<sub>2</sub> experiments gave  $Z_{\text{eff}}$  of 400–450 [146], which agrees with the value obtained in the positron trap [101]. For krypton and argon, the gas-mixture experiments produced similar results to the pure gas experiments in dense gases. Our results for krypton and argon are not in very good agreement with the dense-gas results. We have no definitive explanation of this discrepancy. In principle, systematic errors in our measurements could account for the difference, and more careful measurements for krypton and argon in the positron trap are planned. It is noted that the values measured in the positron trap for argon, krypton, and



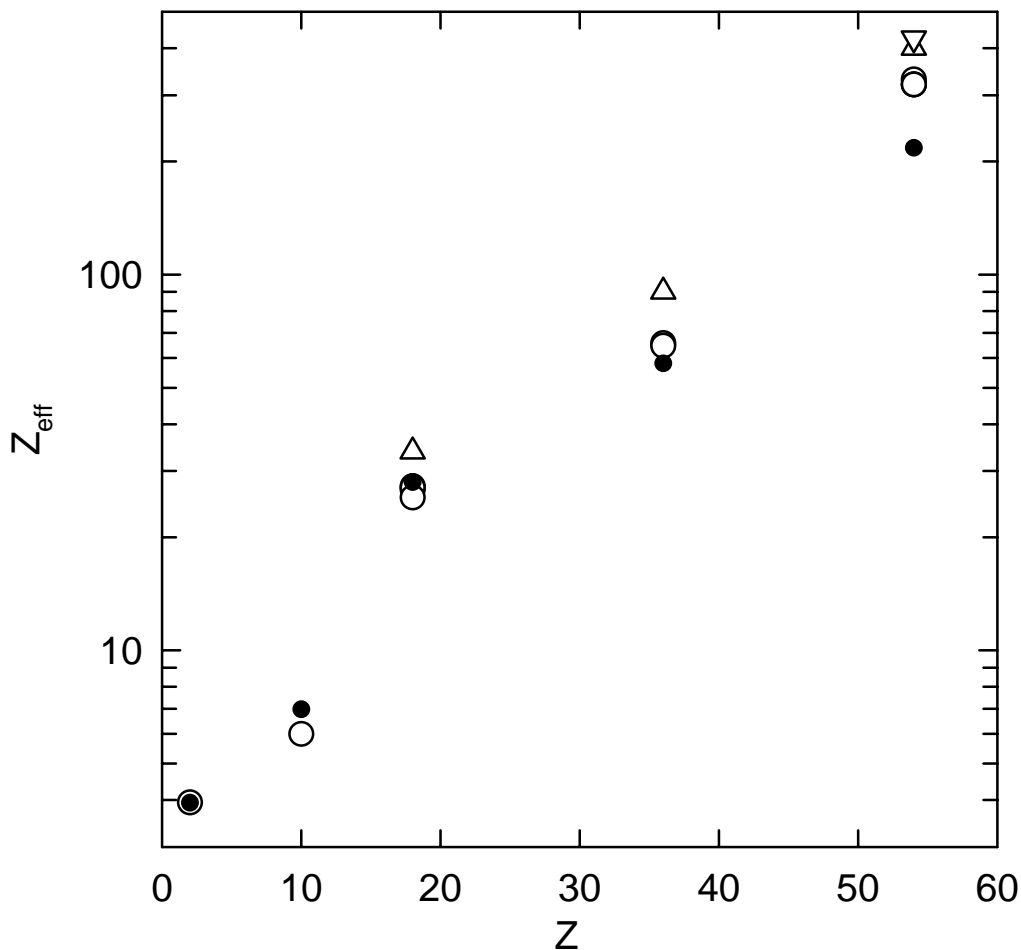


Figure 4.2: Theoretical and experimental values of  $Z_{\text{eff}}$  for noble gases: (●) theoretical values, ( $\Delta$ ) experimental values measured in the positron trap, ( $\circ$ ) values measured in experiments in dense gases, and ( $\nabla$ ) dense gas experiment with  $\text{H}_2$  test-gas mixture. The values measured in the positron trap are generally higher than those in dense gas experiments.

xenon are higher than the theoretical ones (Table 4.1).

#### 4.2.2 Inorganic molecules

Values of  $Z_{\text{eff}}$  for simple inorganic molecules are listed in Table 4.2. Polar and nonpolar molecules are tabulated separately. The molecular dipole moments [104] are also listed in Table 4.2, and it can be seen that polyatomic polar molecules have relatively large values of  $Z_{\text{eff}}$ , with  $Z_{\text{eff}}/Z > 10$ . The exception

Table 4.2: Measured values of  $Z_{\text{eff}}$  for inorganic molecules. The values of dipole moment, DM, have units of debye, D.

Molecule	Formula	$Z$	$Z_{\text{eff}}$	$Z_{\text{eff}}/Z$	DM(D) <sup>a</sup>	Ref.
<b>Diatomic molecules (nonpolar)</b>						
Hydrogen	H <sub>2</sub>	2	14.6	7.3		[76]
			16.02	8.0		[146]
			14.7	7.4		[60]
Deuterium	D <sub>2</sub>	2	14.7	7.4		[60]
Nitrogen	N <sub>2</sub>	14	30.5	2.2		[60]
			28.9	2.1		[137]
Oxygen	O <sub>2</sub>	16	36.7 <sup>†</sup>	2.3		[66]
			40.5	2.5		[60]
<b>Diatomic molecules (polar)</b>						
Carbon monoxide	CO	14	38.5	2.8	0.112	[60]
Nitric oxide	NO	15	34	2.3	0.153	[60]
<b>Polyatomic molecules (nonpolar)</b>						
Carbon dioxide	CO <sub>2</sub>	22	54.7	2.5		[146]
			53	2.4		[60]
Sulfur hexafluoride	SF <sub>6</sub>	70	86.2 <sup>†</sup>	1.2		[66]
			97	1.4		[60]
<b>Polyatomic molecules (polar)</b>						
Ammonia	NH <sub>3</sub>	10	1300	130	1.47	[60]
			1600 <sup>†</sup>	160	1.47	[69]
Water	H <sub>2</sub> O	10	319 <sup>†</sup>	32	1.85	[66]
Nitrous oxide	N <sub>2</sub> O	22	78	3.5	0.167	[60]
Nitrogen dioxide	NO <sub>2</sub>	23	1090	47	0.316	[60]
Methyl chloride	CH <sub>3</sub> Cl	26	15000	580	1.87	[60]
Dichlorodifluoromethane	CCl <sub>2</sub> F <sub>2</sub>	58	750	13	0.51	[55]

<sup>†</sup>Measured in the positron trap, <sup>a</sup>Ref. [104].

is nitrous oxide, which has a small dipole moment. The diatomic molecules, carbon monoxide and nitric oxide, also have relatively small annihilation rates.

At separations much larger than molecular dimensions, the long-range interaction between a positron and a polar molecule is a dipole interaction with force proportional to  $p/r^3$ , where  $p$  is the permanent molecular dipole moment and  $r$  is the separation between the molecule and the positron. This interaction is stronger than that between a positron and a nonpolar molecule, for which

the positron polarizes the molecular electron cloud, inducing a dipole moment and producing a force proportional to  $\alpha/r^4$ , where  $\alpha$  is the polarizability of the molecule.

In the partial wave expansion, the most significant component is the  $s$  wave, where the positron wave function has a finite amplitude at the location of the molecule, since the annihilation rate is the measure of the overlap of positron and electron wave functions. The permanent dipole moment should not affect the scattering cross section for the  $s$  wave considerably. However, the positron affinity may be affected by the dipole moment. It is not clear how dipole moments specifically enhance the annihilation rates.

For nonpolar substances, a correlation between  $Z_{\text{eff}}$  and polarizability for some chemical species has been reported earlier [102,108].

Because of the structural complexity of polyatomic molecules, theoretical values of  $Z_{\text{eff}}$  are available only for a limited number of substances [6]. Positron annihilation on  $\text{H}_2$  has been extensively studied because of the relative simplicity of its structure. A calculation using the Kohn variational method yields a  $Z_{\text{eff}}$  of 10.7 [7], which is smaller than the experimental values (see Table 4.2). The calculation for  $\text{N}_2$  using polarization potentials with a phenomenological cutoff gives  $Z_{\text{eff}} = 18$  [31]. This value is smaller than the experimental values. *Ab initio* calculations using the Kohn variational method for  $\text{N}_2$  are currently being investigated [8]. The calculation for  $\text{NH}_3$  with the fixed-nuclei approximation and without the polarization of molecular orbitals due to the incoming positrons gives  $Z_{\text{eff}} = 241$ , while the calculation including the polarization increases the value to about 500 [71], which is still much smaller than the experimental value of 1300 [60] or 1600 [69].

### 4.2.3 Alkanes and substituted alkanes

Values of  $Z_{\text{eff}}$  for alkanes and substituted alkanes are listed in Table 4.3, and values of  $Z_{\text{eff}}/Z$  are plotted against  $Z$  in Fig. 4.1. For alkanes,  $Z_{\text{eff}}/Z$  increases from  $\sim 10$  for methane to  $\sim 2 \times 10^4$  for hexadecane. These anomalously high values of  $Z_{\text{eff}}/Z$  might be explained by long-lived resonances [134]. It is noted that  $Z_{\text{eff}}/Z$  does not increase between dodecane and hexadecane.

Theoretical calculations of  $Z_{\text{eff}}$  for  $\text{CH}_4$  are available [71]. Using the fixed-nuclei approximation, the values are 46.8 without including the polarization of the molecular orbitals, and 99.5 with the polarization. These values are smaller than the experimental values (see Table 4.3).

Substitution of hydrogen atoms in the alkanes by other atoms dramatically changes  $Z_{\text{eff}}$ . Substitution by fluorine decreases  $Z_{\text{eff}}$ , while substitution by io-

Table 4.3: Measured values of  $Z_{\text{eff}}$  for alkanes and substituted alkanes.

Molecule	Formula	$Z$	$Z_{\text{eff}}$	$Z_{\text{eff}}/Z$	Ref.
<b>Alkanes</b>					
Methane	CH <sub>4</sub>	10	142	14	[146]
			140	14	[60]
			162	16	[110]
Ethane	C <sub>2</sub> H <sub>6</sub>	18	660	37	[60]
			698	39	[110]
Propane	C <sub>3</sub> H <sub>8</sub>	26	3 500	130	[60]
			3 850	150	[110]
Butane	C <sub>4</sub> H <sub>10</sub>	34	11 300 <sup>†</sup>	330	[81]
			15 000	440	[60]
			16 300	480	[110]
<i>iso</i> Butane	C <sub>4</sub> H <sub>10</sub>	34	14 400	420	[110]
Pentane	C <sub>5</sub> H <sub>12</sub>	42	37 800 <sup>†</sup>	900	[81]
Hexane	C <sub>6</sub> H <sub>14</sub>	50	120 000 <sup>†</sup>	2 400	[67]
			98 200 <sup>†</sup>	2 000	[102]
Heptane	C <sub>7</sub> H <sub>16</sub>	58	242 000 <sup>†</sup>	4 200	[81]
Nonane	C <sub>9</sub> H <sub>20</sub>	74	643 000 <sup>†</sup>	8 700	[81]
Decane	C <sub>10</sub> H <sub>22</sub>	82	507 000 <sup>†</sup>	6 200	[66]
Dodecane	C <sub>12</sub> H <sub>26</sub>	98	1 780 000 <sup>†</sup>	18 000	[81]
Hexadecane	C <sub>16</sub> H <sub>34</sub>	130	2 230 000 <sup>†</sup>	17 000	[81]
<b>Deuterated alkanes</b>					
d-Heptane	C <sub>7</sub> D <sub>16</sub>	58	197 000 <sup>†</sup>	3 400	[81]
<b>Perfluorinated alkanes</b>					
Carbon tetrafluoride	CF <sub>4</sub>	42	54.4 <sup>†</sup>	1.3	[102]
Perfluoropropane	C <sub>3</sub> F <sub>8</sub>	90	152 <sup>†</sup>	1.7	[102]
Perfluorohexane	C <sub>6</sub> F <sub>14</sub>	162	535 <sup>†</sup>	3.3	[102]
Perfluorooctane	C <sub>8</sub> F <sub>18</sub>	210	1 064 <sup>†</sup>	5.1	[102]
<b>Perchlorinated alkanes</b>					
Carbon tetrachloride	CCl <sub>4</sub>	74	9 530 <sup>†</sup>	130	[102]
			22 500	300	[110]
Hexachloroethane	C <sub>2</sub> Cl <sub>6</sub>	114	68 600 <sup>†</sup>	600	[102]
<b>Perbrominated alkanes</b>					
Carbon tetrabromide	CBr <sub>4</sub>	146	39 800 <sup>†</sup>	270	[102]
<b>Periodated alkanes</b>					
Carbon tetraiodide	CI <sub>4</sub>	218	7 990 <sup>†</sup>	37	[66]

<sup>†</sup>Measured in the positron trap.

Table 4.4: Measured values of  $Z_{\text{eff}}$  for isomers of pentane. Some of data may be inconsistent with previous measurements due to the ion-gauge readout. All values are measured in the positron trap.

Molecule	Formula	$Z$	$Z_{\text{eff}}$	$Z_{\text{eff}}/Z$	Ref.
Pentane	$\text{CH}_3(\text{CH}_2)_3\text{CH}_3$	42	40 200	957	[69]
2-Methylbutane	$\text{CH}_3\text{C}(\text{CH}_3)\text{H}_2\text{C}_2\text{H}_5$	42	50 500*	1 200	[69]
2,2-Dimethylpropane	$\text{C}(\text{CH}_3)_4$	42	21 400*	510	[69]

\*Ion-gauge sensitivities are estimated.

Table 4.5: Measured values of  $Z_{\text{eff}}$  for alkenes. All values are measured in the positron trap.

Molecule	Formula	$Z$	$Z_{\text{eff}}$	$Z_{\text{eff}}/Z$	Ref.
Ethylene	$\text{C}_2\text{H}_4$	16	1 200	75	[67]
Acetylene	$\text{C}_2\text{H}_2$	14	3 160	226	[69]
1-Hexene	$\text{C}_6\text{H}_{12}$	48	185 000	3 900	[102]
<i>trans</i> 3-Hexene	$\text{C}_6\text{H}_{12}$	48	196 000	4 100	[102]
1,3-Hexadiene	$\text{C}_6\text{H}_{10}$	46	389 000	8 500	[102]
<i>cis</i> 2, <i>trans</i> 4-Hexadiene	$\text{C}_6\text{H}_{10}$	46	413 000	9 000	[102]
<i>trans</i> 2, <i>trans</i> 4-Hexadiene	$\text{C}_6\text{H}_{10}$	46	388 000	8 400	[102]
1,3,5-Hexatriene	$\text{C}_6\text{H}_8$	44	414 000	9 400	[102]

dine, chlorine, or bromine increases  $Z_{\text{eff}}$  by differing amounts.

Isomeric effects of alkanes were studied for three different isomeric configuration of pentane, and the measurements are listed in Table 4.4. We do not observe any systematic differences between these three isomers even though the values of  $Z_{\text{eff}}$  differ by a factor of 2.

#### 4.2.4 Alkenes

The molecular structures and values of  $Z_{\text{eff}}$  are illustrated in Fig. 4.3. Table 4.5 gives values of  $Z_{\text{eff}}$  for various alkene molecules. Introducing one double bond into the alkanes ethane and hexane to form ethylene and hexene, respectively, has the effect of approximately doubling  $Z_{\text{eff}}$ . In the case of hexene, there is no strong dependence of  $Z_{\text{eff}}$  on the location of the double bond. Introducing a second double bond into hexene to form hexadiene further increases  $Z_{\text{eff}}$  by approximately another factor of two. Once again, there is no significant isomeric dependence. Introduction of a third double bond does not change  $Z_{\text{eff}}$


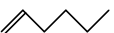
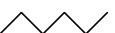
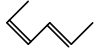
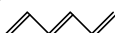
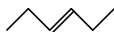
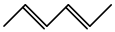
HEXANE	HEXENES	HEXADIENES	HEXATRIENE
		1,3-Hexadiene 	
	1-Hexene 	389,000	
	185,000		
		<i>cis</i> 2, <i>trans</i> 4-Hexadiene 	1,3,5-Hexatriene 
120,000	<i>trans</i> 3-Hexene 	413,000	414,000
	196,000	<i>trans</i> 2, <i>trans</i> 4-Hexadiene 	
		388,000	

Figure 4.3: Values of  $Z_{\text{eff}}$  and structures of alkenes with six carbons.Table 4.6: Measured values of  $Z_{\text{eff}}$  for alcohols, carboxylic acids, and ketones. All values are measured in the positron trap.

Molecule	Formula	$Z$	$Z_{\text{eff}}$	$Z_{\text{eff}}/Z$	DM(D) <sup>a</sup>	Ref.
<b>Alcohols</b>						
Methanol	CH <sub>3</sub> OH	18	1510	84	1.70	[66]
1-Propanol	C <sub>2</sub> H <sub>5</sub> CH <sub>2</sub> OH	34	19900	590	1.68	[66]
<b>Carboxylic acids</b>						
Acetic acid	CH <sub>3</sub> COOH	32	5880	180	1.74	[66]
Propionic acid	C <sub>2</sub> H <sub>5</sub> COOH	40	27200	680	1.75	[66]
<b>Ketones</b>						
Acetone	CH <sub>3</sub> COCH <sub>3</sub>	32	98400	3100	2.88	[66]

<sup>a</sup>Ref. [104].

appreciably as compared to hexadiene.

#### 4.2.5 Oxygen-containing hydrocarbons

Values of  $Z_{\text{eff}}$  for alcohols, carboxylic acids, and ketones are listed in Table 4.6. These measurements focus on chemical trends of  $Z_{\text{eff}}$  in molecules containing

oxygen. Alcohols, carboxylic acids, and ketones each have values of  $Z_{\text{eff}}/Z$  approximately an order of magnitude higher than do alkanes with the same number of carbon atoms. For the three-carbon family of these molecules, it is found that acetone, which has a C=O group, has the highest  $Z_{\text{eff}}/Z$ , and that propionic acid, which has both O–H and C=O groups, has slightly higher  $Z_{\text{eff}}/Z$  than 1-propanol, which has an O–H group. The large dipole moment of acetone (Table 4.6) may be responsible for its high  $Z_{\text{eff}}/Z$  value.

#### 4.2.6 Aromatics and saturated rings

Values of  $Z_{\text{eff}}$  for ring hydrocarbons, substituted rings, aromatics, and other organic molecules are given in Table 4.7. Forming hexane into the cyclic ring compound, cyclohexane, dramatically reduces the value of  $Z_{\text{eff}}$ . A similar decrease is noted when the symmetric ring, benzene, is compared with hexane. The similar values of  $Z_{\text{eff}}$  for benzene and for cyclohexane, compared with the large value for hexane, suggest that symmetry plays a more important role in determining the value of  $Z_{\text{eff}}$  than does the presence of double bonds or delocalized electrons [67]. It is noted, however, that both benzene and cyclohexane lack methyl groups, which might be the reason that  $Z_{\text{eff}}$  is lower in these molecules than in hexane. As in the case of the alkanes, perfluorinating aromatic hydrocarbons to form such compounds as octafluoronaphthalene, hexafluorobenzene, and octafluorotoluene results in a dramatic decrease in  $Z_{\text{eff}}$ .

A number of substituted benzene compounds were studied, and Fig. 4.4 is a summary of these results. Substituting one hydrogen atom in the benzene molecule with any other functional group increases  $Z_{\text{eff}}$ . This is true even for –F, which usually has the property of reducing  $Z_{\text{eff}}$  when substituted for hydrogen atoms. This phenomenon points to the importance of molecular symmetry in reducing  $Z_{\text{eff}}$  in ring compounds. The magnitude of the increase shows a wide variation, depending on the functional group being substituted, varying from a factor of two for –F to a factor of 30 for –NO<sub>2</sub>. In the latter case, the large dipole moment introduced by the –NO<sub>2</sub> substitution may also contribute to the increase in  $Z_{\text{eff}}$  (Table 4.7). Substituting one, four, or five additional fluorines in C<sub>6</sub>H<sub>5</sub>F decreases  $Z_{\text{eff}}$  monotonically, which is consistent with the observation that perfluorocarbons have much lower values of  $Z_{\text{eff}}$  than the analogous hydrocarbons.

In order to test the effect of isomeric symmetry,  $Z_{\text{eff}}$  of xylene isomers (i.e., benzene rings with two substituted –CH<sub>3</sub> groups in various relative positions) were measured. The  $Z_{\text{eff}}$  for *para*-, *ortho*-, and *meta*-xylenes are all identical to within the accuracy of the measurements, and they are not significantly different

Table 4.7: Measured values of  $Z_{\text{eff}}$  for ring molecules and aromatics. All values are measured in the positron trap.

Molecule	Formula	$Z$	$Z_{\text{eff}}$	$Z_{\text{eff}}/Z$	DM(D) <sup>a</sup>	Ref.
<b>Ring hydrocarbons</b>						
Benzene	C <sub>6</sub> H <sub>6</sub>	42	15 000	360	0.00	[67]
			18 000	430	0.00	[102]
Cyclohexane	C <sub>6</sub> H <sub>12</sub>	48	20 000	420	0.00	[67]
Cyclodecane	C <sub>10</sub> H <sub>20</sub>	80	369 000	4 600	0.00	[66]
Naphthalene	C <sub>10</sub> H <sub>8</sub>	68	494 000	7 300	0.00	[102]
Decahydronaphthalene	C <sub>10</sub> H <sub>18</sub>	78	389 000	5 000	0.00	[81]
Anthracene	C <sub>14</sub> H <sub>10</sub>	94	4 330 000	46 000	0.00	[102]
<b>Substituted rings</b>						
Octafluoronaphthalene	C <sub>10</sub> F <sub>8</sub>	132	3 080	23	0.00	[102]
<b>Substituted benzenes</b>						
Toluene	C <sub>6</sub> H <sub>5</sub> (CH <sub>3</sub> )	50	190 000	3 800	0.36	[67]
			155 000	3 100	0.36	[102]
			189 000	3 800	0.36	[81]
<i>para</i> -Xylene	C <sub>6</sub> H <sub>4</sub> (CH <sub>3</sub> ) <sub>2</sub>	58	200 000	3 400	0.00	[67]
<i>ortho</i> -Xylene	C <sub>6</sub> H <sub>4</sub> (CH <sub>3</sub> ) <sub>2</sub>	58	180 000	3 100	0.62	[67]
<i>meta</i> -Xylene	C <sub>6</sub> H <sub>4</sub> (CH <sub>3</sub> ) <sub>2</sub>	58	210 000	3 600	N/A	[67]
Aniline	C <sub>6</sub> H <sub>5</sub> NH <sub>2</sub>	50	400 000	8 000	1.53	[67]
Nitrobenzene	C <sub>6</sub> H <sub>5</sub> NO <sub>2</sub>	64	430 000	6 700	4.22	[67]
Chlorobenzene	C <sub>6</sub> H <sub>5</sub> Cl	58	72 300	1 200	1.69	[66]
Bromobenzene	C <sub>6</sub> H <sub>5</sub> Br	76	172 000	2 300	1.70	[66]
Fluorobenzene	C <sub>6</sub> H <sub>5</sub> F	50	34 000	680	1.60	[67]
1,4-Difluorobenzene	C <sub>6</sub> H <sub>4</sub> F <sub>2</sub>	58	10 700	180	0.00	[66]
Pentafluorobenzene	C <sub>6</sub> HF <sub>5</sub>	82	1 800	22	N/A	[67]
Hexafluorobenzene	C <sub>6</sub> F <sub>6</sub>	90	1 200	13	0.00	[102]
Octafluorotoluene	C <sub>6</sub> F <sub>5</sub> (CF <sub>3</sub> )	114	1 240	11	N/A	[102]
<b>Other</b>						
Pyridine	C <sub>5</sub> H <sub>5</sub> N	42	85 400*	2 030	2.19	[69]

<sup>a</sup>Ref. [104],\*Ion-gauge sensitivity is estimated.

from toluene. Thus, it appears that once the symmetry of the benzene ring is broken by the addition of a methyl group, further substitutions do not have a strong effect. *Para*-, *ortho*-, and *meta*-xylenes have different but small dipole moments. If the isomeric symmetry is not significant in determining  $Z_{\text{eff}}$ , as the



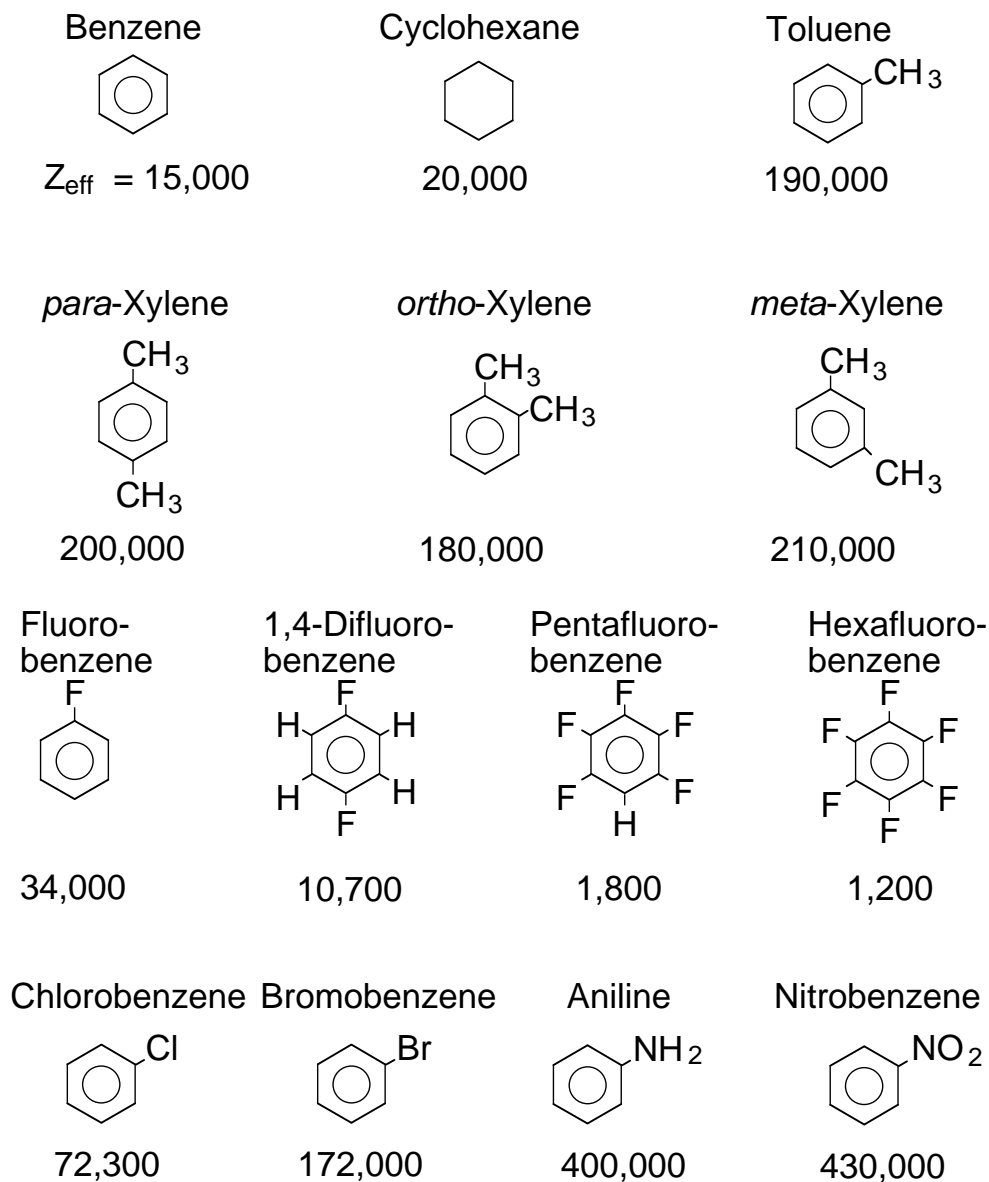


Figure 4.4: Values of  $Z_{\text{eff}}$  and structures of cyclohexane and substituted benzenes. Substitution of one hydrogen atom by any functional group increases  $Z_{\text{eff}}$ , indicating the importance of molecular symmetry in reducing  $Z_{\text{eff}}$  in ring compounds.

xylene data suggest, studies of isomeric symmetry using molecules with larger dipole moments, such as dinitrobenzenes, may give us information about the contribution of the molecular dipole moment to  $Z_{\text{eff}}$  for these molecules, without significantly changing other properties of the molecules.

Table 4.8: Measured values of  $Z_{\text{eff}}$  for other large organic molecules. All values are measured in the positron trap.

Molecule	Formula	$Z$	$Z_{\text{eff}}$	$Z_{\text{eff}}/Z$	Ref.
Tetraethylsilane	$\text{Si}(\text{C}_2\text{H}_5)_4$	82	524 000	6 400	[66]
Glycerol	$\text{C}_3\text{H}_8\text{O}_3$	50	1 470 000	29 000	[81]
Sebacic acid dimethyl ester	$\text{C}_{12}\text{H}_{22}\text{O}_4$	126	7 560 000	60 000	[81]

An important factor in the conventional chemistry of substituted benzenes is whether the substituted group donates or withdraws electrons from the ring. Functional groups such as  $-\text{CH}_3$ , which donate electrons to the ring, tend to activate the ring for electrophilic substitution of a second group, and they induce that substitution to occur at the *ortho* and *para* positions. On the other hand, electron-withdrawing groups like  $-\text{NO}_2$  tend to deactivate the ring, and to direct substitution to the *meta* position. Our data show no evidence that this effect influences the value of  $Z_{\text{eff}}$ . For example, the *meta*-director  $-\text{NO}_2$  produces a value of  $Z_{\text{eff}}$  similar to that resulting from the *ortho*-, *para*-director  $-\text{NH}_2$ , while  $-\text{Cl}$ ,  $-\text{Br}$ ,  $-\text{F}$ ,  $-\text{CH}_3$ , and  $-\text{NH}_2$ , which are all *ortho*-, *para*-directors, have very different values of  $Z_{\text{eff}}$ .

Pyridine has similar electronic structure to benzene. Its  $Z_{\text{eff}}$  (see Table 4.7) is several times larger than that of benzene, pointing to the importance of molecular symmetry in determining  $Z_{\text{eff}}$ . This molecule also has finite dipole moment.

As can be seen in Table 4.8, the values of  $Z_{\text{eff}}/Z$  for some large molecules, such as anthracene, glycerol, and sebacic acid dimethyl ester, are higher than those of large alkanes, in which  $Z_{\text{eff}}$  values are saturated, namely those of dodecane and hexadecane. In the framework of the model described by Eq. (4.6), this might imply that values of  $\sigma_{\text{res}}$  for these molecules are larger than those for large alkanes.

#### 4.2.7 Deuterated hydrocarbons

Comparison of a deuterated molecule to a analogous protonated molecule provides unique information about the annihilation process. Deuteration of molecules does not change their electronic structure,<sup>2</sup> but significantly changes the vibrational modes of the molecules. Annihilation rates of deuterated and protonated hydrocarbons are measured and presented in this subsection. The values of  $Z_{\text{eff}}$

<sup>2</sup>Deuteration of molecules actually changes the electronic structure of the molecules slightly. Deuterons are heavier than protons, and this causes the carbon-hydrogen bond length to change. However, this change is much smaller than the change in the vibrational modes.

Table 4.9: Measured values of  $Z_{\text{eff}}$  for protonated and deuterated alkanes. All values are measured in the positron trap and presently unpublished. The last column is the ratio of  $Z_{\text{eff}}$  for protonated alkanes to those for deuterated alkanes. Some of data may be inconsistent with previous measurements due to the ion-gauge readout.

Molecule	$n$	Protonated ( $C_nH_{2n+2}$ )	Deuterated ( $C_nD_{2n+2}$ )	Ratio
		$Z_{\text{eff}}$		
Methane	1	222	214	0.96
Hexane	6	105 000	116 000	1.10
Heptane	7	355 000	341 000	0.96
Octane	8	585 000	408 000	0.70
Nonane	9	666 000	641 000	0.96
Decane	10	728 000	1 930 000	2.65

for deuterated molecules are obtained using the ion-gauge sensitivity calibration of analogous protonated molecules, which should be a reasonable approximation.

#### 4.2.7.1 Deuterated alkanes

Annihilation rates of deuterated and protonated alkanes are measured systematically and listed in Table 4.9. Some inconsistency with other tabulated values may be noted as discussed earlier due to the ion-gauge readout error. However, the values listed in Table 4.9 were measured sequentially using the same ion-gauge readout, and the relative error between deuterated and protonated alkanes is small ( $< 10\%$ ).

The ratio of  $Z_{\text{eff}}$  for deuterated alkanes to those for protonated alkanes is listed in the last column of the table and plotted in Fig. 4.5 for comparison. Contrary to the data of deuterated benzenes in the previous publication [66], which is also described in Sec. 4.2.7.2, annihilation rates for the deuterated and protonated alkanes, except for decane, are identical within the experimental error, as can be seen in the figure. These data do not support the picture of the positron forming a long-lived resonance state with the molecule, transferring its kinetic energy to the vibrational modes of the molecule. The treatment of Christophorou *et al.* [22,23] for electron-molecule collisions assumes the electron transferring its kinetic energy to all vibrational modes of the molecule statistically. The positron may only be interacting with lower frequency modes involving C-C bonds or chain bending but not the C-H (or C-D) bonds, which may explain our observation.

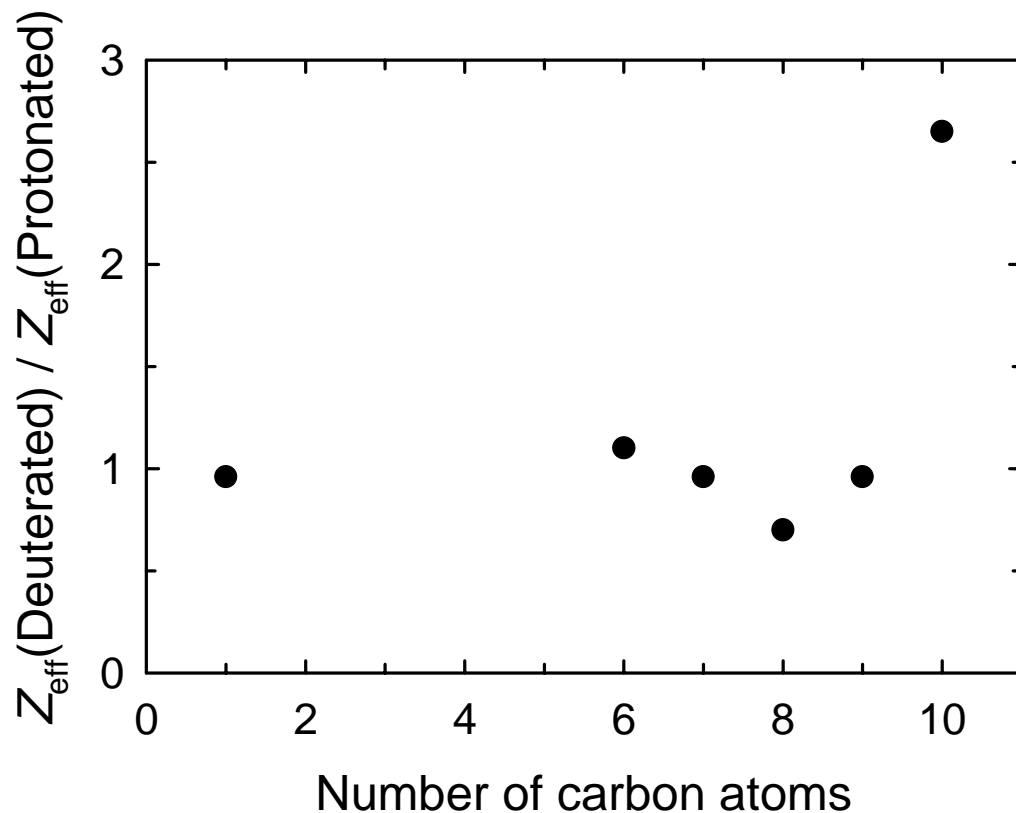


Figure 4.5: Ratio of  $Z_{\text{eff}}$  for deuterated alkanes to those for protonated alkanes plotted against the number of carbon atoms,  $n$ .

The reason for the large difference in the annihilation rates between deuterated and protonated decanes (Table 4.9) is not known at this moment. One possibility is that the deuterated decane sample may have been contaminated.

#### 4.2.7.2 Deuterated benzenes

The annihilation rates of protonated, partially deuterated, and fully deuterated benzenes are listed in Table 4.10, and the structures of these benzenes are also illustrated in Fig. 4.6. As can be seen, deuterated benzenes have higher  $Z_{\text{eff}}$  than the fully protonated benzene. Benzene- $d$  ( $\text{C}_6\text{H}_5\text{D}$ ) and benzene-1,3,5- $d_3$  ( $\text{C}_6\text{H}_3\text{D}_3$ ) have higher  $Z_{\text{eff}}$  than benzene ( $\text{C}_6\text{H}_6$ ) and benzene- $d_6$  ( $\text{C}_6\text{D}_6$ ). This may point to the importance of molecular symmetry discussed in Sec. 4.2.6.

Table 4.10: Measured values of  $Z_{\text{eff}}$  for deuterated benzenes. All values are measured in the positron trap.

Molecule	Formula	$Z_{\text{eff}}$	Ref.
Benzene	$\text{C}_6\text{H}_6$	15 000	[67]
		18 000	[102]
Benzene- <i>d</i>	$\text{C}_6\text{H}_5\text{D}$	36 900	[66]
Benzene-1,3,5- <i>d</i> <sub>3</sub>	$\text{C}_6\text{H}_3\text{D}_3$	43 800	[66]
Benzene- <i>d</i> <sub>6</sub>	$\text{C}_6\text{D}_6$	30 500	[66]

#### 4.2.8 Partially fluorinated hydrocarbons

As can be seen in Sec. 4.2.3, alkanes have very large annihilation rates. In contrast the analogous perfluorinated alkanes have a few orders of magnitude smaller annihilation rates. The transition from the large annihilation rates to the small rates may provide us with insights into determining the physical process responsible for the anomalously large annihilation rates observed for large hydrocarbons. Hydrogen atoms in hydrocarbon molecules can be selectively replaced with fluorine atoms to form partially fluorinated hydrocarbons, and studies of these molecules are discussed in this subsection.

The experimentally measured annihilation rates of partially fluorinated hydrocarbons are listed in Table 4.11. Some inconsistency with previously tabulated values may also be noted for this table due to the ion-gauge readout error as discussed earlier.

An interesting trend is that the molecules with one fluorine atom have the highest annihilation rates among the molecules with the same number of carbon atoms. Further fluorination reduces the annihilation rates gradually to the lowest value for perfluorinated molecules. It is noted that the molecules with one fluorine atom are highly dipolar. However, the effect of permanent dipole moments to the annihilation rates is not understood as discussed earlier (Sec. 4.2.2).

Gribakin attempted to explain this effect of increased  $Z_{\text{eff}}$  for one substituted fluorine atom [52] in terms of large scattering cross section as discussed in Sec. 4.1.2. He calculated the scattering lengths of partially fluorinated methanes, employing the zero-range potential approximation [32], and the trend of annihilation rates at room temperature are in reasonable agreement with this model. This theory also predicts the dependence of annihilation rate on positron momentum  $p_{e+}$  to be

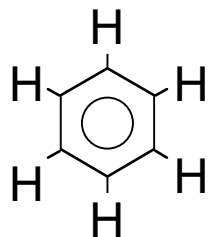
$$Z_{\text{eff}}(p_{e+}) \propto \frac{1}{\kappa^2 + p_{e+}^2}, \quad (4.7)$$

Table 4.11: Measured values of  $Z_{\text{eff}}$  for partially fluorinated hydrocarbons. All measurements are performed in the positron trap and unpublished. Some of data may be inconsistent with previous measurements due to the ion-gauge readout.

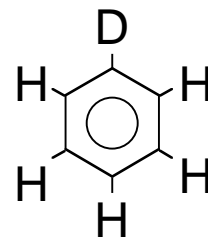
Molecule	Formula	$Z$	$Z_{\text{eff}}$
<b>1-carbon molecules</b>			
Methane	$\text{CH}_4$	10	308
Methyl fluoride	$\text{CH}_3\text{F}$	18	1390 <sup>a</sup>
Difluoromethane	$\text{CH}_2\text{F}_2$	26	799 <sup>a</sup>
Trifluoromethane	$\text{CHF}_3$	34	247 <sup>a</sup>
Carbon tetrafluoride	$\text{CF}_4$	42	73.5
<b>2-carbon molecules</b>			
Ethane	$\text{C}_2\text{H}_6$	18	1780
Fluoroethane	$\text{C}_2\text{H}_5\text{F}$	26	3030 <sup>a</sup>
1,1,1-Trifluoroethane	$\text{CF}_3\text{CH}_3$	42	1600 <sup>a</sup>
1,1,2-Trifluoroethane	$\text{CHF}_2\text{CH}_2\text{F}$	42	1510 <sup>a</sup>
1,1,1,2-Tetrafluoroethane	$\text{CF}_3\text{CH}_2\text{F}$	50	1110 <sup>a</sup>
1,1,2,2-Tetrafluoroethane	$\text{CHF}_2\text{CHF}_2$	50	467 <sup>a</sup>
Hexafluoroethane	$\text{C}_2\text{F}_6$	66	149 <sup>a</sup>
<b>3-carbon molecules</b>			
Propane	$\text{C}_3\text{H}_8$	26	2350
2,2-Difluoropropane	$\text{CH}_3\text{CF}_2\text{CH}_3$	42	8130 <sup>a</sup>
1,1,1-Trifluoropropane	$\text{CF}_3\text{C}_2\text{H}_5$	50	3350 <sup>a</sup>
Perfluoropropane	$\text{C}_3\text{F}_8$	90	317
<b>6-carbon molecules</b>			
Hexane	$\text{C}_6\text{H}_{14}$	50	151000
1-Fluorohexane	$\text{CH}_2\text{FC}_5\text{H}_{11}$	58	269000 <sup>a</sup>
Perfluorohexane	$\text{C}_6\text{F}_{14}$	162	630
<b>Benzene-based molecules</b>			
Benzene	$\text{C}_6\text{H}_6$	42	20300
Fluorobenzene	$\text{C}_6\text{H}_5\text{F}$	50	45100
1,2-Difluorobenzene	$\text{C}_6\text{H}_4\text{F}_2$	58	32800 <sup>a</sup>
1,3-Difluorobenzene	$\text{C}_6\text{H}_4\text{F}_2$	58	13100 <sup>a</sup>
1,4-Difluorobenzene	$\text{C}_6\text{H}_4\text{F}_2$	58	13500
1,2,4-Trifluorobenzene	$\text{C}_6\text{H}_3\text{F}_3$	66	10100 <sup>a</sup>
1,2,4,5-Tetrafluorobenzene	$\text{C}_6\text{H}_2\text{F}_4$	74	2760 <sup>a</sup>
Pentafluorobenzene	$\text{C}_6\text{HF}_5$	82	1930
Hexafluorobenzene	$\text{C}_6\text{F}_6$	90	499

<sup>a</sup>Ion-gauge sensitivity is approximated.

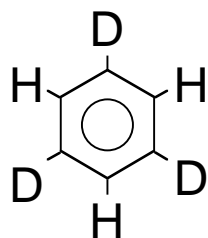
## Benzene



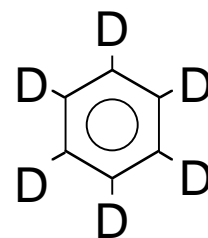
$$Z_{\text{eff}} = 15,000$$

Benzene-*d*

$$36,900$$

Benzene-1,3,5*d*<sub>3</sub>

$$43,800$$

Benzene-*d*<sub>6</sub>

$$30,500$$

Figure 4.6: Values of  $Z_{\text{eff}}$  and structures of deuterated benzenes studied. Deuterated benzenes have higher values of  $Z_{\text{eff}}$  as compared to the ordinary benzene.

where  $\kappa$  is the inverse of scattering length. If the trend of annihilation rates for partially fluorinated methanes are explained by the model described here, this equation indicates a stronger annihilation rate dependence on positron temperature for  $\text{CH}_3\text{F}$  than for  $\text{CH}_4$ . However, a preliminary measurement by Kurz *et al.* [73] suggests that the annihilation rates depend similarly for  $\text{CH}_3\text{F}$  and  $\text{CH}_4$ , which disagree with the prediction. Further measurements of the dependence of

$Z_{\text{eff}}$  on positron temperature are warranted. Even if Gribakin's theory were to explain the trend of annihilation rates for partially fluorinated hydrocarbons, it is not expected to explain the anomalously large annihilation rates. Even if the scattering length is very large ( $\kappa \sim 0$ ), the annihilation rate is limited by the thermal momentum of the positron, as can be seen from Eq. (4.7).

### 4.3 Discussion

In this section, studies closely related to annihilation rate measurements are discussed. The empirical scaling of annihilation rates discovered by Murphy and Surko [102] is presented in Sec. 4.3.1. Tinkle *et al.* developed a technique for heating electron (or positron) plasmas [138]. This method is applied to measure the dependence of annihilation rate on positron temperature, which is presented in Sec. 4.3.2. The latest theoretical progress in this area is summarized in Sec. 4.3.3, including a recent attempt to explain the anomalously large annihilation rates for large organic molecules [77]. Other issues are discussed in Sec. 4.3.4, and a summary is given in Sec. 4.3.5.

#### 4.3.1 Empirical scaling of annihilation rates

Murphy and Surko discovered previously a linear relationship between  $\log(Z_{\text{eff}})$  and  $(E_i - E_{\text{Ps}})^{-1}$  for molecules without double bonds [102], where  $E_i$  is the ionization potential of the molecule [15, 40, 82, 119], and  $E_{\text{Ps}} = 6.8$  eV is the binding energy of a positronium atom (see Appendix B for values of  $E_i$ ). This relationship holds for alkanes, substituted alkanes, noble gases, and all nonpolar molecules studied thus far and is illustrated in Fig. 4.7. It should be noted that plotting the data as any function of  $E_i$  would also collapse the data on a single curve. Choosing  $(E_i - E_{\text{Ps}})^{-1}$  results in the curve approximating a straight line on a semi-log plot. No theory explains this relationship; however, Murphy and Surko previously pointed out that this empirical scaling might suggest a model in which a positronium atom moves in the electrostatic field of a positive ion [102].

Murphy and Surko found that the linear relation between  $\log(Z_{\text{eff}})$  and  $(E_i - E_{\text{Ps}})^{-1}$  does not hold for molecules with double bonds [102]. However, some of these molecules do come close to the linear relation, as shown in Fig. 4.8. This figure shows data for oxygen-containing hydrocarbons and simple molecules with dipole moments and/or double bonds. Oxygen-containing hydrocarbons lie slightly below the line. Most of the simple molecules lie close to the line, with the exception of  $\text{O}_2$ ,  $\text{NH}_3$ ,  $\text{NO}_2$ , and  $\text{NO}$ . Any systematic trends for these molecules have not been identified.



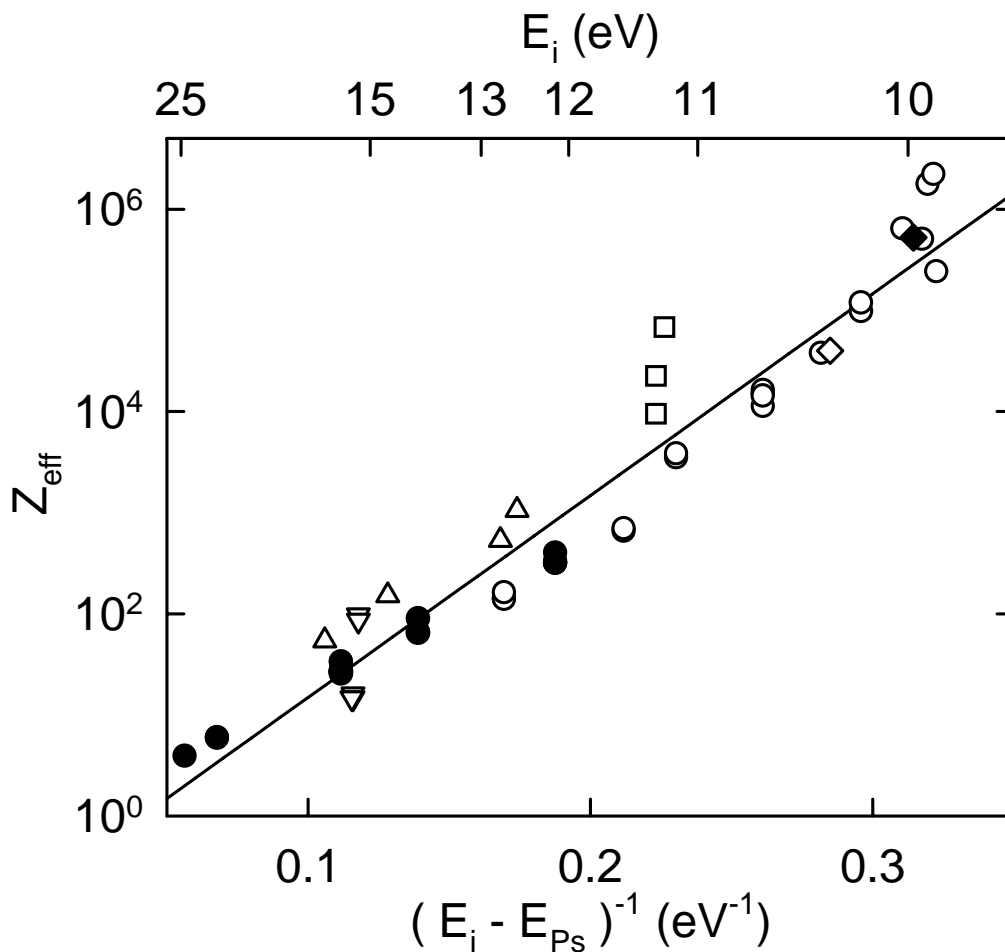


Figure 4.7: Values of  $Z_{\text{eff}}$  for non-polar molecules containing only single bonds are plotted against  $(E_i - E_{\text{Ps}})^{-1}$ , where  $E_i$  is ionization potential of molecule (labeled on top of graph), and  $E_{\text{Ps}} = 6.8$  eV is the binding energy of a positronium atom: ( $\bullet$ ) noble gases, ( $\nabla$ ) simple nonpolar molecules, ( $\circ$ ) alkanes, ( $\Delta$ ) perfluorinated alkanes, ( $\square$ ) perchlorinated alkanes, ( $\diamond$ ) perbrominated alkane, and (solid diamond) tetraethylsilane. The solid line is a linear regression to the data. The ionization potentials of perchlorinated alkanes and the largest alkanes are not known accurately, which could account for larger deviations from the line for these molecules.

Figure 4.9 shows the same plot for alkenes, ring hydrocarbons, and substituted benzenes. The majority of these molecules are quite far from the fitted line to the data in Fig. 4.7, and  $Z_{\text{eff}}$  values seem to reach a saturation around  $Z_{\text{eff}} \approx 5 \times 10^5$  for alkenes and substituted benzenes. This saturation may be a result of a positron-molecule resonance time,  $\tau_{\text{res}}$ , being larger than

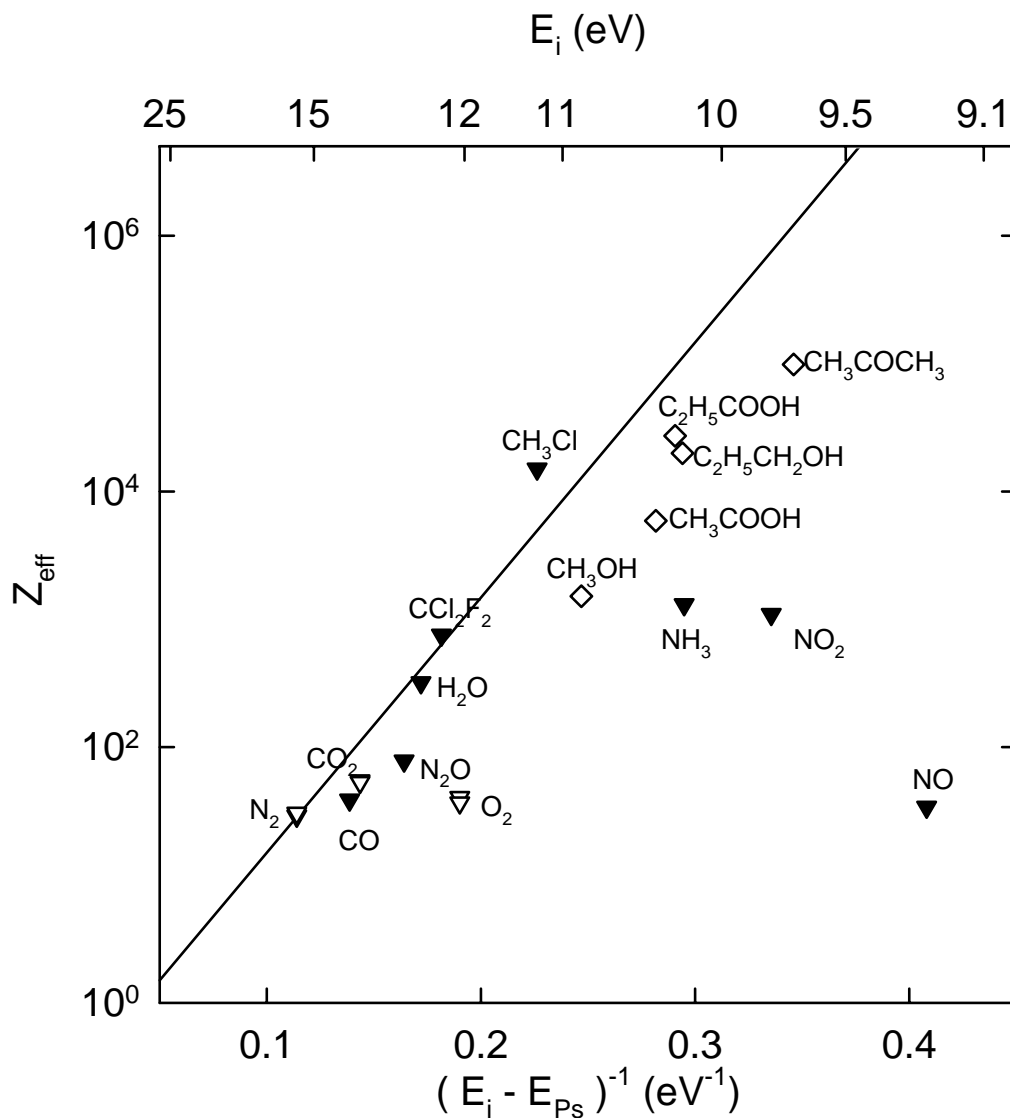


Figure 4.8: Values of  $Z_{eff}$  plotted against  $(E_i - E_{Ps})^{-1}$  for oxygen-containing hydrocarbons and small molecules with a dipole moment and/or double bonds : (▽) simple nonpolar molecules with double bonds, (solid triangle down) simple polar molecules, and (◇) oxygen-containing hydrocarbons. The solid line is the linear regression from Fig. 4.7.

the spin-averaged annihilation time for a positronium atom (i.e., in the notation of Sec. 4.1.1,  $\tau_{res} \geq \tau_0$ ), which, as discussed in Sec. 4.1.1, might lead to such a saturation. The value of  $Z_{eff}$  for anthracene is an order of magnitude larger than this saturated value, which could possibly be explained as follows:  $Z_{eff}$  depends

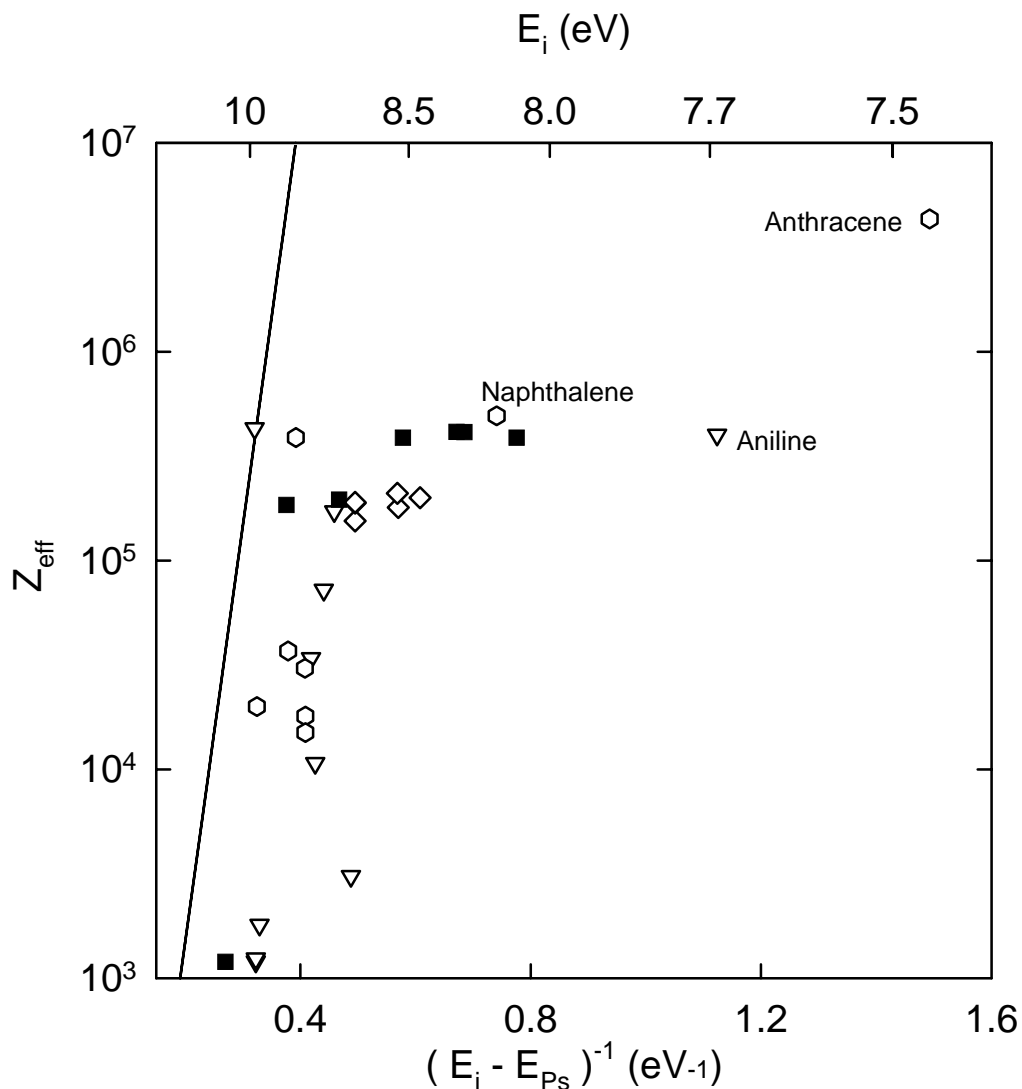


Figure 4.9: Values of  $Z_{\text{eff}}$  plotted against  $(E_i - E_{\text{Ps}})^{-1}$  for alkenes, ring hydrocarbons, and substituted benzenes: (solid square) alkenes, (open hexagon) ring hydrocarbons, ( $\diamond$ ) toluene and xylenes and ( $\nabla$ ) other substituted benzenes. The solid line is the linear regression from Fig. 4.7. Note that the range of  $(E_i - E_{\text{Ps}})^{-1}$  plotted is much larger than those in Figs. 4.7 and 4.8.

both on the resonance formation cross section,  $\sigma_{\text{res}}$ , and the resonance time,  $\tau_{\text{res}}$ , as shown in Eq. (4.3). An order of magnitude increase in  $\sigma_{\text{res}}$  is reasonable for a large molecule such as anthracene as compared with the alkenes, substituted benzenes, and naphthalene, which could account for the higher saturation value of  $Z_{\text{eff}}$ .

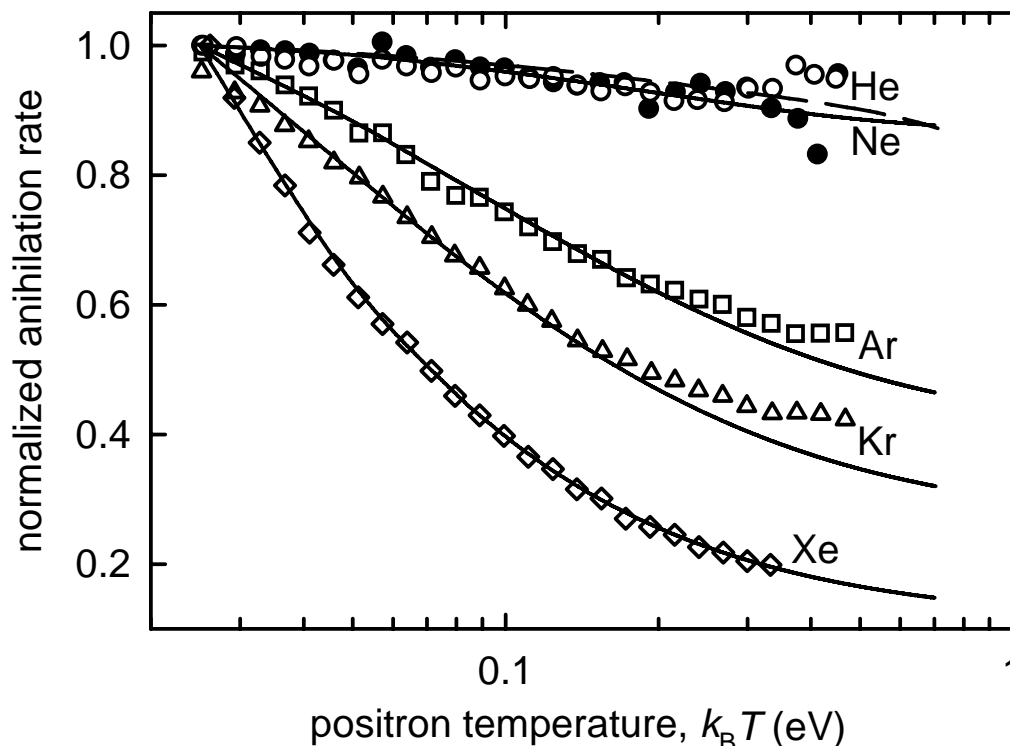


Figure 4.10: Dependence of annihilation rates of noble gases on positron temperature (taken from Ref. [74]). Experimental data: ( $\bullet$ ) He, ( $\circ$ ) Ne, ( $\square$ ) Ar, ( $\triangle$ ) Kr, and ( $\diamond$ ) Xe. Also shown are theoretical calculations: (- -) Kohn variational approximation for He [140], and (—) polarized orbital approximation [91,92,94].

### 4.3.2 Dependence of annihilation rates on positron temperature

Tinkle *et al.* developed a technique for heating the positron gas confined in the positron trap by applying RF noise to one of the electrodes [138]. Using this technique, Kurz *et al.* were able to make the first systematic measurements of the dependence of annihilation rates on positron temperature for noble gas atoms [74]. Although I was not directly involved with this work, I briefly review the results here, since they provide an important part of our understanding of the positron-atom interaction. The measured values of  $Z_{\text{eff}}$  are plotted in Fig. 4.10, where the data are normalized to the room-temperature values. The theoretically calculated temperature dependences (based on the polarized orbital approximation [91,92,94], except for He [140]) are also shown in the figure. These predictions are in excellent agreement with experiment. This agreement is somewhat surprising, since the predicted absolute values of  $Z_{\text{eff}}$  at room temperature for krypton and xenon [94] do not agree well with the measurements [39,66], as

can be seen in Table 4.1. Recently, Kurz *et al.* have made preliminary measurements of dependence of annihilation rates on positron temperature for a small number of hydrocarbons [73]. These measurements are expected to provide an additional constraint to theoretical models (e.g., Secs. 4.2.8 and 4.3.3.2).

### 4.3.3 Recent theoretical work

#### 4.3.3.1 Semi-empirical approach

The anomalously large annihilation rates observed for large organic molecules [60, 134] have not been theoretically understood, and a model for explaining the large annihilation rates in the constraint of other experimental evidences, which are presented in this chapter, has been a challenge. Recently, Laricchia and Wilkin have attempted a semi-empirical approach to explain this phenomena [77]. Motivated by the empirical scaling described in Sec. 4.3.1, their model assumes that the incoming positron forms a positronium atom inside a molecule in the uncertainty principle time scale of

$$\Delta t \sim \frac{\hbar}{|E_{e^+} - E_i + E_{Ps}|}. \quad (4.8)$$

They argue that, in this time scale, the positron in the virtual positronium atom annihilates by picking off one of the other bound electrons in the molecule, where the electron density around the positron is enhanced by polarization. This model is consistent with the scaling of annihilation rates with  $(E_i - E_{Ps})$  for positrons with energy  $E_{e^+} \ll (E_i - E_{Ps})$ , and reasonable agreement with observed room-temperature annihilation rates is seen [77].

They interpret their model as predicting that the annihilation rates diverges at  $E_{e^+} \sim (E_i - E_{Ps})$  with the form

$$Z_{\text{eff}} \propto \frac{1}{|E_{e^+} - E_i + E_{Ps}|}. \quad (4.9)$$

Motivated by this model, Humberston and Van Reeth have performed precise numerical calculations of positron annihilation rate of helium just below the positronium formation threshold [65], and they have observed a divergence in the annihilation rate. The nature of the divergence is, however, much faster than that expected from the model by Laricchia and Wilkin. The divergence observed by Humberston and Van Reeth can be understood by the divergence in the scattering length as discussed in Sec. 4.1.2, not due to the uncertainty principle. An experiment using the narrow energy-spread positron beam recently developed in our laboratory [44] to study  $Z_{\text{eff}}$  near the positronium formation

threshold energy may give us deeper insight into the nature of the interaction at the threshold for Ps formation.

#### 4.3.3.2 Large scale calculations for molecules

Annihilation rate measurements for a wide range of molecules have now been made, as can be seen in Sec. 4.2. However, theoretical work on annihilation rates for molecules had been limited to the simplest molecules (Sec. 4.2.2). Recently, da Silva *et al.* have made the first large-scale calculation of a hydrocarbon molecule with an anomalously large annihilation rate, namely ethylene ( $\text{C}_2\text{H}_4$ ), using the Schwinger multichannel method [29]. The scaling of annihilation rates with  $(E_i - E_{\text{Ps}})^{-1}$  suggests that the physics involved in the observed anomalously high annihilation rates may be dominated by pseudo-positronium atom formation in the field of the molecular ion. Their calculation of annihilation rate including the pseudo-positronium formation channel brings the annihilation rate close to the observed value. In addition, the recent measurement of annihilation rate dependence on positron temperature for this molecule by Kurz *et al.* [73] is also in reasonable agreement with their calculation.

#### 4.3.4 Other issues

##### 4.3.4.1 Noble gas atoms

The relatively simple atomic structure of the noble gases provides a test of our understanding of low-energy positron-atom interactions. Even in this case, there are discrepancies between experimental values measured in the positron trap and theoretical values based on polarized orbital calculations [94] (see Table 4.1) for the case of krypton and xenon. The data presented here indicate that reexamination of the theory might be warranted. Recently, Dzuba *et al.* have theoretically investigated the effect of the virtual positronium formation channel on the annihilation of noble gas atoms [39], as suggested in the scaling described in Sec. 4.3.1. Even though they have not calculated the annihilation rates, their analyses provide useful insights into positron-atom interactions.

##### 4.3.4.2 Reproducibility of measurements

For earlier studies, only a small number of positrons were available, and consequently, uncertainties of a factor of two are possible in the measured values of  $Z_{\text{eff}}$  [134]. Subsequently, considerably more positrons have become available, and the main source of error is now the 20% uncertainty in the pressure of the

test gas. It is likely that the early measurement of  $Z_{\text{eff}}$  of nonane (see Table 4.3) is higher than the recent measurement of  $Z_{\text{eff}}$  of decane for this reason.

#### 4.3.4.3 Delocalized $\pi$ bonds in benzene

As a result of earlier studies, it was suggested that the reduction of  $Z_{\text{eff}}$  in benzene as compared with hexane might be due to the presence of delocalized  $\pi$ -bonding electrons in the benzene ring [102]. However, measurements for cyclohexane, which contains no delocalized electrons, yield a value for  $Z_{\text{eff}}$  similar to benzene, indicating that delocalized electrons may not be responsible for this effect.

#### 4.3.4.4 Determination of positron annihilation sites in a molecule

The determination of positron annihilation sites in a molecule can give a stringent constraint on a theoretical model of annihilation processes. This kind of information can be obtained from studies of the Doppler broadening of the 511-keV annihilation  $\gamma$ -ray line. The earliest study of this type concentrated on hydrogen, because of its importance in the production of astrophysical positron annihilation radiation [14]. Tang *et al.* began more comprehensive studies of the energy spectra of annihilation radiation in a variety of molecules, including hydrocarbons and perfluorocarbons [136]. These studies have now been extended to include many of the compounds reported in this chapter. We have made significant progress in this area recently [69, 70], which is the subject of the next chapter (Ch. 5).

#### 4.3.5 Current state of annihilation rate studies

The anomalously large annihilation rates have still not been explained theoretically, even though some attempts have been made. The deuterated alkane studies described in Sec. 4.2.7.1 seem to rule out the possibility of positron forming long-lived compound with the target molecule by transferring its kinetic energy to the vibrational modes. The scaling of annihilation rates described in Sec. 4.3.1 points to a process involving electronic excitation (e.g., highly correlated electron-positron complex in the field of a positive molecular ion) being responsible for the observed annihilation rates. The enhancement in the scattering cross section alone is not likely to explain the observation as discussed in Sec. 4.2.8. An inelastic channel other than molecular vibration may be responsible for the formation of long-lived positron-molecule compounds, but if such a channel exists, it has not been identified.

## 4.4 Concluding remarks on annihilation rate measurements

In this chapter, positron annihilation rates on molecules studied in a positron trap have been presented. These measurements are compared with those done using other techniques. Where more than one measurement is available for a particular molecule, the data are, in general, in reasonable agreement. The data exhibit a number of chemical trends and illustrate the importance of electronic structure and symmetries. Even though theoretical progress has been made recently, features of the results such as the anomalously large annihilation rate observed for large organic molecules have not been understood. A systematic survey of annihilation rates for various molecules presented in this chapter provides stringent constraints for the development of theoretical models to explain the observed trends, including the anomalously large annihilation rates.



## Chapter 5

# Annihilation $\gamma$ -ray spectra

### 5.1 Introduction

Extensive measurements of the momentum distributions of annihilating electron-positron pairs have been performed in solid and liquid targets [124], and they provide information about the annihilation processes and other properties of materials. In this chapter, a technique for measuring the momentum distribution is applied to make systematic measurements in gaseous media, which are sufficiently tenuous so that the interaction of positrons with an individual atom or molecule can be isolated and studied.

Earlier measurements of this type in gases were mainly performed in high density using a different technique from the one described here. As discussed in Sec. 5.2, one disadvantage of the earlier method is that positronium atom formation can take place during the slowing down of the positrons, and subsequent annihilation of the thermalized positronium atoms can obscure the free positron annihilation signal. We avoid the annihilation signals from positronium atoms by the use of the positron trap. The signals from positronium atoms during a measurement are eliminated by cooling the positrons below the formation threshold before the sample gas is introduced.

Previous experiments of Doppler-broadened  $\gamma$ -ray spectra in Penning traps [14, 136] demonstrated the feasibility of the use of stored positrons for spectral measurements. Subsequent improvements in positron moderation [49, 100] and trapping efficiency, as well as in the gas handling system, have now enhanced the signal-to-noise ratio by two orders of magnitude. This has permitted a range of new experiments, including detailed comparison of the annihilation line shape with theoretical calculations [140], the simulation of astrophysical positron annihilation [68], and the localization of the sites of positron annihilation in

complex molecules.

In this chapter, a systematic study of positrons interacting with a wide variety of atoms and molecules is described. Data are presented for noble gases, inorganic molecules, alkanes, alkenes, aromatics, substituted hydrocarbons, as well as fully and partially fluorinated hydrocarbons. Important results include demonstration of the ability to resolve, for the first time in gaseous media, non-Gaussian features in the line shapes and the detection of more than one annihilation site in molecules, including distinguishing annihilation on the C-H bond from that on the fluorine atom in partially fluorinated hydrocarbons. The data presented also indicate that in hydrocarbons annihilation on the C-H bond from that on the C-C bond can be distinguished. In all molecules studied, the data are consistent with the positrons annihilating predominantly with valence electrons. A study of halogenated hydrocarbons is also presented. This study shows that the positrons annihilate on the halogen atoms with a linewidth very similar to that of the related noble gas atom, particularly in the case of the larger halogens. The systematic studies presented in this chapter provide useful constraints on theories of low-energy positron-atom and positron-molecule interactions.

This chapter is organized in the following manner. In Sec. 5.2, previous experiments to measure the momentum distributions of annihilating electron-positron pairs are reviewed. The results of the experiments are described in Sec. 5.3, including the results of an extensive study of partially fluorinated hydrocarbons. (The experimental setup was described previously in Sec. 3.6.) Detailed analyses of spectral line shapes are presented in Sec. 5.4. In Sec. 5.5, the implications of these results for current theoretical work and for progress in other areas of positron-molecule interactions are discussed. A brief set of concluding remarks is presented in Sec. 5.6. The subject discussed in this chapter is published in Ref. [69].

## 5.2 Momentum distribution measurements

An electron-positron pair annihilates by emitting two quanta of 511-keV  $\gamma$  rays at an angle of  $180^\circ$  in the center-of-mass frame of the two particles. However, in the laboratory frame, the  $\gamma$  rays carry away the initial momentum of the center of mass of the pair. Thus, as illustrated in Fig. 5.1, the angle of emission of the two photons relative to one another deviates slightly from  $180^\circ$  due to the perpendicular components of the momentum of the electron-positron pair,  $p_x$  and  $p_y$ . The  $\gamma$  rays are Doppler shifted in energy due to the longitudinal momentum component of the pair,  $p_z$ . When  $p_x, p_y \ll m_0c$ , the angle of deviation,  $\theta$ , can

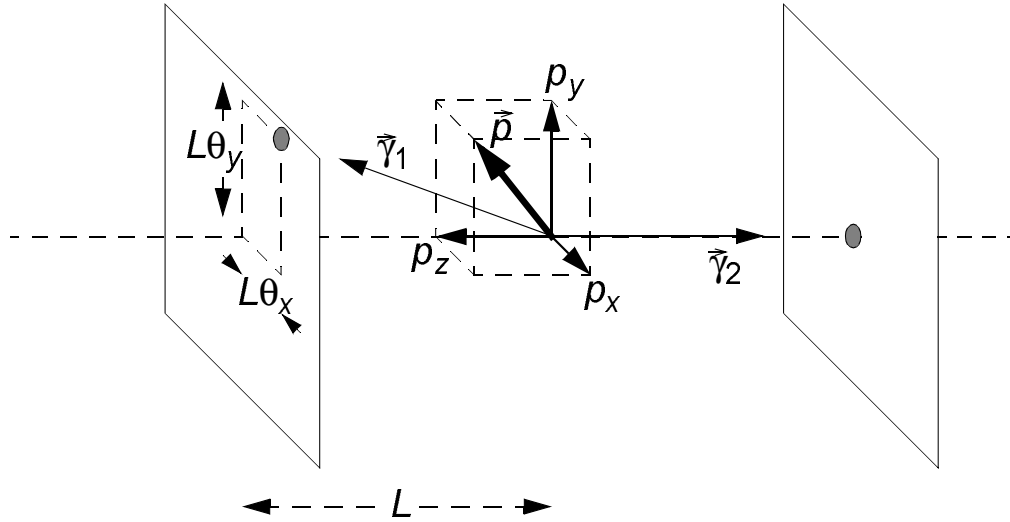


Figure 5.1: Illustration of the momentum of an annihilating electron-positron pair,  $\vec{p}$ , and the resulting  $\gamma$ -ray momenta,  $\vec{\gamma}_1$  and  $\vec{\gamma}_2$ . An annihilation event is observed with two detectors placed  $180^\circ$  with respect to the annihilation site at distance,  $L$ . The longitudinal component of  $\vec{p}$ ,  $p_z$ , shifts the energies of  $\gamma$  rays, and the tangential components,  $p_x$  and  $p_y$ , deflect the  $\gamma$  rays by an angle  $\theta = (\theta_x^2 + \theta_y^2)^{1/2}$ . (The angle of deflection is exaggerated in this figure.)

be expressed as

$$\theta_j \simeq \frac{p_j}{m_0 c}, \quad (5.1)$$

where  $j = x$  or  $y$ ,  $m_0$  is the rest mass of the electron, and  $c$  is the speed of light. The Doppler shift in the energy,  $\Delta E$ , is given by

$$\Delta E = \frac{p_z}{2m_0 c} E_0 = \frac{c p_z}{2}, \quad (5.2)$$

where  $E_0 = m_0 c^2$  is the rest mass energy of the electron. The perpendicular components of the momentum of the annihilating pair can be studied by measuring the angular correlation of two  $\gamma$  rays. The longitudinal component can be measured by observing the Doppler broadening of the  $\gamma$ -ray spectrum using high-resolution solid-state detectors such as lithium-drifted or intrinsic germanium detectors.

When annihilation follows thermalization of the positrons in the medium, e.g., with the characteristic energy of  $(3/2)kT = 0.04$  eV (corresponding to room temperature), the momentum of the annihilating pairs is typically dominated by the momenta of the electrons. Techniques for measuring the momentum distributions of the annihilation  $\gamma$  rays were developed initially for the studies

of positron annihilation in condensed media [115]. These techniques have been applied to studies of positron-gas interactions as well [26]. When the medium is a crystalline solid,  $p_x$  and  $p_y$  can be distinct. For example, the anisotropy in two dimensions has been observed and studied in some materials [111]. When the medium under investigation is a liquid or gas, the momentum distribution is rotationally averaged, and the three momentum components are equivalent. In this case, the angular deviation  $\theta$  and the energy spread  $\Delta E$  are related by

$$\Delta E = m_0 c^2 \frac{\theta}{2}, \quad (5.3)$$

and angular correlation and Doppler-broadening measurements can be compared.

### 5.2.1 Annihilation $\gamma$ -ray angular correlation measurements

The technique of angular correlation of annihilation radiation (ACAR) was developed to determine the perpendicular components of the momenta of annihilating electron-positron pairs in solids, liquids, and dense gases [115]. Initially, the measurements were performed in a one-dimensional geometry [11] in which two  $\gamma$ -ray detectors are located behind slit collimators on opposite sides of the annihilation region. One of the detectors is scanned as a function of the angle between the two detectors, and coincident events are recorded. One advantage of the ACAR method is its high resolution. Typical angular resolutions achievable are about 0.65 mrad [143], which is equivalent to the  $\gamma$ -ray energy resolution of 0.2 keV using Eq. (5.3).

In order to obtain high resolution, the slits must be placed as far from the annihilation cell as possible, typically tens of meters. This results in reduced count rates due to the small solid angle subtended by the detector at the sample. In order to obtain both high resolution and a large number of counts in a reasonable amount of time, one would like to have as many positrons as possible annihilating in a small volume. This condition can be satisfied in solid and liquid targets [13, 130], but in this case, annihilation may involve the interaction of a positron with multiple atoms or molecules. In contrast, in gaseous media the two-body assumption is more likely to be met, but ACAR measurements are more difficult because the mean free path of positrons in gases is relatively large and results in a large annihilation region and low count rates. The first ACAR measurements in gaseous media were reported by Heinberg and Page in 1957 [59]. However, their study was focused on positronium atoms in which the information content of the signal is less sensitive to the details of the spectra. The introduction of the 2-D ACAR detector [143] has enabled measurements

in the gas phase with significantly increased count rates. For 2-D ACAR, two relatively large NaI crystals with position-sensitive detectors attached replace the detector/slit combinations. The position-sensitive detectors can accurately identify the location of scintillations produced by  $\gamma$ -rays without much loss of count rate. The first quantitative ACAR results of free positrons annihilating on atoms in gaseous media were done by Coleman *et al.* using a 2-D ACAR detector [26].

### 5.2.2 Doppler-broadened $\gamma$ -ray spectral measurements

For the experiments described in this chapter, an alternative method of obtaining the momenta of the annihilating electron-positron pairs was used. The Doppler broadening of the annihilation line was directly measured using a high-energy-resolution solid-state  $\gamma$ -ray detector (an intrinsic germanium detector), in conjunction with a multi-channel analyzer (MCA). This yields the longitudinal component,  $p_z$ , of the annihilating pair's momentum, which is equivalent to either of the other two components in an isotropic medium such as a gaseous target. One advantage of the Doppler-broadening technique is that a high count rate can be obtained since the detector can be placed close to the annihilation region, and this results in a large collection solid angle. This permits measurements in diffuse media, such as low-pressure gases [14, 126, 136]. Another advantage of this technique is the compactness of the equipment and the ease of installation. As described in Ch. 7, this technique can also be applied to studies of positron annihilation in the interstellar medium, where ACAR techniques are inapplicable. However, one disadvantage of the Doppler-broadening technique is its relatively poor resolution. For example, an intrinsic Ge detector typically has an energy resolution of  $\sim 1$  keV at 511 keV, as compared with the equivalent ACAR resolution of 0.2 keV. In the experiments described here, an intrinsic Ge detector is used to take advantage of the high count rate in diffuse media where positrons are interacting with low-pressure gas atoms or molecules.

Lynn *et al.* employed an improved implementation of the Doppler-broadening approach, which utilizes two high-resolution Ge detectors placed  $180^\circ$  with respect to the annihilation region [84]. This technique can dramatically increase the signal-to-noise ratio of the data. Use of this technique allowed them to detect positron annihilation on inner-shell electrons in condensed media. This method can, in principle, also be used for studies of positron annihilation in gaseous media, which are discussed in Sec. 5.5.

## 5.3 Results

In this section, the results of the Doppler broadening of the  $\gamma$ -ray spectra from positrons annihilating on a variety of atoms and molecules in the Penning trap are reported. The results from previous studies of momentum distributions and theoretical calculations are also tabulated and compared.

Typical spectra from our experiment are shown in Fig. 5.2 along with the detector response. The annihilation lines shown are the spectra from  $\text{H}_2$  and Ne, which are the narrowest and widest lines observed, respectively. The observed linewidths correspond to the positrons annihilating predominantly with the valence electrons of the atoms and molecules. However, we also have evidence of annihilation on inner-shell electrons, and this will be discussed in Sec. 5.3.9 and in Ch. 6. As can be seen in Fig. 5.2, the detector width is substantially narrower than the observed annihilation lines. The high precision of the measurements is evident from the small scatter in the data. The total number of  $\gamma$ -ray counts in a spectrum is about  $10^6$  unless otherwise stated. For the experimentally measured spectra presented in figures, the error bars shown represent the expected statistical uncertainties in spectral amplitude due to the finite number of  $\gamma$ -ray counts. Spectra were recorded in 12 1-hour time segments, and the linewidth was calculated from each segment. The tabulated linewidths were obtained by averaging these linewidths. The variations were typically 0.01 to 0.02 keV. Measurements of some substances were repeated in separate runs on different days, and those linewidths generally agree within 0.01 keV. The uncertainty in the detector response is at most 0.01 keV. The experimental precision of the linewidths is estimated to be typically 0.02 keV.

In the remainder of this section, annihilation line data for a variety of substances are presented. Some of the tables also list the annihilation rates (in terms of  $Z_{\text{eff}}$ ), where they are relevant in the discussion. The sources of the values are listed in Ref. [66] and in Ch. 4 unless otherwise noted. The values of the previously measured linewidths from ACAR measurements are quoted in keV as converted from the ACAR linewidths using Eq. (5.3).

### 5.3.1 Noble gases

The simple electronic structure of noble gas atoms has made them attractive candidates for studies of positron-atom interactions. Comparison between experiments [26] and theories [39,91–94] are available for all of these atoms. Previous theoretical calculations were based on the polarized orbital approximation, with the exception of the helium studies [17,38,140].

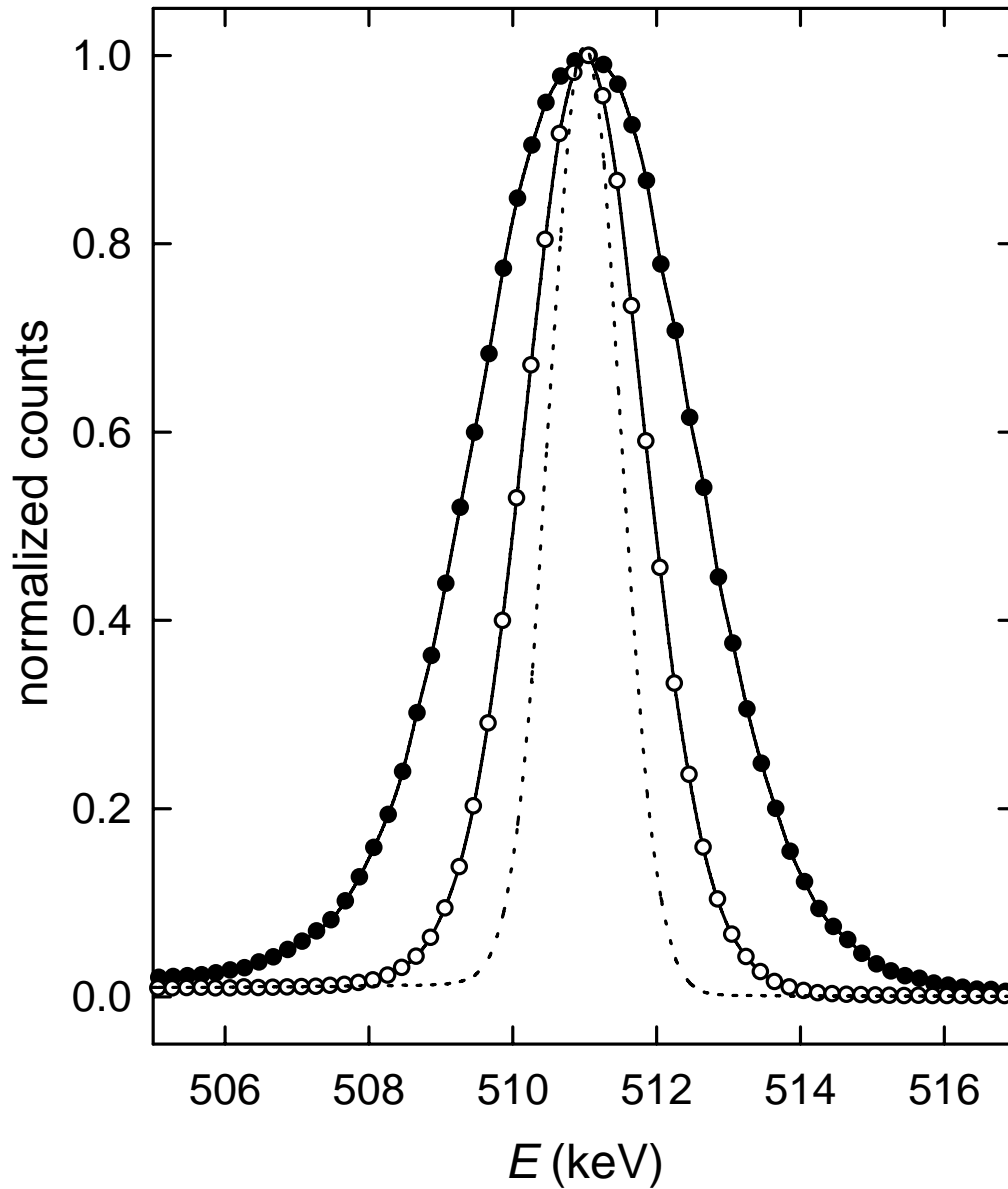


Figure 5.2: Observed spectra from H<sub>2</sub> (o) and Ne (•) plotted on a linear scale. Solid lines are drawn to guide the eye. For the purpose of comparison, the 514.02-keV line from <sup>85</sup>Sr (· · ·) is shifted to 511 keV, which represents the detector response. The spectra are normalized to unity at the peak.

A qualitative understanding of the linewidths of the noble gases can be obtained by considering the simple approximation of the positron in the static potential of the atom in its Hartree-Fock ground state. While this theory gives

Table 5.1: The  $\gamma$ -ray linewidths for noble gases obtained from Gaussian fits to the data (in keV). For comparison, experimental values from other methods as well as theoretical values are listed.

Gas	This study	Shizuma <sup>a</sup>	Coleman <sup>b</sup>	Stewart <sup>c</sup>	Theory <sup>d</sup> (static)	Theory
Helium	2.50	2.01	2.63	2.4	2.53	2.50 <sup>e</sup> 2.20 <sup>f</sup> 2.45 <sup>g</sup> 2.50 <sup>h</sup>
Neon	3.36	2.04	3.19	3.32	3.82	3.73 <sup>i</sup>
Argon	2.30	1.96	2.86	2.61	2.64	2.81 <sup>j</sup>
Krypton	2.09	N/A	2.65	2.63	2.36	2.50 <sup>k</sup>
Xenon	1.92	1.69	2.58	2.43	2.06	2.22 <sup>k</sup>

<sup>a</sup>Ref. [126], <sup>b</sup>Ref. [26], <sup>c</sup>Ref. [130], <sup>d</sup>Ref. [53] <sup>e</sup>Ref. [140], <sup>f</sup>Ref. [17], <sup>g</sup>Ref. [93], <sup>h</sup>Ref. [38], <sup>i</sup>Ref. [91], <sup>j</sup>Ref. [92], and <sup>k</sup>Ref. [94].

a significant underestimate of  $Z_{\text{eff}}$ , the  $\gamma$ -ray linewidths are in reasonable agreement with experiment (Table 5.1) [53]. This indicates that the momentum distribution of the electrons in the atomic ground state is the most significant factor in determining the linewidths. The experimentally measured linewidths are consistently smaller than the predictions of this simple theory.

In Table 5.1, we compare our  $\gamma$ -ray spectra for noble gases with the previous measurements as well as with theoretical calculations. The theoretical calculations predict the general trend of the experimental linewidths even though the calculated values differ from our measurements.

### 5.3.1.1 Helium

Helium is the simplest stable atomic gas, and it has been studied extensively. Rigorous calculations are possible for positron-helium interactions. Measurements for helium in our system are restricted by the limited capacity of our cryogenic pumps for this gas so that the data quality is not as good as those for other gases. The experimentally measured spectrum is shown in Fig. 5.3 together with a very recent calculation [140] using the Kohn variational method. Excellent agreement can be seen between experiment and theory, extending over three orders of magnitude in spectral amplitude. These data provide the first experimental evidence for deviations from the empirical Gaussian line shape described above and shown by the dashed line in Fig. 5.3. While such deviations



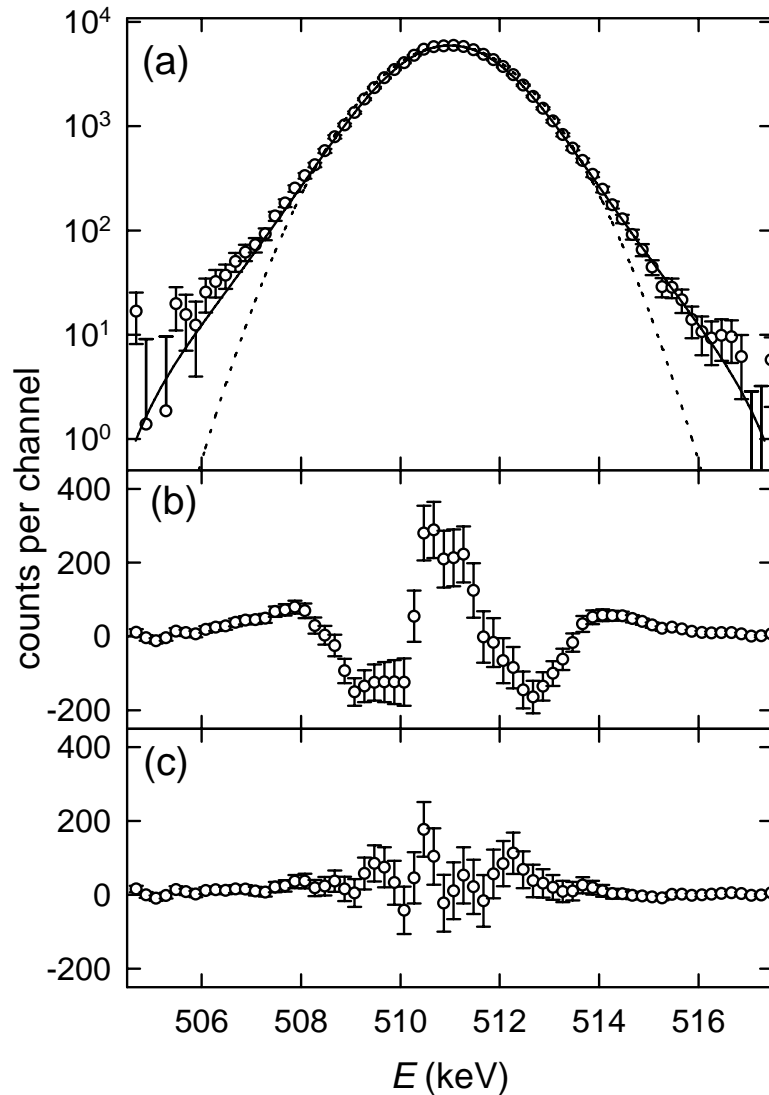


Figure 5.3: (a) Annihilation  $\gamma$ -ray spectrum for positrons interacting with helium atoms: (o), experimental measurements; (—) theoretical prediction of Ref. [140], convolved with the response of the Ge detector; (· · ·) Gaussian function fit to the experimental data. (b) Residuals from the Gaussian fit. (c) Residuals from the theoretical calculation.

are expected, previous experiments were not sufficiently precise to discern them.

### 5.3.1.2 Neon, argon, krypton, and xenon

Spectra for neon, argon, krypton, and xenon are shown in Fig. 5.4, and the values of the linewidths are listed in Table 5.1. The linewidth for neon is the largest.

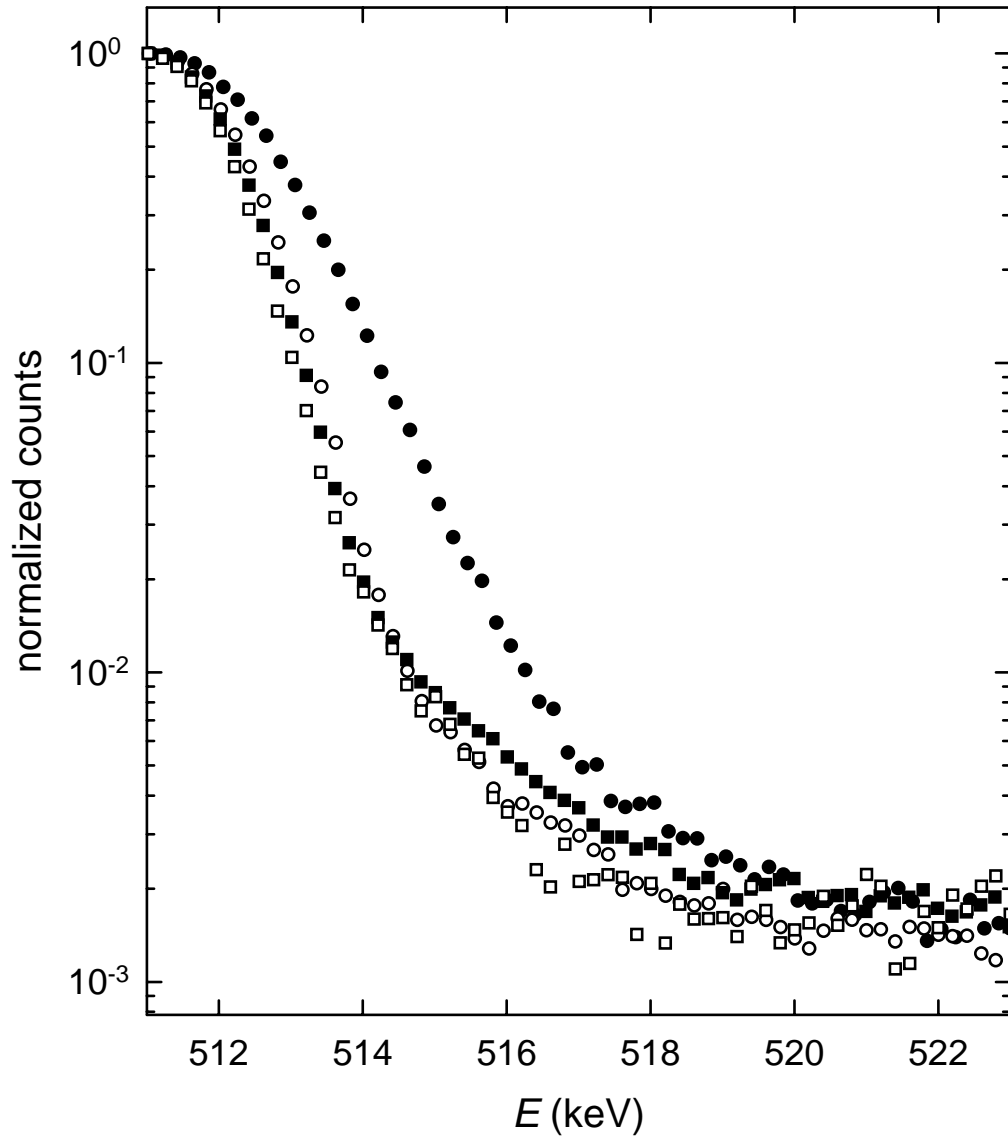


Figure 5.4: Experimentally measured  $\gamma$ -ray spectra from noble gases: ( $\bullet$ ) neon, ( $\circ$ ) argon, (solid square) krypton, and ( $\square$ ) xenon. The peak heights are normalized to unity. The spectra shown are for the higher energy side of the  $\gamma$ -ray line since the step function in the detector response is absent in this region, and consequently the data quality is better.

In fact, it is the widest line observed for any atom or molecule. For atoms larger than neon, the linewidths decrease as the sizes of the atoms increase. Calculations using the polarized-orbital approximation are listed in Table 5.1

[91,92,94]. The higher momentum components in Kr as compared to Ar can be seen by the crossing of the data around 515 keV. This crossing was predicted by the static Hartree-Fock approximation, and the theory indicates that the crossing is due to a larger fraction of positrons annihilating with inner-shell electrons in Kr [53]. (Inner-shell electron annihilations will be discussed in more detail in Sec. 5.3.9 and in Ch. 6.) The agreement between the experimental and theoretical values for these noble gases is not as good as that for helium, probably reflecting the difficulty in performing accurate calculations for all but the simplest atoms.

### 5.3.1.3 Previous measurements from other experiments

Selected values of the linewidths measured for the noble gases are listed in Table 5.1. Stewart *et al.* [130] performed ACAR measurements in condensed media, while Coleman *et al.* [26] obtained 2D-ACAR measurements from gaseous targets at a pressure of 1 atm. High-energy positrons were directly injected into the gas cells in these experiments. Thus, these ACAR spectra include a contribution from the annihilation of thermalized positronium atoms. This appears as a narrow peak in the spectrum, superimposed on the annihilation of free positrons on atoms, which appears as a wide component in the spectrum. The free-positron component was subtracted assuming Gaussian line shapes for both contributions. The linewidths from these measurements are qualitatively similar to our measured values, although the absolute values are larger. This discrepancy may come from the high sample gas pressures in the ACAR experiments, which can introduce three-body interactions. Also, the positronium contributions in the ACAR experiments were relatively large, especially for the larger noble gases, which makes the extraction of the free positron component more difficult. The only previous Doppler-broadening studies in the gas phase were reported by Shizuma *et al.* [126]. Although they did not tabulate linewidths, we have estimated numerical values from their graphical data (Table 5.1). Their values are significantly narrower than other measurements and theoretical predictions. The reason for the discrepancy is not clear.

### 5.3.2 Inorganic molecules

Molecules are significantly more complicated than atoms, and consequently theoretical calculations exist for only a limited number of molecules. Experimentally measured linewidths are listed in Tables 5.2 and 5.3 for the inorganic molecules that we have studied.

Table 5.2: The  $\gamma$ -ray linewidths from a Gaussian fit to the data for  $\text{H}_2$ , along with other measurements and calculations. The value of  $Z_{\text{eff}}$  is 14.6 [76].

Reference	$\Delta E$ (keV)
This study	$1.71 \pm 0.02$
Briscoe <sup>a</sup>	1.66
Brown <sup>b</sup>	$1.56 \pm 0.09$
Darewych <sup>c</sup>	1.70
Ghosh <sup>d</sup>	1.93

<sup>a</sup>ACAR measurement in liquid  $\text{H}_2$  (6.5 mrad) [13], <sup>b</sup>Doppler-broadening  $\gamma$ -ray spectrum measurement in gas [14], <sup>c</sup>theoretical calculation (6.65 mrad) [30], and <sup>d</sup>theoretical calculation (7.54 mrad) [43].

Table 5.3: The  $\gamma$ -ray linewidths for inorganic molecules (using Gaussian fits). (See Ref. [66] for the sources of  $Z_{\text{eff}}$  values.)

Molecule	Formula	$\Delta E$ (keV)	$Z_{\text{eff}}$
Nitrogen	$\text{N}_2$	2.32	30.5
Oxygen	$\text{O}_2$	2.73	36.7
Carbon monoxide	$\text{CO}$	2.23	38.5
Carbon dioxide	$\text{CO}_2$	2.63	54.7
Water	$\text{H}_2\text{O}$	2.59	319
Sulfur hexafluoride	$\text{SF}_6$	3.07	86.2
Ammonia	$\text{NH}_3$	2.27	1600 <sup>a</sup>

<sup>a</sup>Ref. [69].

### 5.3.2.1 Hydrogen

$\text{H}_2$  is the simplest molecule, and its significance in astrophysical positron annihilation has attracted interest from both experimentalists [14] and theorists [30,43]. The astrophysical aspects of our measurements are discussed in Ch. 7. Our measured spectrum for hydrogen is shown in Fig. 5.5 along with theoretical predictions for the line shape [30,43]. The measured value of the linewidth of  $1.71 \pm 0.02$  keV is compared with other measurements and with theoretical predictions in Table 5.2. All of the experimental measurements and the value calculated by Darewych are similar, while the prediction by Ghosh *et al.* is much larger.

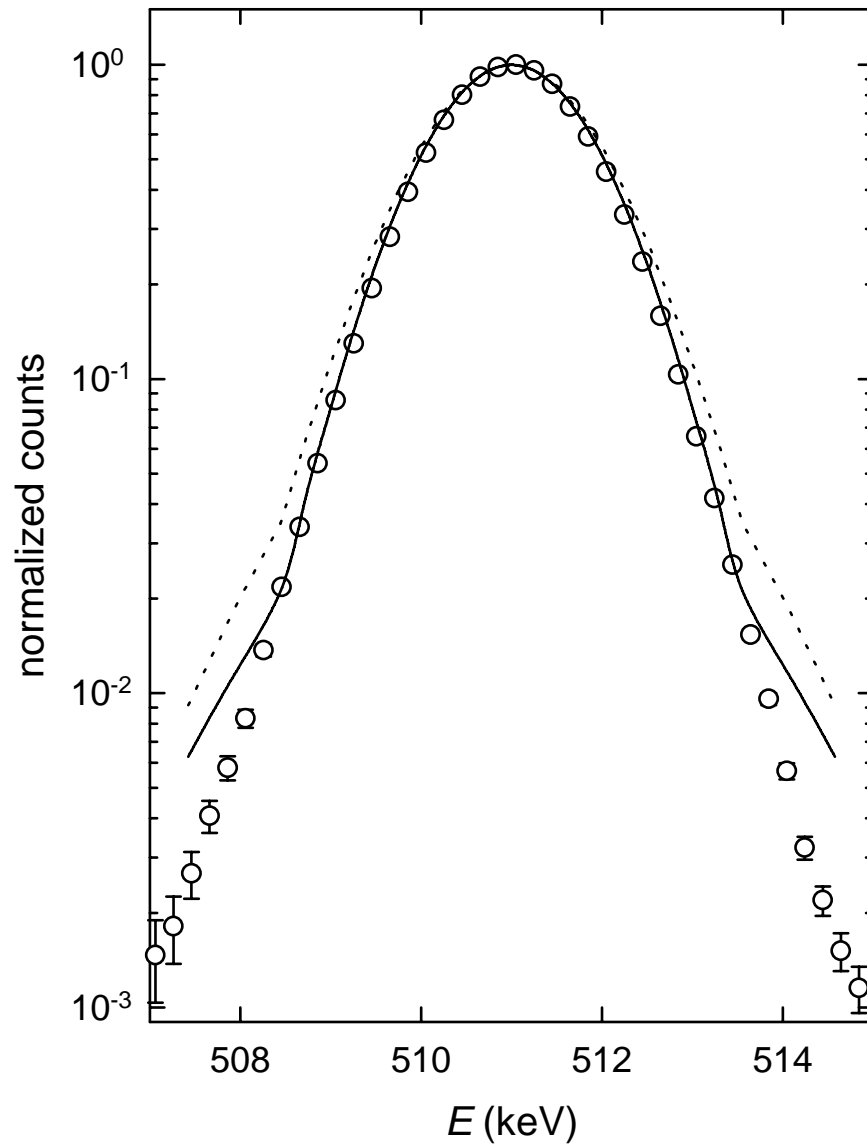


Figure 5.5:  $\gamma$ -ray spectrum from positron annihilation on molecular hydrogen: (o) observed spectrum from our measurement, (—) theoretical calculation of Ref. [30], and (---) theoretical calculation of Ref. [43].

### 5.3.2.2 Other gases

**Nitrogen** An ACAR measurement in liquid  $N_2$  gave  $\Delta E = 2.25$  keV (8.8 mrad) [130], which is in reasonable agreement with our measured value of 2.32 keV. The only theoretical calculation available gives a linewidth of 1.34 keV

(5.28 mrad) [43], which is much narrower than the experimental values.

**Carbon monoxide and carbon dioxide.** Carbon monoxide stands out in that the line shape exhibits the largest departure from a Gaussian of any molecule that we have studied, as shown in Fig. 5.6. This is due to a small fraction of positrons annihilating with electrons having high momenta. Since this molecule is relatively simple, it may be an interesting subject for theoretical calculations. In contrast to carbon monoxide, as shown in Fig. 5.6, carbon dioxide has only a weakly non-Gaussian line shape.

**Sulfur hexafluoride** Sulfur hexafluoride has very high electron affinity, and it is well known as an electron scavenger [58]. In contrast, with regard to the interaction with positrons, it has a very low annihilation rate for a molecule of this size ( $Z_{\text{eff}} = 86.2$ ). The annihilation line is almost as wide as neon. We note that the electronic structure of the fluorine atoms in many molecules, including  $\text{SF}_6$ , is similar to the closed-shell structure of neon. For example, sulfur hexafluoride has a linewidth very similar to the perfluorinated alkanes. This suggests that annihilation in all of these cases occurs predominantly on the fluorine atoms, which are expected to have a close-shell structure similar to neon atoms.

**Ammonia** Ammonia has an anomalously large annihilation rate ( $Z_{\text{eff}}/Z \sim 100$ ) [60]. It has a linewidth comparable to that of the alkanes. Ammonia has a significant dipole moment, but it is not known, at present, how this would affect the linewidth.

### 5.3.3 Alkanes

The linewidths for the alkanes are listed in Table 5.4. Methane has the narrowest linewidth, 2.09 keV. The linewidth increases to a value around 2.3 keV for the larger alkanes. While cyclohexane has a value of  $Z_{\text{eff}}$  about an order of magnitude smaller than hexane (Table 4.3), the linewidth of the  $\gamma$ -ray spectrum is only slightly larger than that of hexane. Considering saturated hydrocarbons with five carbon atoms, there are three different isomeric configurations, and data for them are shown in Table 5.4. While their  $\gamma$ -ray spectra are identical to within the experimental error, the values of annihilation rates,  $Z_{\text{eff}}$ , differ by approximately a factor of two. In general, we have not been able to detect any systematic relationship between  $Z_{\text{eff}}$  and linewidth for the hydrocarbons or for any of the other molecules studied.

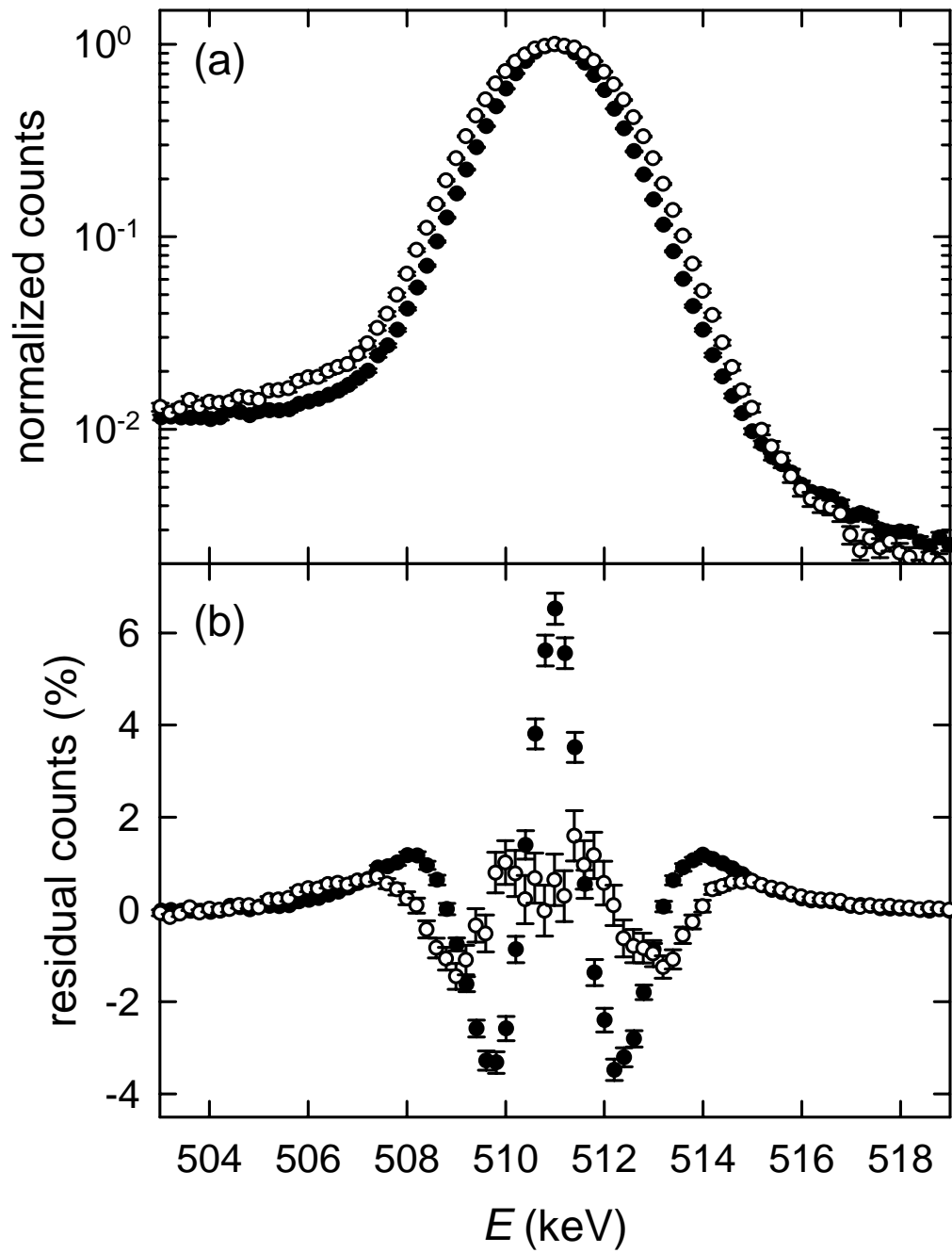


Figure 5.6: (a)  $\gamma$ -ray spectra for positrons annihilating with ( $\bullet$ ) CO and ( $\circ$ ) CO<sub>2</sub>. (b) Residuals from the Gaussian fits. The data and residuals are normalized to the peak height of the spectra.

Table 5.4: The  $\gamma$ -ray linewidths for hydrocarbons (using Gaussian fits). (See Ref. [66] for the sources of  $Z_{\text{eff}}$  values.)

Molecule	Formula	$\Delta E$ (keV)	$Z_{\text{eff}}$
<b>Alkanes</b>			
Methane	CH <sub>4</sub>	2.09	142
Ethane	C <sub>2</sub> H <sub>6</sub>	2.18	1 780 <sup>a</sup>
Propane	C <sub>3</sub> H <sub>8</sub>	2.21	3 500
Butane	C <sub>4</sub> H <sub>10</sub>	2.28	11 300
Pentane	C <sub>5</sub> H <sub>12</sub>	2.24	40 200 <sup>a</sup>
Hexane	C <sub>6</sub> H <sub>14</sub>	2.25	120 000
Nonane	C <sub>9</sub> H <sub>20</sub>	2.32	643 000
Dodecane	C <sub>12</sub> H <sub>26</sub>	2.29	1 780 000
Cyclohexane	C <sub>6</sub> H <sub>12</sub>	2.31	20 000
<b>5-carbon alkanes</b>			
Pentane	CH <sub>3</sub> (CH <sub>2</sub> ) <sub>3</sub> CH <sub>3</sub>	2.24	40 200 <sup>a</sup>
2-Methylbutane	CH <sub>3</sub> C(CH <sub>3</sub> )H <sub>2</sub> C <sub>2</sub> H <sub>5</sub>	2.23	50 500 <sup>a</sup>
2,2-Dimethylpropane	C(CH <sub>3</sub> ) <sub>4</sub>	2.23	21 400 <sup>a</sup>
<b>2-carbon molecules with different saturation level</b>			
Ethane	C <sub>2</sub> H <sub>6</sub>	2.18	1 780 <sup>a</sup>
Ethylene	C <sub>2</sub> H <sub>4</sub>	2.10	1 200
Acetylene	C <sub>2</sub> H <sub>2</sub>	2.08	3 160 <sup>a</sup>
<b>Aromatic hydrocarbons</b>			
Benzene	C <sub>6</sub> H <sub>6</sub>	2.23	15 000
Naphthalene	C <sub>10</sub> H <sub>8</sub>	2.29	494 000
Anthracene	C <sub>14</sub> H <sub>10</sub>	2.45	4 330 000
Toluene	C <sub>6</sub> H <sub>5</sub> CH <sub>3</sub>	2.28	190 000

<sup>a</sup>Ref. [69].

In earlier work based on measurements of linewidths for four hydrocarbons, Tang *et al.* concluded that it was likely that the positrons interact primarily with C–H bond electrons in these molecules [136]. In order to test the possibility of positrons annihilating with C–C bond electrons using our improved data, we plot in Fig. 5.7 the linewidths,  $\Delta E$ , as a function of the fraction of valence electrons in C–C bonds for the alkanes including cyclohexane. The fact that  $\Delta E$  increases approximately linearly with the number of valence electrons in C–C bonds suggests that positrons are annihilating with C–C bond electrons. In principle, annihilation on C–H bond electrons can be separated from annihila-



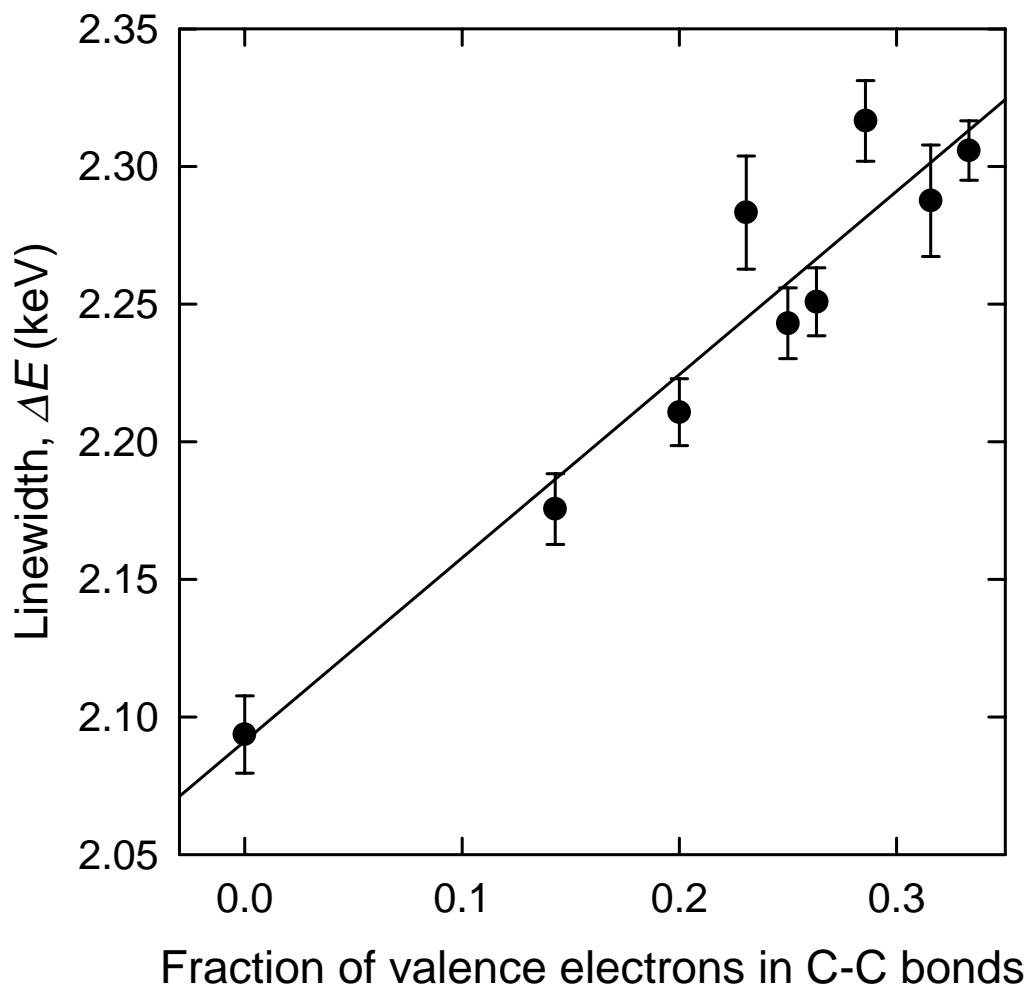


Figure 5.7: The Gaussian linewidth,  $\Delta E$ , plotted against the fraction of valence electrons in C-C bonds for alkane molecules, assuming two electrons each in the C-C and C-H bonds. The solid line is a fit to the data.

tion on C-C bond electrons assuming that each bond has its own characteristic linewidth. Then the linear combination of these linewidths weighted by the number of bond electrons should yield the observed linewidths. From a linear regression of the data in Fig. 5.7, we estimate the linewidths associated with the C-H bond and C-C bond electrons to be 2.09 keV and 2.76 keV, respectively.

The momentum distributions for the C-C bond and C-H bond electrons have been calculated previously [24]. Using the graphs of the calculated momentum distributions in Ref. [24], we estimate the predicted linewidths of C-H bond and C-C bond to be 2.06 keV and 2.42 keV, respectively. The predicted linewidth

for C–H bond electrons agrees reasonably well with our experimentally measured value of 2.09 keV. However, the linewidth extrapolated for the C–C bond electrons is in greater disagreement. These linewidths were calculated using the “static” approximation in which the effect of the positron was not included. As can be seen in the case for noble gases, wave functions without including the effect of the positron can give the qualitative estimates, but not the quantitative comparisons. Therefore, it is difficult to distinguish whether this discrepancy in the linewidth associated with the C–C bond is caused by the inadequacy of the approximation used in the calculations or by the validity of the assumption that positrons annihilate equally with any valence electron and the assumption that each bond has a characteristic linewidth.

This conclusion is in agreement with positron annihilation momentum distributions for liquid hexane and decane measured by using ACAR techniques [24]. Calculated momentum distributions for C–H and C–C bond electrons were compared with the observed ACAR spectra, and it was concluded that positrons annihilate with both C–H and C–C bond electrons.

#### 5.3.4 Alkane, alkene, and alkyne

Alkenes and alkynes are generally more reactive than alkanes because the  $\pi$  bond is weaker than the  $\sigma$  bond. The smallest members of the alkane, alkene, and alkyne families are ethane, ethylene, and acetylene, respectively. The values of the linewidths for these molecules are listed in Table 5.4. They show that, as the bond saturation level is reduced, the linewidths decrease. One possible explanation of this trend is that for the alkenes and alkynes, positrons can annihilate with  $\pi$ -bond electrons, which are less tightly bound and consequently have a smaller momentum distribution than that of the  $\sigma$ -bond electrons. Assuming that each chemical bond has its own characteristic linewidth and that the linear combination of these linewidths weighted with the number of bond electrons yields the observed linewidths, we estimate the linewidth of the C–C  $\pi$  bonds to be 1.48 and 1.73 keV for ethylene and acetylene, respectively, using the C–H bond and C–C  $\sigma$ -bond values of 2.09 and 2.76 keV. We would hope that these results would stimulate further theoretical work in this area.

#### 5.3.5 Aromatics

Aromatic compounds have very different electronic and geometrical structures compared to alkanes. The values of the linewidths from our measurements are listed in Table 5.4 for the smaller aromatic molecules benzene, naphthalene, and anthracene and for some of the substituted benzenes.

Table 5.5: The  $\gamma$ -ray linewidths for fully halogenated carbons (using Gaussian fits). (See Ref. [66] for the sources of  $Z_{\text{eff}}$  values.)

Molecule	Formula	$\Delta E$ (keV)	$Z_{\text{eff}}$
Carbon tetrafluoride	CF <sub>4</sub>	3.04	54.4
Carbon tetrachloride	CCl <sub>4</sub>	2.29	9 530
Carbon tetrabromide	CBr <sub>4</sub>	2.09	39 800

The existence of polycyclic aromatic hydrocarbons (PAH) in the interstellar media has been deduced from infrared measurements [2,3]. It was found that the PAH's have very large annihilation cross sections and, it has been conjectured that these molecules may contribute significantly to astrophysical positron annihilation [132]. This facet of the research is discussed in Ch. 7. Measurements of larger PAH's, such as pyrene, were attempted, but were not successful due to the low-vapor pressure of these substances.

### 5.3.6 Fully halogenated carbons

The linewidths for fully halogenated carbons are listed in Table 5.5 where we have ordered these molecules by the size of the halogen. The linewidths decrease from CF<sub>4</sub>, CCl<sub>4</sub>, to CBr<sub>4</sub>. This trend is very similar to that of the noble gas atoms; neon, argon, and krypton (Table 5.1). In addition, the linewidths are almost identical to those of analogous noble gas atoms, particularly for the larger halogens, as one would expect if the valence electrons of the carbon atoms were completely transferred to the halogen atoms. In particular, comparing the halocarbons and noble gas atoms, the linewidths are 3.04 (3.36) for CF<sub>4</sub> (Ne); 2.29 (2.30) for CCl<sub>4</sub> (Ar); and 2.09 (2.09) for CBr<sub>4</sub> (Kr). These data provide evidence that, in halocarbon molecules, the positron annihilates with the valence electrons of the halogen atoms.

The difference in the linewidths for hydrocarbons and perfluorocarbons are significant; hydrocarbons have large annihilation rates and relatively narrow linewidths, while perfluorocarbons have low annihilation rates and wide linewidths. It was concluded by Tang *et al.* [136] that positrons annihilate predominantly with C–H bonds in hydrocarbons and with fluorine atoms in perfluorinated molecules. In order to examine further the localization of positron annihilation in a molecule, exploiting the easily distinguishable annihilation linewidths for fluorine atoms and the C–H bonds, we have studied a series of partially fluorinated hydrocarbons. These results are discussed in the next subsection.

Table 5.6: The  $\gamma$ -ray linewidths for partially fluorinated hydrocarbons (using Gaussian fits).

Molecule	Formula	$\Delta E$ (keV)
Methane	CH <sub>4</sub>	2.09
Methyl fluoride	CH <sub>3</sub> F	2.77
Difluoromethane	CH <sub>2</sub> F <sub>2</sub>	2.86
Trifluoromethane	CHF <sub>3</sub>	2.85
Carbon tetrafluoride	CF <sub>4</sub>	3.04
Ethane	C <sub>2</sub> H <sub>6</sub>	2.18
Fluoroethane	C <sub>2</sub> H <sub>5</sub> F	2.62
1,1,1-Trifluoroethane	CF <sub>3</sub> CH <sub>3</sub>	2.95
1,1,2-Trifluoroethane	CHF <sub>2</sub> CH <sub>2</sub> F	2.91
1,1,1,2-Tetrafluoroethane	CF <sub>3</sub> CH <sub>2</sub> F	3.00
1,1,2,2-Tetrafluoroethane	CHF <sub>2</sub> CHF <sub>2</sub>	2.97
Hexafluoroethane	C <sub>2</sub> F <sub>6</sub>	3.04
Propane	C <sub>3</sub> H <sub>8</sub>	2.21
2,2-Difluoropropane	CH <sub>3</sub> CF <sub>2</sub> CH <sub>3</sub>	2.78
1,1,1-Trifluoropropane	CF <sub>3</sub> C <sub>2</sub> H <sub>5</sub>	2.86
Perfluoropropane	C <sub>3</sub> F <sub>8</sub>	3.05
Hexane	C <sub>6</sub> H <sub>14</sub>	2.25
1-Fluorohexane	CH <sub>2</sub> FC <sub>5</sub> H <sub>11</sub>	2.46
Perfluorohexane	C <sub>6</sub> F <sub>14</sub>	3.09
Benzene	C <sub>6</sub> H <sub>6</sub>	2.23
Fluorobenzene	C <sub>6</sub> H <sub>5</sub> F	2.43
1,2-Difluorobenzene	C <sub>6</sub> H <sub>4</sub> F <sub>2</sub>	2.66
1,3-Difluorobenzene	C <sub>6</sub> H <sub>4</sub> F <sub>2</sub>	2.52
1,4-Difluorobenzene	C <sub>6</sub> H <sub>4</sub> F <sub>2</sub>	2.53
1,2,4-Trifluorobenzene	C <sub>6</sub> H <sub>3</sub> F <sub>3</sub>	2.71
1,2,4,5-Tetrafluorobenzene	C <sub>6</sub> H <sub>2</sub> F <sub>4</sub>	2.77
Pentafluorobenzene	C <sub>6</sub> HF <sub>5</sub>	2.89
Hexafluorobenzene	C <sub>6</sub> F <sub>6</sub>	2.95

### 5.3.7 Partially fluorinated hydrocarbons

The experimentally measured  $\gamma$ -ray linewidths of a series of partially fluorinated hydrocarbons are summarized in Table 5.6, and a typical  $\gamma$ -ray spectrum is shown in Fig. 5.8(a). As pointed out earlier, the hydrocarbons have significantly

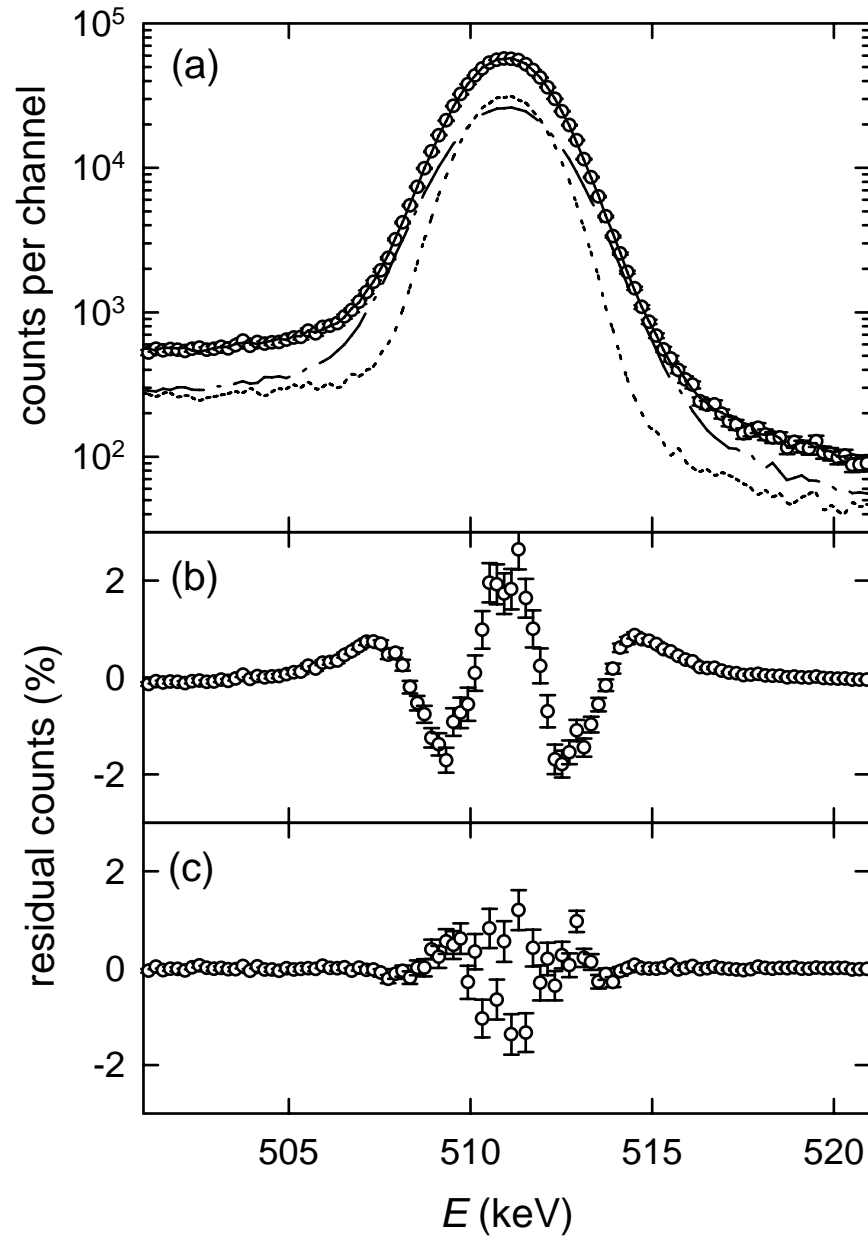


Figure 5.8:  $\gamma$ -ray spectrum from positron annihilation on fluoroethane: (a) ( $\circ$ ) observed spectrum, and (—) fit to the spectrum using a combination of the experimentally measured ethane and hexafluoroethane spectra. The two components in the fit are also shown: ( $\cdots$ ) the ethane spectrum and ( $-\cdot-$ ) the hexafluoroethane spectrum. The fraction of the area in the ethane component is 47.9 %, while that in hexafluoroethane is 52.1 %. (b) Residuals from a Gaussian fit ( $\chi_r^2 = 28.8$ ) plotted as a percentage of the peak height of the spectrum. (c) Residuals from the two spectrum fit ( $\chi_r^2 = 1.4$ ).

narrower linewidths than the perfluorocarbons [136]. This substantial difference between the two annihilation linewidths has now made it possible for us to distinguish multiple annihilation sites in a single molecule.

For the purpose of this analysis, the annihilation line shape cannot be modeled adequately with a Gaussian, as is evident from the residuals in Fig. 5.8(b) and the corresponding values of  $\chi_r^2$ , which are of the order of 20 to 40. However, at present, we do not know of an appropriate general functional form for the annihilation  $\gamma$ -ray line shape. Consequently, in order to separate the line shapes for the partially fluorinated hydrocarbons into two components, we fitted the spectra with a linear combination of the experimentally observed spectra for the analogous hydrocarbon and perfluorocarbon molecules. This fit has the amplitudes of the hydrocarbon and perfluorocarbon components as only two free parameters. A typical fit and residual are shown in Figs. 5.8(a) and (c). The fit produces  $\chi_r^2$  of order of unity, indicating that the model of fitting with the two experimentally measured spectra is an excellent one.

The area under the perfluorocarbon spectral component can yield the relative fraction of positrons annihilating on the fluorine atoms. This fraction is then normalized by the fraction of valence electrons on fluorine atoms in the perfluorinated molecule to take into account the annihilation on C-C bond electrons. The normalized fraction is plotted in Fig. 5.9 as a function of the fraction of the total number of valence electrons on the fluorine atoms. The good correlation between these two quantities, as seen in Fig. 5.9, suggests that the positrons annihilate with equal probability on any valence electrons. In this analysis, we have assigned eight valence electrons to each fluorine atom, assuming the formation of a closed shell neon-like structure, and two electrons each to a C-H bond and to a C-C  $\sigma$  bond. For a delocalized C-C  $\pi$  bonds in benzene, a total of six electrons is assumed in a benzene ring. We have assumed, for simplicity, that the line shape of annihilation from C-C bond electrons are the same as that from C-H bond electrons. As indicated in Sec. 5.3.3, this is probably not strictly correct, but it is likely to be a reasonable approximation since the number of C-C bond electrons is small compared to the total number of valence electrons, and the C-C bond linewidth is not as wide as that from fluorine atoms.

The only theoretical prediction we are aware of regarding positron localization in molecules is the study of positron attachment using approximate molecular orbital theory by Schrader and Wang [123]. A study of ethylene and its fluoro derivatives predicts that the positron is likely to be found preferentially in the vicinity of the hydrogen atoms. (e.g., for  $C_2H_3F$ , 99% of the positron density is in the vicinity of the two hydrogen atoms attached to one carbon atom.) Our experimental results do not confirm this prediction.

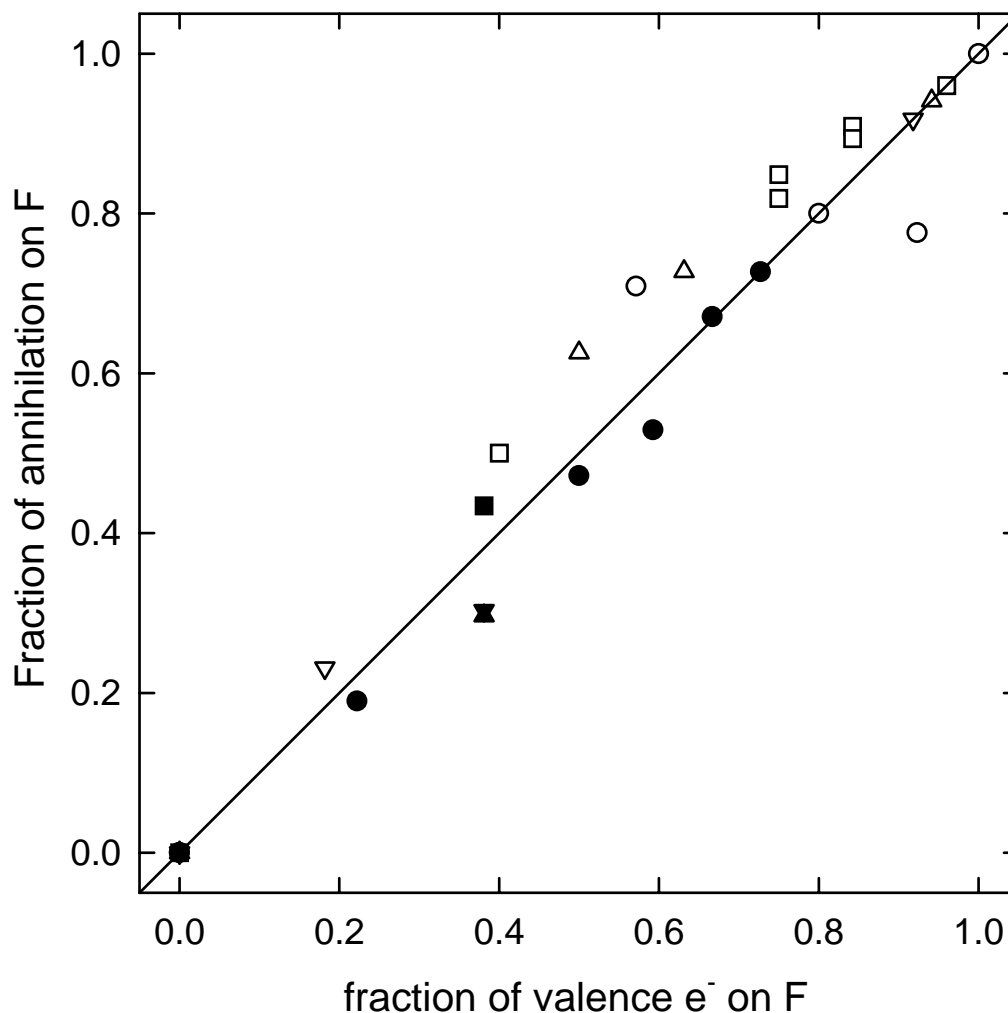


Figure 5.9: Normalized fraction of positrons annihilating on fluorine atoms plotted against the fraction of the valence electrons on fluorine atoms. The fraction of annihilation on perfluorocarbons is obtained with the two-spectrum fitting procedure. This fraction is normalized with the fraction of valence electrons in fluorine atoms in the perfluorocarbons: (○) one-carbon (i.e., methane-based) molecules, (□) two-carbon (ethane-based) molecules, (△) three-carbon (propane-based) molecules, (▽) six-carbon (hexane-based) molecules. Filled symbols are for six-carbon (benzene-based) molecules with (solid square) 1,2-difluorobenzene, (solid triangle up) 1,3-difluorobenzene, (solid triangle down) 1,4-difluorobenzene, and (●) other six-carbon (benzene-based) molecules.

We have measured three different isomeric configurations of difluorobenzenes. The 1,2-difluorobenzene has a higher fraction of positron annihilation on the fluorine atoms than does the 1,3- or 1,4-difluorobenzene. This may be due to

Table 5.7: The  $\gamma$ -ray linewidths for other organic molecules (using Gaussian fits). (See Ref. [66] for the sources of  $Z_{\text{eff}}$  values.)

Molecule	Formula	$\Delta E$ (keV)	$Z_{\text{eff}}$
Methanol	CH <sub>3</sub> OH	2.59	1 510
Tetraethylsilane	Si(C <sub>2</sub> H <sub>5</sub> ) <sub>4</sub>	2.37	524 000
Nitrobenzene	C <sub>6</sub> H <sub>5</sub> NO <sub>2</sub>	2.47	430 000
Pyridine	C <sub>5</sub> H <sub>5</sub> N	2.34	85 400 <sup>a</sup>

<sup>a</sup>Ref. [69].

the dipole moment, which is the largest for the 1,2-isomer.

### 5.3.8 Other organic molecules

The linewidths of four other molecules are listed in Table 5.7. Methanol has a  $Z_{\text{eff}}$  value an order of magnitude larger than methane. The O–H group also increases the annihilation  $\gamma$ -ray linewidth. Pyridine has a similar electronic structure to benzene. It has a higher  $Z_{\text{eff}}$  value and a somewhat larger linewidth.

### 5.3.9 Annihilation on inner-shell electrons

Our data show that positrons annihilate predominantly with the valence electrons in atoms or molecules. The potential exerted by the atomic nucleus on a positron is repulsive, so that the amplitude of the positron wave function is small near the inner-shell electrons. However, a small fraction of positrons can tunnel through this repulsive potential and annihilate with inner-shell electrons. The typical linewidth from inner-shell electron annihilation is expected to be  $\Delta E > 5$  keV [53], and a study of inner-shell electron annihilation requires a detailed study of this region of  $\gamma$ -ray spectra. Evidence of inner-shell electron annihilation can be seen in our data for Ar and Kr (Fig. 5.4). Using the amplitude of spectra around 516 keV, where we expect that the contribution from valence electron annihilation is small, we estimate the upper bound of inner-shell electron annihilation contribution to be 2% and 3% for Ar and Kr, respectively. A similar analysis of carbon monoxide data indicates the upper bound on inner-shell annihilation to be 3% in this molecule, which may explain the large deviation from a Gaussian line shape discussed in Sec. 5.3.2. This bound on inner-shell annihilation in hexane is 1%, which is smaller than those for Ar and Kr. As a consistency check, we estimate the upper bound for H<sub>2</sub> (which does not have inner-shell electrons) to be 0.1%, which is much smaller than those of the



Table 5.8: Values of  $\chi_r^2$  from fits to various models.

Molecule	1 Gauss. Eq. (3.3)	Non-interacting H Eq. (5.6)	Gauss. convolved to Eq. (5.6) Eq. (5.7)	2 Gauss. Eq. (C.1)
Hydrogen	14.9	9.7	1.4	2.0
Krypton	33.4	32.6	17.1	2.3
Hexane	9.9	65.0	5.8	1.4

substances with inner-shell electrons. A more detailed description of inner-shell electron annihilation is presented in Ch. 6 [70].

## 5.4 Spectral analysis beyond the 1-Gaussian approximation

The analyses of the measured spectra discussed thus far were done using either a single-Gaussian approximation or using a combination of the experimentally measured line shapes (e.g., in the case of the partially fluorinated hydrocarbons). As discussed in Sec. 5.3, we have observed departures from Gaussian line shapes, and examples are shown in Figs. 5.10 and 5.11. We have also attempted to use other functional forms for fitting the observed spectra. Values of  $\chi_r^2$  from various fits are summarized in Table 5.8 for hydrogen, krypton, and hexane as examples. For the hydrogen atom, in the approximation that the positron does not perturb the electron wave function, the line shape is predicted to be  $1/[1+C^2(E-E_0)^2]^3$ , where  $C = 4\pi a_0/(hc) = 0.536 \text{ eV}^{-1}$ ;  $a_0$  is the Bohr radius, and  $h$  is the Planck constant [64]. Motivated by this prediction, we convolved the function

$$g(E) = 1/[1 + b(E - E_0)^2]^3 \quad (5.4)$$

with the detector response, which we parameterize by

$$r(E) = B_1 \exp \left[ - \left( \frac{E - E_0}{a\Delta E_{\text{det}}} \right)^2 \right] + B_2 \text{erfc} \left( \frac{E - E_0}{a\Delta E_{\text{det}}} \right) + B_3. \quad (5.5)$$

We tried to fit the resulting function,

$$G(E) = \int_0^\infty g(E')r(E - E')dE', \quad (5.6)$$

to some of the observed spectra, using  $\Delta E_{\text{det}} = 1.16 \text{ keV}$ , and  $E_0$ ,  $B_1$ ,  $B_2$ ,  $B_3$ , and  $b$  as the fitting parameters. Examples of the fits and the residuals using Eq. (5.6) are shown in Figs. 5.10 and 5.11. As indicated in Table 5.8, these

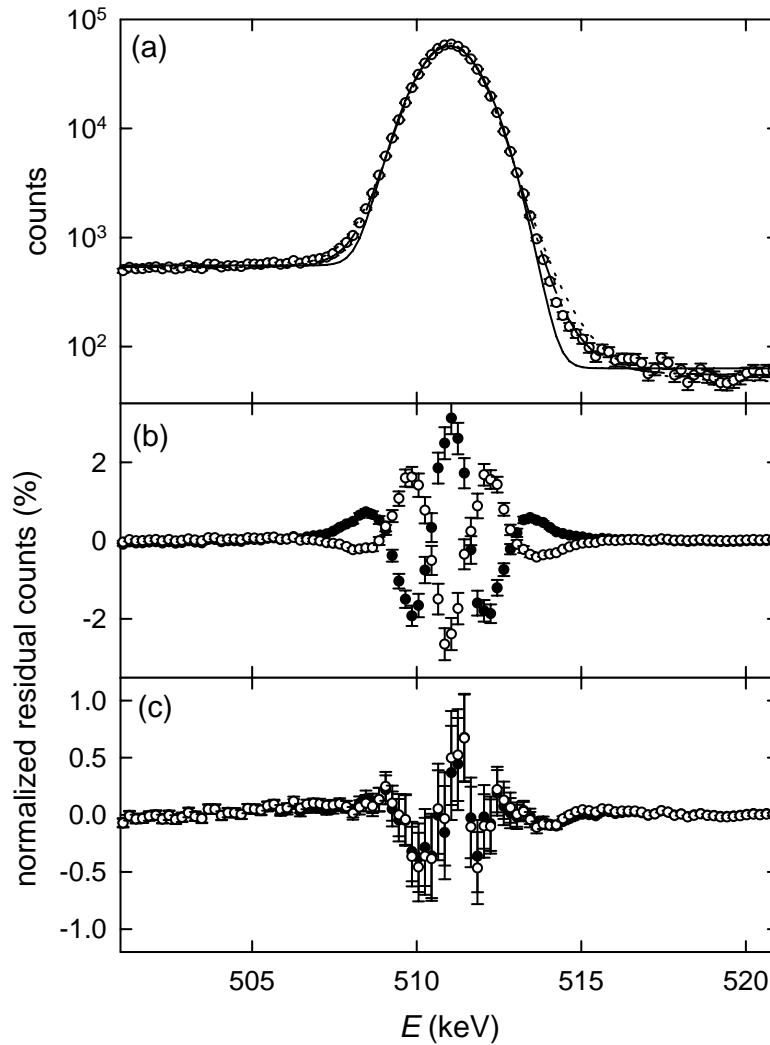


Figure 5.10: (a)  $\gamma$ -ray spectrum of  $\text{H}_2$ : (o) observed spectrum; (—) Gaussian fit [Eq. (3.3)]; ( $\cdots$ ) fit with non-interacting atomic hydrogen functional form [Eq. (5.6)]; and (---) fit with Gaussian convolved non-interacting H form [Eq. (5.7)]. (b) ( $\bullet$ ) residuals from the Gaussian fit and (o) residuals from the non-interacting hydrogen fit. (c) ( $\bullet$ ) residuals from the Gaussian convolved non-interacting hydrogen fit and (o) residuals from the 2-Gaussian fit [Eq. (C.1)].

fits produced generally larger values of  $\chi_r^2$  than the Gaussian fits [Eq. (3.3)], especially for the hydrocarbons. Fits to the hydrogen, helium, and xenon spectra with this functional form created slightly smaller  $\chi_r^2$  values than those from the Gaussian fits, but these values are still much greater than unity.

It is interesting to note that the residuals from the Gaussian fits [Eq. (3.3)]

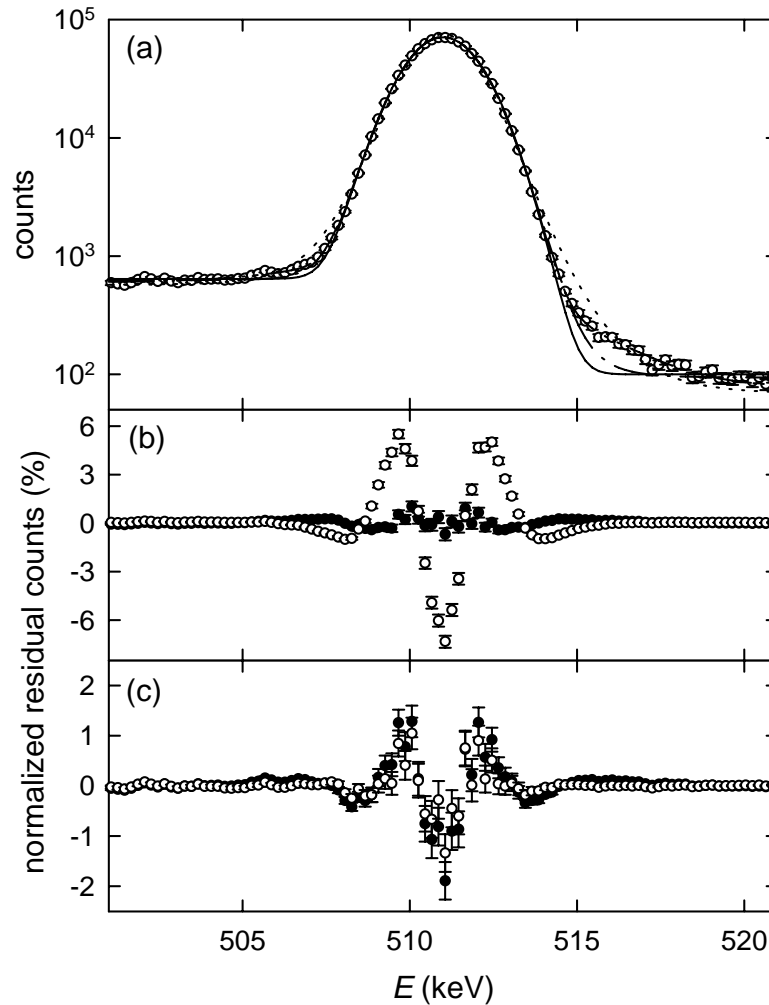


Figure 5.11: (a)  $\gamma$ -ray spectrum of hexane ( $C_6H_{14}$ ): ( $\circ$ ) observed spectrum; (—) Gaussian fit [Eq. (3.3)]; ( $\cdots$ ) fit with non-interacting atomic hydrogen functional form [Eq. (5.6)]; ( $-\cdot-$ ) fit with Gaussian convolved non-interacting H form [Eq. (5.7)], and (---) fit with 2-Gaussian fit [Eq. (C.1)]. (b) ( $\bullet$ ) residuals from the Gaussian fit and ( $\circ$ ) residuals from the non-interacting hydrogen fit. (c) ( $\bullet$ ) residuals from the Gaussian convolved non-interacting hydrogen fit and ( $\circ$ ) residuals from the 2-Gaussian fit.

are positive at the peak, while the residuals from fits with Eq. (5.6) are negative. A Gaussian line shape is expected from positrons annihilating with free electrons having a thermal momentum distribution. The potential exerted by the nuclei in the atoms or molecules will tend to increase the population of high momentum components of the electrons. There are two different interactions that can account for the difference between the observed spectra and the func-

tional form Eq. (5.4), which is derived in the approximation that the positron does not disturb the electronic configuration of a hydrogen atom. One is the presence of the other electrons in the atom or molecule. The other is the effect of the positron on the atom or molecule. The fact that the distribution lies between the form of Eq. (5.4) and the Gaussian shape indicates that the distribution is more “relaxed” compared to Eq. (5.4), in other words, the distribution is more free-electron like. The effect of other electrons seems to be strong, as can be seen by the poor fit to Eq. (5.6) for the case of hydrocarbons. In principle, measurement of  $\gamma$ -ray spectra from atomic hydrogen is possible [151], and it would indicate the magnitude of the effect of the positron on the momentum distribution.

Since the actual line shape lies somewhere between the Gaussian shape and Eq. (5.4), we attempted fitting another function, which is the line shape from Eq. (5.4),  $g(E)$ , convolved with a Gaussian having a variable width  $\Delta E$ ;

$$h(E) = \int_0^\infty g(E') \exp \left[ - \left( \frac{E - E' - E_0}{a\Delta E} \right)^2 \right] dE'. \quad (5.7)$$

This was an attempt to take into account the degree to which electrons “relax” from the potential exerted by the nuclei due to the effect of the nearby positron. This function,  $h(E)$ , was then convolved with the detector response given by Eq. (5.5) and used for the actual fit. This function has 6 free parameters. As can be seen in Figs. 5.10(a) and (c), it fits spectra of some atoms and molecules reasonably well, but does not fit others such as argon and krypton.

We have also tried to fit two Gaussians to the data. This fitting function produces values of  $\chi_r^2$  around unity, and the residuals are generally within the error bars as can be seen in Figs. 5.10(c) and 5.11(c). However, the widths of two Gaussians and the relative amplitude of the second Gaussian are highly correlated, and we know of no physical meaning for such a line shape. Nonetheless, the two Gaussian fit is a convenient way of representing the data more accurately with an analytic form. The fitting procedure using two Gaussians is discussed in Appendix C, along with a compilation of the fitting parameters for various atoms and molecules resulting from this analysis.

## 5.5 Discussion

Previous theoretical studies of positron annihilation in gases have focused on understanding annihilation rates. This is likely due, at least in part, to the fact that experimental data for annihilation rates are available for a variety of substances, while, previous to our positron trap experiments, there have been relatively few

ACAR and  $\gamma$ -ray Doppler broadening studies of atoms and molecules, except for media sufficiently dense that multiple atom and molecule effects may not be neglected. Consequently, we expect that the data presented here will be useful for comparison with the predictions of theoretical models of low-energy positron-molecule interactions. As described above, we have recently carried out such a comparison for the case of helium, resulting in excellent agreement [140].

In order to calculate either annihilation rates or  $\gamma$ -ray line shapes, the combined wave function for the positron and electrons must be calculated. Once the wave function is known, calculation of either the annihilation rate or the Doppler-broadened annihilation line shape is straightforward. Specific calculations that would be useful include prediction of the  $\gamma$ -ray spectra for annihilation on noble gases, where theory and experiment are not in good agreement except for helium; inorganic molecules such as nitrogen and carbon monoxide, which showed strong non-Gaussian features; the C–H and C–C bonds in alkanes; the  $\sigma$  and  $\pi$  bonds in aromatics such as benzene; and calculations for halocarbons.

We described an unsuccessful attempt to find a physically meaningful “universal line shape” beyond the single Gaussian applicable to a variety of atoms and molecules. Theoretical insights on this subject would be of value. Does such a general function exist, and if so, what is its physical interpretation?

Regarding possible improvements in experimental capabilities, we now have the ability to vary the temperature of the trapped positrons in a systematic way, and a study of annihilation rates in noble gases has been recently carried out, varying the temperature of the positron gas from room temperature to about 0.6 eV [74]. Thus, in the near future, we should be able to provide data on the effect of positron temperature on  $\gamma$ -ray linewidths. The increased temperature of the positrons may, for example, change the fraction of annihilations at specific sites in molecules, and we will be able to search for this effect.

It is interesting to note that our measurements of the temperature dependence of annihilation rates on noble gas atoms [74] agree well with calculations using the polarized-orbital approximation [91–94]. However, the absolute values of the annihilation rates [25] are underestimated in these calculations, and the predicted  $\gamma$ -ray linewidths (described in Sec. 5.3.1) are larger than those that are observed. Thus calculations in this approximation are capable of capturing the temperature dependences, but not the absolute annihilation rates or the  $\gamma$ -ray spectra.

Our  $\gamma$ -ray spectral measurements on partially fluorinated hydrocarbons indicate that positrons annihilate with equal probability with any of the valence electrons. In addition, the data from the alkanes are also consistent with annihilation with equal probability on any valence electron. At present, we do

not see how the  $\gamma$ -ray spectral measurements give direct information about the physical process responsible for the anomalously large annihilation rates. It is interesting to note that, as discussed in Sec. 5.3.1, the “static” approximation gives reasonably good estimates for the  $\gamma$ -ray linewidths, but not for the annihilation rates. This may point to the importance of short-range correlation between the positron and electrons in calculating annihilation rates, which is reasonable, since the overlap in the positron and electron wave functions determines the annihilation rate. This correlation does not seem to be critical for the calculation of the  $\gamma$ -ray spectra.

## 5.6 Concluding Remarks

In this chapter, we have presented measurements of the Doppler broadening of the annihilation  $\gamma$ -ray line, which complement other studies of positron-molecule interactions. Measurements were performed on a wide variety of substances, including noble gases, inorganic molecules, alkanes, aromatics, and substituted alkanes. The precision of the measurements is sufficiently high that, for the first time in gaseous media, one can distinguish non-Gaussian features in the line shapes. In the case of helium, the measurements are in excellent agreement with new, state-of-the-art theoretical calculations.

We have also shown that we are able to distinguish annihilation on specific sites in molecules, such as on fluorines and on C–H bonds in partially fluorinated hydrocarbons. These partially fluorinated hydrocarbon data indicate that positrons annihilate with equal probability on the valence electrons. Interpretation of our data for alkanes is also consistent with this statistical model, where the valence electrons are those in the C–H and C–C bonds in this case. The results presented in this chapter for the  $\gamma$ -ray spectra from positron annihilation will provide useful tests of theoretical models of positron-atom and positron-molecule interactions.

## Chapter 6

# Positron annihilation with inner-shell electrons in noble gas atoms

The inner-shell electron annihilation, which was described briefly in Sec. 5.3.9, is discussed here. This work is published in Ref. [70].

### 6.1 Introduction

Positrons annihilate predominantly with valence electrons in insulators or with conduction electrons in metals because of the repulsive potential exerted on the positron by the nuclei. However, a small fraction of the positrons can tunnel through this repulsive potential and annihilate with inner-shell electrons. In the work presented here, we detect inner-shell annihilation by measuring the momentum distribution of the annihilating electron-positron pairs by the Doppler broadening of the annihilation  $\gamma$  rays. Inner-shell annihilation has been studied previously for positrons interacting with condensed matter targets using a clever coincidence technique with two detectors [9,84]. This technique improves the signal-to-noise ratio, which in turn enables one to explore the high momentum region of the spectra. The interactions in condensed matter, however, are very different from the isolated interaction of a positron with a single atom discussed here. For example, in metals the positron forms a Bloch wave under the periodic potential generated by the ions, while positron annihilation in a single atom is a scattering process. We confine positrons for a long time in the positron trap, so that they can be used efficiently, as discussed in Ch. 3. Using this positron trap, we have been able to obtain sufficiently good statistics to identify inner-shell

annihilation using a single detector.

In this chapter we present precise measurements of the annihilation  $\gamma$ -ray spectra for argon, krypton, and xenon. The measured spectra are compared with calculations based on the Hartree-Fock (HF) approximation. The high momentum components in the spectra provide a quantitative measure of the fraction of positrons that annihilate with inner-shell electrons. This is the first experimental study of positrons annihilating with inner-shell electrons in isolated two-body positron-atom interactions.

## 6.2 Experiment

Measurements of the  $\gamma$ -ray spectra are performed using a technique similar to previous measurements as discussed in Sec. 3.6 [69, 136]. The data were taken for 12 h for argon and krypton and for 58 h for xenon. The spectra were taken in 1-h time segments, and the drift in the detector (less than 0.01 keV in 12 h) was carefully monitored. The number of positrons in each fill was adjusted to minimize  $\gamma$ -ray pile-up.

## 6.3 Results

The observed spectra were first fitted with the Gaussian function, similarly to that discussed in Ch. 5. The step function and the baseline were then subtracted, after convolution of the step function with the fitted Gaussian width. The amplitudes of the step function and the baseline were determined by requiring that the spectrum be zero at energies far (e.g., 15 keV) from the centroid of the peak (511 keV).

The corrected spectra for xenon, krypton, and argon are shown in Figs. 6.1, 6.2, and 6.3, respectively. The error bars represent the expected statistical variation in spectral amplitude due to counting statistics. The spectra can be resolved over four orders of magnitude in spectral amplitude, and this is crucial in separating the contribution to the annihilation signal due to inner-shell electrons from that due to electrons in the outermost shell. In Figs. 6.1, 6.2, and 6.3, only the high energy side of the symmetric  $\gamma$ -ray line is shown, since this region has greater statistical significance due to absence of the Compton scattering component. The measured and calculated spectra are normalized so that  $\int_0^\infty f(E)dE = 1$ , where  $f(E)$  is the amplitude of the spectrum at  $\gamma$ -ray energy,  $E$ . The theoretically predicted spectra shown in Figs. 6.1, 6.2, and 6.3 have been convolved with the Gaussian detector response, which has a full width at half maximum (FWHM) of 1.16 keV.



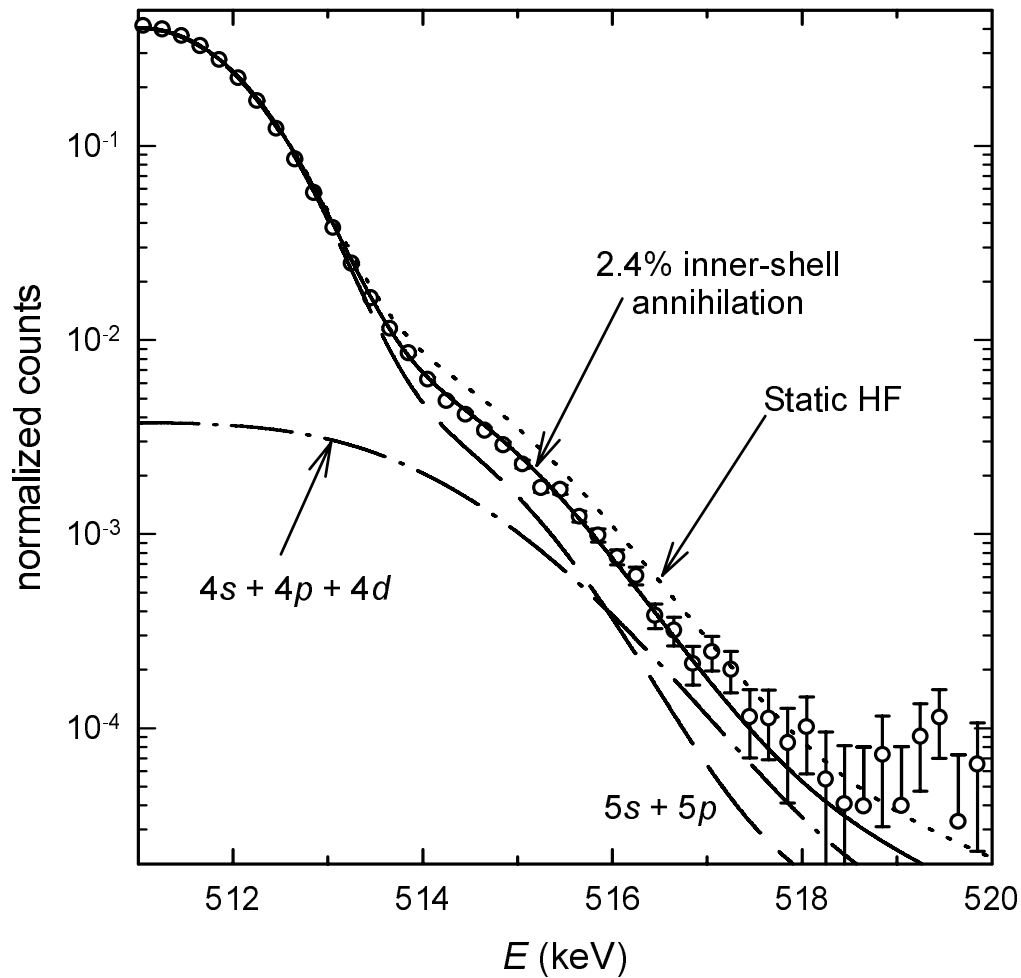


Figure 6.1: The Doppler-broadened  $\gamma$ -ray spectrum resulting from positrons annihilating on xenon atoms at  $p = 2 \times 10^{-6}$  Torr. Shown are the experimental data ( $\circ$ ); the static Hartree-Fock calculation ( $\cdots$ ); the best fit to the data ( $—$ ), which includes a 2.4% contribution from the states with principle quantum number  $(n - 1) = 4$ ; the contribution from the outer-shell states with  $n = 5$  ( $- - -$ ); and that from the inner-shell states with  $(n - 1) = 4$  ( $- \cdot -$ ).

In order to identify the contributions of inner-shell electrons to the annihilation  $\gamma$ -ray spectra, the line shapes were calculated using the static HF approximation [70]. In this approximation, the wave function of the positron at thermal energies is calculated from the Schrodinger equation using the potential of the HF atomic ground state, and annihilation  $\gamma$ -ray spectra are determined for electrons in each atomic subshell. The annihilation fractions,  $\zeta$ , and the associated

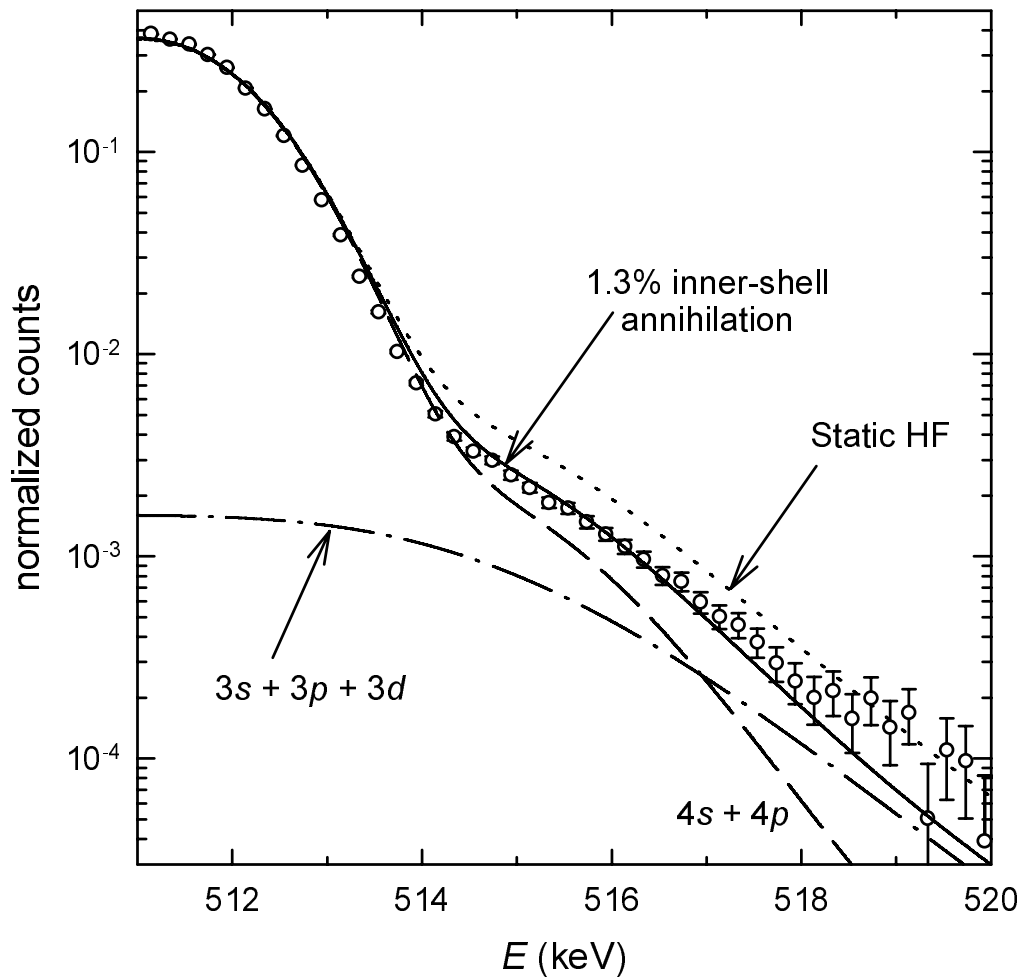


Figure 6.2: The Doppler-broadened  $\gamma$ -ray spectrum resulting from positrons annihilating on krypton atoms at  $p = 9 \times 10^{-6}$  Torr. The notation is similar to that in Fig. 6.1.

line shapes (FWHM),  $\Delta E$ , for electrons from the two outer shells with principal quantum numbers  $n$  and  $n - 1$  are summarized in Table 6.1 for argon, krypton, and xenon ( $n = 3, 4, 5$ , respectively). The sum of the annihilation fractions for the two outer subshells  $\zeta_{nl}$  and those from the three (or two, for argon) inner subshells  $\zeta_{(n-1)l}$  is normalized to unity. There is good agreement between the widths and shapes of the  $\gamma$ -ray spectra obtained in the static HF approximation and the experimental data (see Table 6.1 and Figs. 6.1, 6.2, and 6.3).

As expected, the main contribution to the annihilation probability comes from the outer-shell electrons. The linewidths from inner-shell annihilation (3.3–

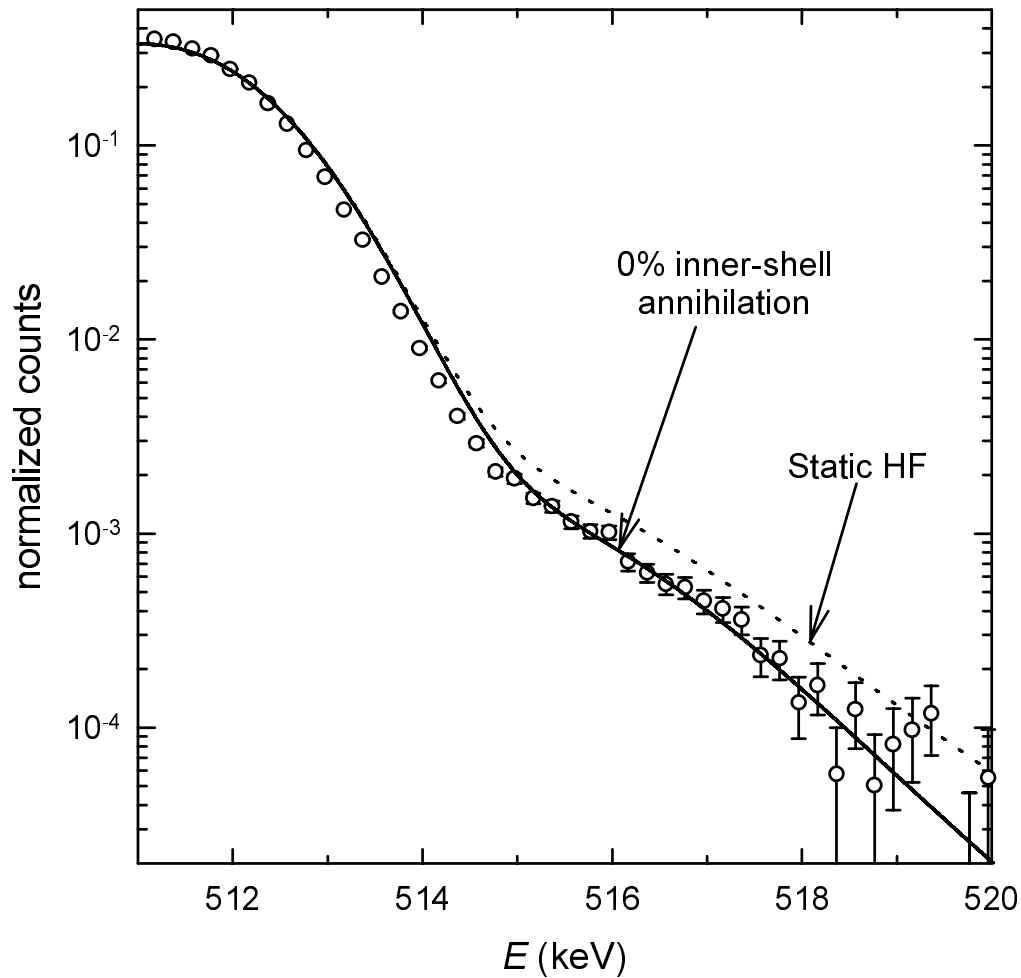


Figure 6.3: The Doppler-broadened  $\gamma$ -ray spectrum resulting from positrons annihilating on argon atoms at  $p = 2 \times 10^{-5}$  Torr. The notation is similar to that in Fig. 6.1.

9.4 keV) are much larger than those from outer shells (1.4–2.9 keV) due to the higher momenta of the former. The values of  $\zeta_{(n-1)l}$  are roughly proportional to the number of electrons in the  $s$ ,  $p$ , and  $d$  subshells, namely 2, 6, and 10, respectively. The lack of an inner  $d$  subshell for argon (only 8 electrons in the inner shell as compared to 18 for krypton and xenon) results in a lower total annihilation fraction from inner-shell electrons relative to krypton and xenon (Table 6.1). The reason for  $\zeta_{(n-1)d}$  in xenon being greater than  $\zeta_{(n-1)d}$  in krypton is the more diffuse character of the  $d$  orbital in xenon; the radial density of the  $(n-1)d$  orbital in xenon peaks at 0.75 a.u., as compared to 0.4 a.u. for  $(n-1)d$

Table 6.1: The FWHM of annihilation  $\gamma$ -ray spectra,  $\Delta E$  (in keV), and partial contributions to the annihilation probability from the subshells of noble-gas atoms,  $\zeta$ , calculated in the static Hartree-Fock approximation.

Shell	Argon		Krypton		Xenon	
	$\Delta E$	$\zeta$	$\Delta E$	$\zeta$	$\Delta E$	$\zeta$
$np$	2.89	0.808	2.56	0.804	2.22	0.791
$ns$	1.86	0.181	1.66	0.164	1.41	0.161
$(n-1)d$	–	–	8.85	0.021	6.73	0.036
$(n-1)p$	9.41	0.008	7.65	0.009	5.80	0.009
$(n-1)s$	5.18	0.003	4.35	0.003	3.34	0.003
total	2.65	1	2.38	1	2.06	1
experiment	2.30	–	2.09	–	1.92	–
$(n-1)$ tot., th.	–	0.012	–	0.033	–	0.048
$(n-1)$ fit	–	< 0.002	–	0.013	–	0.024

in krypton, and the value of  $\Delta E$  is smaller for the  $d$  orbital in xenon.

As can be seen from Figs. 6.1 and 6.2, a contribution from the shell with principal quantum number  $(n-1)$  is essential to account for the shape of the high-energy tail in the spectra of xenon and krypton. However, it appears that the static HF approximation overestimates the values of  $\zeta_{n-1}$  by about a factor of two. There are positron-electron correlation effects, not treated by the static approximation, which preferentially enhance the annihilation rate for the most weakly bound electrons, i.e., the outer-shell electrons. On the other hand, they do not affect much of the shape of the  $\gamma$ -ray spectra, as suggested by the agreement observed in Figs. 6.1, 6.2 and 6.3. This enables us to treat the fraction of annihilations with the inner-shell electrons as a fitted parameter,  $\zeta_{n-1}^*$ , to obtain a more precise estimate of this effect. Thus, we are able to achieve good agreement (shown as the solid line in Fig. 6.1) over four orders of magnitude in spectral amplitude with  $\zeta_{n-1}^* = 0.024$ , compared with the static HF value of  $\zeta_{n-1} = 0.048$  for xenon (Table 6.1). Figure 6.2 shows the results of this analysis for krypton, with similarly good agreement for the spectral line shape. In this case, the fitted value,  $\zeta_{n-1}^* = 0.013$ , which is approximately 40% of that predicted by the static HF calculation. For argon (Fig. 6.3) the comparison between the measurement and the theory cannot accurately determine the contribution of inner-shell annihilation events. We estimate  $\zeta_{n-1}^* < 0.002$ , which is less than 20% of the value predicted by the static theory.

We note that, in the analysis presented in Asoka-Kumar *et al.* (Ref. [9]), the

high-momenta “shoulder” of the  $\gamma$ -ray spectrum was fitted by the inner-shell annihilation contribution alone. It is clear from our work that the outer-shell annihilation spectra also possess this “shoulder”-like feature due to oscillations in the structure of the outer-shell electron wave functions. Neglect of this would result in an overestimate of the fraction of inner-shell annihilation.

While good agreement for the annihilation  $\gamma$ -ray spectra is achieved using simple static HF theory, there is considerable evidence that the positron wave function obtained in this approximation is not correct. For example, the HF approximation fails to reproduce positron-atom scattering and seriously underestimates the total annihilation rate [39]. There is a strong attractive potential between the positron and the atom due to polarization of the atom by the electric field of the positron and virtual positronium formation [39,54]. As a result, the actual positron wave function near the atom is much larger than that predicted by the static approximation. There are also short-range correlation effects due to the electron-positron interaction. These interactions enhance the total wave function at small electron-positron separations and further increase the annihilation rate. However, as seen from Figs. 6.1, 6.2 and 6.3, these effects seem to have little influence on the shapes of the  $\gamma$ -ray spectra. In particular, the  $\gamma$ -ray spectra are expected to be insensitive to short-range electron-positron correlation effects, since the spectra depend only on the momentum of the electron-positron pairs, and their center-of-mass momenta are weakly affected by this correlation. This means that the annihilation spectra are basically determined by the momentum distribution of the atomic electrons, which are described well by the HF approximation.

There are correlational corrections, which can account for the discrepancy between the theoretical and experimental  $\Delta E$  (Table 6.1). As discussed above, correlations also lead to a large enhancement of the annihilation rates, which is greater for the weakly bound outer-shell electrons. Accordingly, the fitted  $\zeta_{(n-1)}^*$  values are smaller than  $\zeta_{(n-1)}$  from the static HF calculation.

The robust nature of the shapes of the  $\gamma$ -ray spectra in atoms should be of help in analyzing the details of positron interactions in more complicated systems such as molecules and solids. For example, the annihilation  $\gamma$ -ray spectra can provide quantitative information about preferential sites of positron annihilation in molecules [69].

An important implication of the inner-shell annihilation is the emission of Auger electrons and the consequent formation of doubly ionized atoms. The positron-induced Auger electron emission has been observed in condensed matter [142]. The work described here opens up a possibility of the Auger spectroscopy in gaseous media. Our work suggests that the doubly ionized atoms, associated

with Auger electron emission, should be observable, e.g., using time-of-flight mass spectrometry [63,109]. We expect the highest production of doubly ionized atoms for heavier atoms such as krypton and xenon since they have large inner-shell annihilation fractions.

## 6.4 Concluding remarks for inner-shell electron annihilation

In summary, our experimental results demonstrate that positron annihilation with inner-shell electrons can be studied in a quantitative manner in isolated atomic systems. While a simple static HF calculation was used successfully to identify the inner-shell electron contribution, the relative fraction of annihilations with inner-shell electrons is not predicted accurately by this theory. We hope that these results will motivate further theoretical work in this area.

## Chapter 7

# Positron annihilation in the interstellar media

Simulations of positron annihilation in the interstellar media (ISM) have previously been studied [14, 68]. Since these publications, new information has emerged from observations with various instruments on the Compton Gamma Ray Observatory (GRO). In this chapter, positron annihilation in the ISM is discussed. After an introduction (Sec. 7.1), a brief summary of current understanding of positron annihilation is described in Sec. 7.2. The observational evidence of the existence of interstellar polycyclic aromatic molecules (PAH's) is discussed in Sec. 7.3, followed by our positron annihilation study in a simulated ISM, namely, hydrogen-PAH mixture, in Sec. 7.4, and this chapter is summarized in Sec. 7.5.

### 7.1 Introduction

The 511-keV positron annihilation line is the strongest  $\gamma$ -ray line of astrophysical origin [80, 117], and it has been studied extensively, both observationally and theoretically [16, 128, 141]. The narrow energy spread of the observed annihilation line is interpreted as coming from positrons that have been slowed down to a few eV before annihilating on either free electrons or on electrons in molecules of the ISM. The physics of positron slowing and annihilation in the ISM has been the subject of many analytical models and numerical simulations [46, 56]. One scenario postulates that the positrons thermalize with the ISM and then annihilate on neutral gas atoms and molecules [141]. In this case, the line shape of the  $\gamma$ -ray spectrum would be determined entirely by the temperature and chemical composition of the ISM. In this kind of interstellar environment, PAH's

may contribute significantly to the positron annihilation, since these molecules have anomalously high annihilation rates as discussed earlier, even though their abundance is much lower than that of hydrogen atoms.

Another scenario for the fate of astrophysical positrons involves annihilation following in-flight positronium atom formation by interaction with neutral gas atoms and molecules. In this scenario, the  $\gamma$ -ray line shape would be qualitatively different from that of annihilation on neutral atoms and molecules, and would depend on the dynamics of the slowing-down process. The effects of the temperature of annihilating media have also been studied theoretically [56]. Other scenarios include the effects of interstellar dust and molecular clusters [152].

The technique we have developed for accumulating and storing cold positrons in a vacuum of less than  $10^{-9}$  torr provides a tool for studying low-energy positron-molecule interactions in an environment relevant to that of the ISM. We have previously measured annihilation rates [66, 67, 101, 102, 134] and annihilation  $\gamma$ -ray spectra [69, 70, 136], and discovered that large organic molecules, such as PAH's, have anomalously high annihilation rates (attributed to resonance binding of the positron to the molecule) [134] with measurably different  $\gamma$ -ray spectra from that of hydrogen as described in Ch. 5 [69, 136].

## 7.2 Positrons in the interstellar media

Recently, the Gamma Ray Observatory has increased our knowledge of astrophysical positron annihilation dramatically [20, 33, 113, 114]. The strongest sources of positron annihilation  $\gamma$  rays are those associated with our Galaxy. The spatial distribution of the radiation has been observed to show three distinct features: a central bulge, the galactic plane, and an enhancement or extension of emission at positive latitudes above the galactic center [33, 113]. The time variation of radiation intensity, previously noted in balloon experiments, was not observed by the GRO [114].

An observed  $\gamma$ -ray spectrum from these Galactic regions is shown in Fig. 7.1. This spectrum is taken using a NaI(Tl)-CsI(Na) detector, and the energy resolution at 511 keV is  $\sim 9\%$ . The data were fitted over the energy range 0.05-4.0 MeV with a function consisting of a single powerlaw, a photopeak line fixed in energy and width at 511 keV and 2.5 keV, respectively, and a positronium continuum component. The fitted photopeak and positronium components corresponds to a positronium fraction of  $0.98 \pm 0.04$  [113], which indicates that almost all of Galactic positrons form positronium atoms. This spectral analysis of annihilation radiation makes the scenario of direct positron annihilation on atoms and molecules less likely for the positrons associated with our Galaxy.



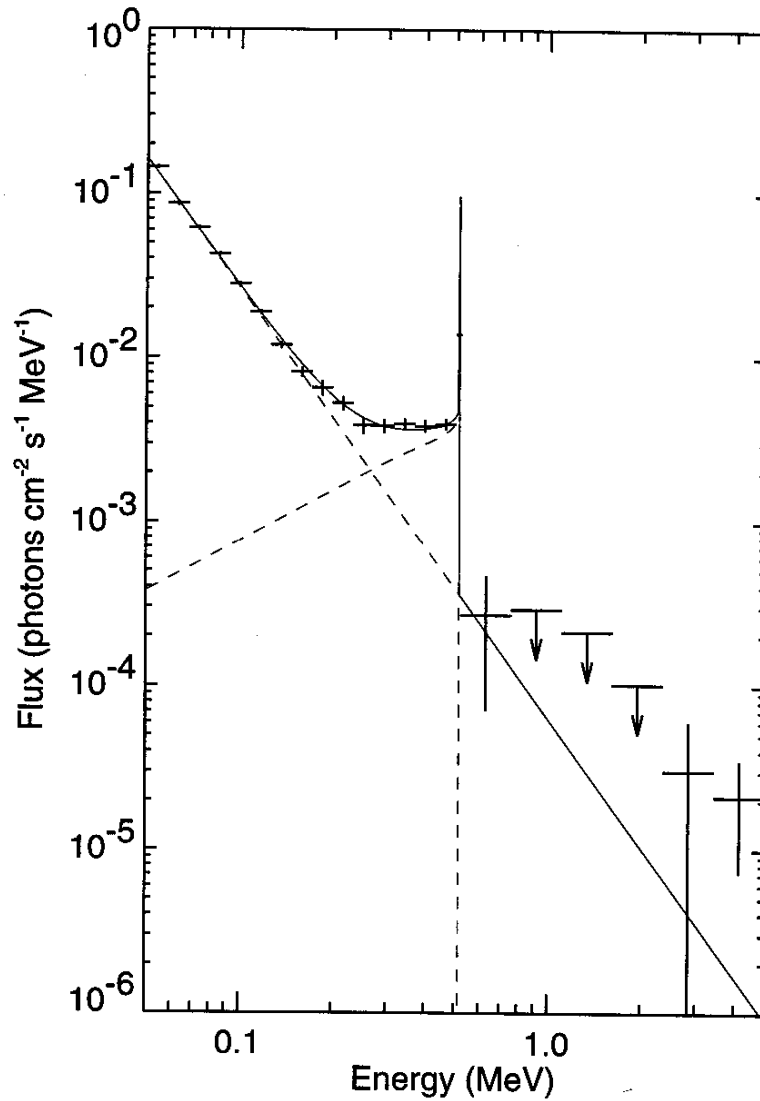


Figure 7.1: Positron annihilation  $\gamma$ -ray spectrum from the Galactic center. The data were fitted with a model function consisting of a single powerlaw, a photopeak line, and a positronium continuum component. The dashed lines show the contribution of each of these components. (Taken from Ref. [113].)

Higher energy resolution spectra are shown in Fig. 7.2. They were measured using a Ge detector on a balloon, and the energy resolution is  $\sim 2\text{keV}$ . The linewidth from the April 26 observation is  $1.3 \pm 0.7 \text{ keV}$ , while that from the May 7 is  $3.6 \pm 1.0 \text{ keV}$ .

The positronium fraction of nearly unity and the narrow annihilation line

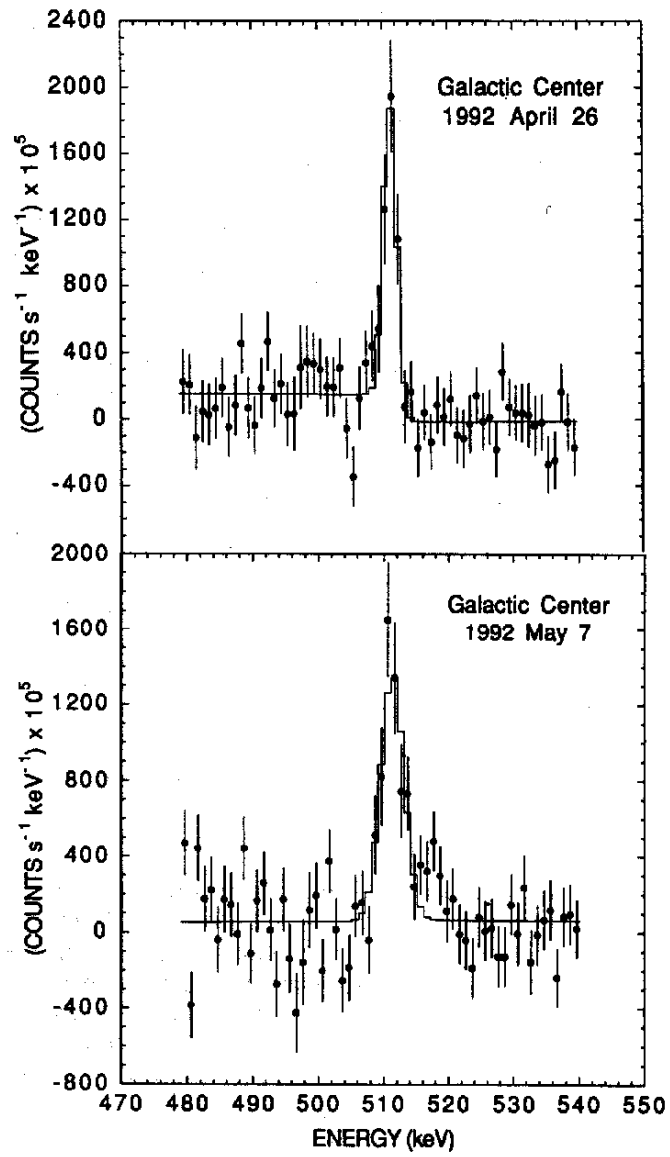


Figure 7.2: Positron annihilation  $\gamma$ -ray spectrum from the Galactic center. (Taken from Ref. [79].)

suggest that the positrons annihilate in a warm ( $\sim 10^4$  K) and either neutral or partially ionized medium [83].

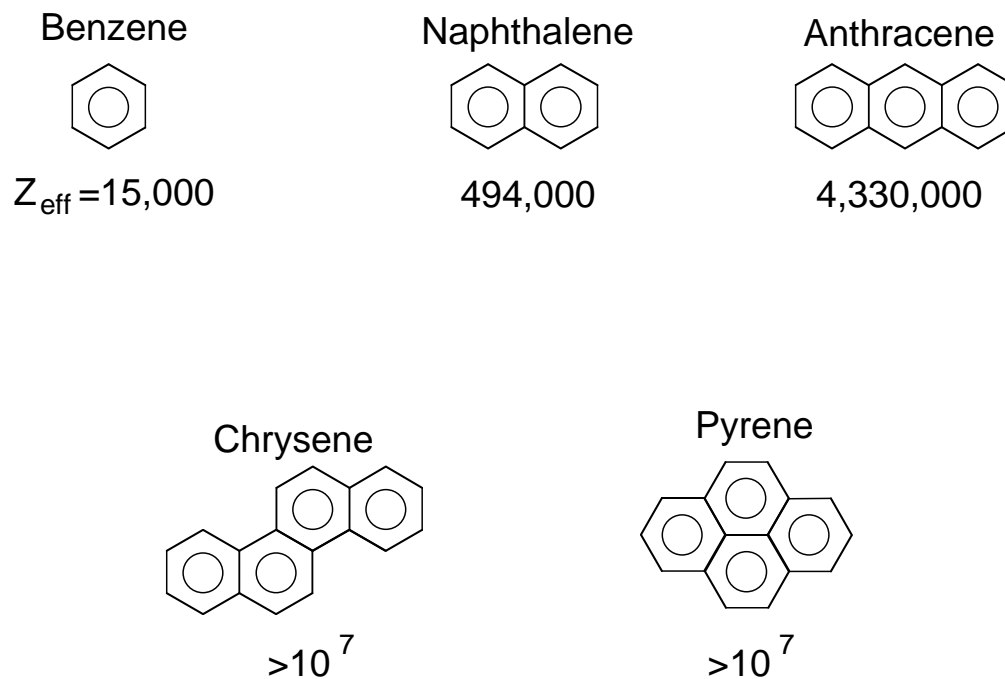


Figure 7.3: Molecular structures and  $Z_{\text{eff}}$  of polycyclic aromatic hydrocarbons. Measured values of  $Z_{\text{eff}}$  are shown for benzene, naphthalene, and anthracene, and estimated values of  $Z_{\text{eff}}$  are also indicated for chrysene and pyrene. As discussed in the text, these latter molecules may be significant sources of astrophysical  $\gamma$ -ray radiation from positron annihilation.

### 7.3 Interstellar molecules

The anomalously high values of  $Z_{\text{eff}}$  observed for many molecules have implications for astrophysical processes [132]. There exist extensive sets of infrared spectral measurements indicating that hydrocarbons are present in the ISM [2, 3, 41, 78, 105, 112, 135]. The molecules have been identified as polycyclic aromatic hydrocarbons (PAH), and their molecular concentration is  $\sim 10^{-7}$  of that of hydrogen [105]. Stability analyses of these molecules indicate that PAH's with 4 to 9 aromatic rings (examples of which are shown in Fig. 7.3) dominate the interstellar PAH population [3]. Chrysene and pyrene are the smallest of the PAH molecules known to be present in the ISM. At present, we are only able to study the two- and three-ring PAH's, naphthalene and anthracene, in the positron trap because the larger PAH's have very low vapor pressure. However, we believe that these two PAH's are representative of the family, in that all hydrocarbons studied previously, including the single ring benzene, the two-

ring naphthalene, and three-ring anthracene, have larger  $\gamma$ -ray linewidths than that of hydrogen [64,69], and we expect this to extrapolate to the larger PAH's. Moreover, we have noted a systematic increase in the annihilation rates for the PAH's as one adds more rings. This trend should continue up to some saturation level, where the resonance binding time becomes comparable to the annihilation time scale. The saturated value could be as high as  $10^6$  or greater than that of atomic hydrogen, which is 8.0 [64], so that the interstellar PAH molecules may contribute significantly to the annihilation of slow positrons in the ISM, due to their anomalously high annihilation rates, even though the PAH molecules are present in only small concentrations as pointed out earlier. This positron annihilation on PAH's would then be reflected in the 511-keV annihilation  $\gamma$ -ray line shape from the ISM [132,133]. These measurements have led us to simulate positron annihilation in a cold medium similar to the cold cloud phase of the ISM.

## 7.4 Astrophysical positron annihilation simulation

In this section, we describe an experiment to measure the annihilation  $\gamma$ -ray spectrum from a simulated ISM consisting of molecular hydrogen and a PAH, namely naphthalene, at room temperature. To our knowledge, this is the first experimental simulation of astrophysical positron annihilation in a mixed gas medium. Section 7.4.1 describes the experiment in more detail. In Sec. 7.4.2, we present the annihilation data and describe the analysis, while Sec. 7.5 summarizes the chapter, and discusses the implications of the experiment for the analysis of astrophysical data.

### 7.4.1 Description of the experiment

This experiment was performed using the same technique to the  $\gamma$ -ray study described in Ch. 5. The pressures of molecular hydrogen and naphthalene were adjusted so that approximately equal number of  $\gamma$  rays originate from annihilation on each of the sample gases. The numerical values are listed in Table 7.1. Note that, although the naphthalene has four orders of magnitude lower pressure than that of hydrogen, it nonetheless contributes significantly to the annihilation, owing to its anomalously large annihilation cross section [102].

### 7.4.2 Experimental results

The observed spectrum from positrons annihilating on the mixture of molecular hydrogen and naphthalene molecules is shown in Fig. 7.4. The Gaussian func-

Table 7.1: The fraction of annihilations on each component:  $\Delta F$ —calculated from fit to data;  $\Delta F_p$ —calculated from pressure and  $Z_{\text{eff}}$ .

Molecule	Pressure (torr)	$Z_{\text{eff}}$	Width (keV)	$\Delta F_p$	$\Delta F$
Hydrogen	$3.0 \times 10^{-5}$	14.7 <sup>a</sup>	1.71	21%	51%
Naphthalene	$3.5 \times 10^{-9}$	494 000 <sup>b</sup>	2.29	79%	49%

<sup>a</sup>Ref. [60]. <sup>b</sup>Ref. [102].

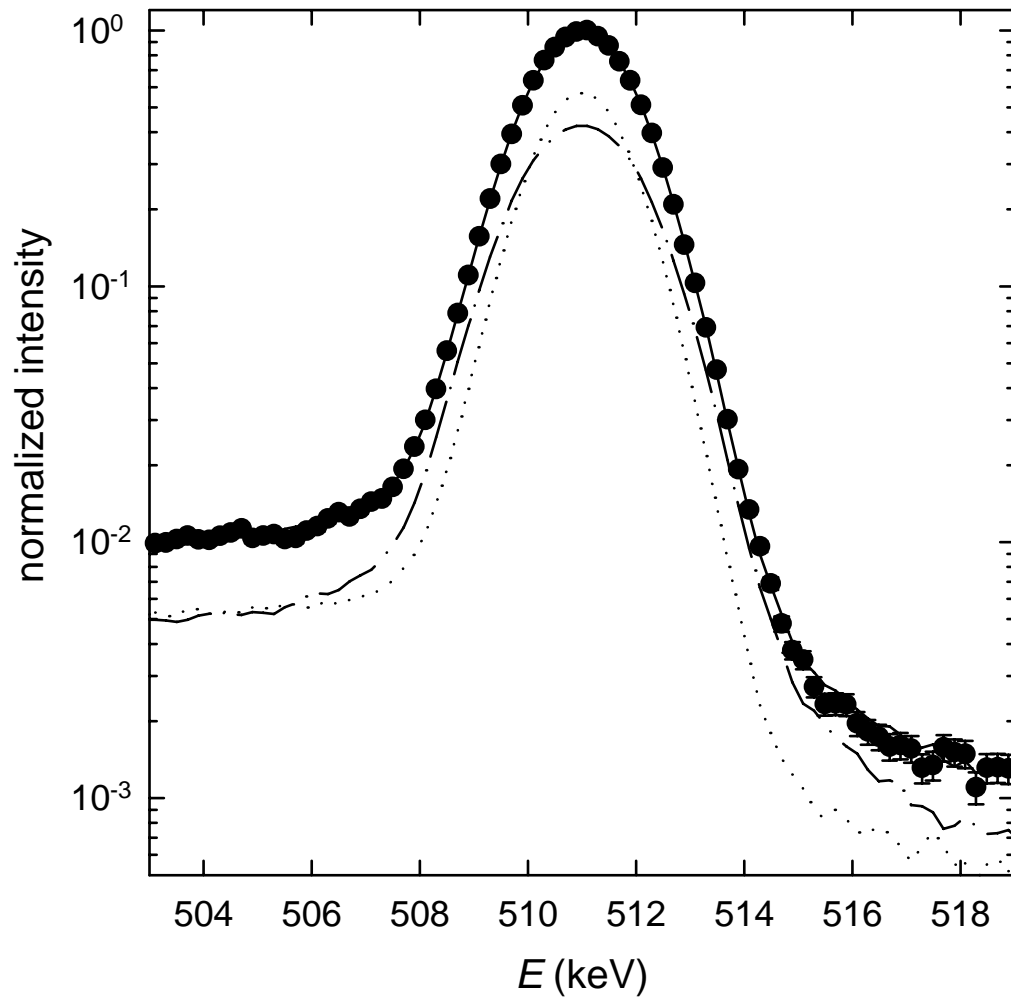


Figure 7.4:  $\gamma$ -ray line for positrons annihilating on mixture of hydrogen and naphthalene molecules: ( $\cdots$ ) annihilation spectrum from molecular hydrogen; ( $-\cdot-$ ) annihilation spectrum from naphthalene; ( $-$ ) combined fit to annihilation spectrum from the mixed medium.

tion, Eq. (3.3), was fit to the data producing a linewidth of 2.01 keV. However, the fit parameter  $\chi_n^2$  was 13.4, which indicates that a single Gaussian does not model the data adequately.

In order to find a better fitting function, the spectra from annihilation on  $\text{H}_2$  and naphthalene were measured separately. Then, a superposition of these two spectra was fit to the mixed-gas data by adjusting the relative weights of the two components, as described in Sec. 5.3.7. The fit has only two free parameters, namely, the weights of the  $\text{H}_2$  and of the naphthalene spectra. The resulting fit and the separate components from  $\text{H}_2$  and naphthalene are plotted on Fig. 7.4. The fit produced  $\chi_n^2 = 0.98$ , indicating that the choice of the individually measured component spectra as fitting functions is a very good model. By integrating the area under each component, the fractions of positrons annihilating on  $\text{H}_2$  and on naphthalene can be calculated (see Table 7.1).

Annihilation fractions were also calculated independently using the pressures and annihilation rates listed in Table 7.1. The annihilation rates are expressed in terms of the normalized rates  $Z_{\text{eff}}$  [66]. The total annihilation rate of each component is proportional to the  $Z_{\text{eff}}$  and partial pressure of the molecule. The annihilation fractions are calculated comparing the data for  $\text{H}_2$  and naphthalene. These fractions differ by a factor of four from the fractions calculated with the two-spectrum fitting procedure. Uncertainties in measuring the low naphthalene pressure ( $\sim 10^{-9}$  torr) using an ionization vacuum gauge could be in error by as much as 50%, which would account for a large part of this discrepancy.

## 7.5 Summary of positron annihilation in the interstellar media

We have demonstrated a method for analyzing  $\gamma$ -ray spectra from positrons annihilating on gas mixtures. These data introduce the possibility of identifying the minority constituents of the ISM from the  $\gamma$ -ray spectra, assuming a scenario in which positrons thermalize and then annihilate on neutral atoms and molecules in the ISM. In practice, such an analysis would involve building up a library of annihilation line shapes for candidate molecules in the ISM, and using them to fit the astrophysical measurements. At present, the signal-to-noise ratio of astrophysical data is too low to attempt such fits, but these kinds of analyses may be possible in the future using high-resolution data from orbital missions [145].

For the experiment described here, molecular hydrogen was used for convenience, but in principle experiments with atomic hydrogen are also possible [151].

At present, annihilation studies of PAH's larger than naphthalene are difficult because of the low vapor pressures of these molecules. To eliminate this restriction, a "hot cell" could be used in order to perform studies of these molecules. In the future, experiments to test other scenarios for positron annihilation in the ISM could be carried out in the positron trap, such as interaction with dust and clusters, as well as the annihilation by in-flight positronium formation.

Recent observation makes the scenario of low-energy positrons annihilating with neutral atoms and molecules unlikely to account for the intense annihilation radiation from the Galaxy. However, annihilation radiation from the cold cloud of the ISM may be used to perform chemical analysis simulated in this chapter.





## Chapter 8

# Conclusion

### 8.1 Summary of this dissertation

Atomic and molecular physics studies using positrons has gained renewed interests since the introduction of studies in positron traps, as discussed in this dissertation. The range of molecules studied has increased dramatically due to the ability to conduct studies at low test-gas pressures, where two-body interactions can be isolated and studied. The positrons used in these experiments have a well-defined energy distribution, and the number of positrons available is much larger than in previous experiments. This results in a considerable increase in the signal-to-noise ratio of the measurements.

Using these trapped positrons, annihilation rates of various molecules were studied systematically (Ch. 4). Anomalously large annihilation rates have been observed previously for large organic molecules [60, 110, 134]. The annihilation rate data exhibit a number of chemical trends and highlight the importance of the electronic structure of the molecule. The empirical scaling of the rates with molecular ionization potentials and the positronium binding energy [102] suggests that a highly correlated positron-electron pair moving in the field of molecular positive ion dominates the physics involved. Even though attempts have now been made, the anomalously high annihilation rates and this empirical scaling have not yet been understood theoretically.

The spectra of the 511-keV annihilation line for various molecules were systematically studied (Ch. 5). The observed spectra are Doppler broadened mainly due to the momenta of annihilating electrons, which are bound to the molecule. These spectra give information about the quantum states of the electrons. The observed spectrum for helium was compared to a recent theoretical calculation, resulting in an excellent agreement. The data from alkanes and partially fluori-

nated hydrocarbons indicated that positrons annihilate with an equal probability with any valence electron in these molecules. Inner-shell electron annihilation was detected in gaseous media for the first time, and a study of this effect on noble gases was presented in Ch. 6.

The anomalously large annihilation rates measured for polycyclic aromatic hydrocarbons have implications for positron annihilation in the ISM. These molecules are expected to have very high annihilation rates, which leads us to conjecture that the annihilation  $\gamma$  rays from the ISM may contain information about these molecules. A laboratory experiment in a simulated ISM is presented in Ch. 7.

## 8.2 Future work

As shown in this dissertation, a broad survey of annihilation rates and  $\gamma$ -ray spectral measurements using room-temperature positrons is more or less completed. We have developed two techniques to change the energy distribution of positrons in the positron trap. The first technique is to heat positron plasmas by applying a RF noise to one of the electrodes, and as discussed in Sec. 4.3.2, it has been successfully applied to measure the dependence of annihilation rates on positron temperature for noble gases. Extending this type of measurement to hydrocarbons, where the anomalously high annihilation rates are observed, will be fruitful. In particular, a large scale calculation of positron annihilation on ethylene ( $\text{C}_2\text{H}_4$ ) is available [29], and a comparison with experimental data will help to verify the validity of the calculation.

The second technique is the generation of positron beams with very narrow energy spread ( $\sim 0.018$  eV) [44]. The first technique is limited in the useful range of positron energies ( $< 0.5$  eV), since application of large RF noise kicks positrons out of the trapping potential well. The monoenergetic beam is expected to be a powerful tool for atomic and molecular physics studies, since positrons with well-defined energies can probe the molecules under study in a precise way. The empirical scaling indicates that the parameter  $(E_i - E_{\text{Ps}})$  is important for room-temperature positrons. For higher energy positrons, the parameter  $(E_{e^+} - E_i + E_{\text{Ps}})$  is the energy difference from the positronium formation threshold, and it may play an important role. Recent theories predict resonance behavior in annihilation rates at  $(E_{e^+} - E_i + E_{\text{Ps}}) \sim 0$ , and this can potentially be observed experimentally using the monoenergetic positron beam.

The  $\gamma$ -ray spectral studies suggest that positrons annihilate equally with any valence electron in molecules, while the empirical scaling suggests that the physics involved may be dominated by highly correlated electron-positron pairs.

Near the positronium formation threshold, this picture of equal probability of annihilation may break down, and we may be able to study this effect using the technique described above.

Positron annihilation is a qualitatively different way of ionizing molecules from conventional methods, and studies of the ions formed after positron annihilation are potentially useful in mass spectroscopy applications. Previously, mass spectroscopy of positive molecular ions in our positron trap has been attempted, and these studies showed that there was a large probability of fragmentation for alkanes [109, 147–149]. Hulett *et al.* have discovered that the resulting molecular ions were predominantly unfragmented when the incident positron energy is tuned near the positronium formation threshold [63]. This effect can be studied more systematically using the monoenergetic positron beam described above. Our positron trap is not optimized for time-of-flight mass spectrometry, and the application of ion cyclotron mass spectrometry may prove useful for these experiments [144].

Currently the substances we can study are limited to those which have sufficiently high vapor pressures at room temperature. Installation of a hot cell would enable us to study other substances, which could give us useful physical insights. Metal vapors, such as Cd, Zn and Hg, have relatively low ionization energies, and we could test the validity of the empirical scaling for these atoms. If the empirical scaling holds for atoms, then these metal are expected to have  $Z_{\text{eff}} > 10^5$ . These atoms are simple enough that the theoretical calculation can be performed and compared with experiments. At elevated temperatures, we may also be able to perform more realistic simulations of positron annihilation in the ISM.

### 8.3 Concluding remarks

In the past several years we have systematically studied annihilation on a variety of atoms and molecules using positron trapping techniques. As a result of these studies, we have gained significant physical insights into the interaction of low-energy positrons with molecules. We now have a considerable body of data, which can be compared with theoretical models. A number of outstanding issues still remain to be addressed. The work presented here demonstrates the utility of the positron trap as a tool for atomic and molecular physics. Presently, new experimental techniques are being developed that can increase the range of positron energies and the variety of chemical species that can be studied, and these developments are expected to further enhance our understanding of physics involved in this area.



## Appendix A

# Ion gauge sensitivity calibration for gases and molecular vapors

As described in Sec. 3.5, the ion gauge sensitivities for the test gases are necessary to measure the pressure precisely and, in turn, to obtain the annihilation rate,  $Z_{\text{eff}}$ . Where available, published pressure gauge sensitivities were used [10]. For those substances for which data were not available, we measured the sensitivities using a technique similar to that described in Ref. [10]. The sensitivities for the molecules discussed in this dissertation are listed in Table A.1. As can be seen from the table, for the molecules where both our measurements and previously published data [10] are available, the values are in good agreement (in most cases agreeing to better than 10%).

Table A.1: Sensitivities of ion gauge response,  $R$ , relative to that of nitrogen gas.

Molecule	Formula	Measured $R$	$R$ from Ref. [10]
<b>Noble gases</b>			
Helium	He	0.20	0.20
Neon	Ne	n/a	0.33
Argon	Ar	1.23	1.32
Krypton	Kr	1.77	1.92
Xenon	Xe	2.72	2.78
<b>Inorganic molecules</b>			
Hydrogen	H <sub>2</sub>	n/a	0.44
Nitrogen	N <sub>2</sub>	1	1
Oxygen	O <sub>2</sub>	n/a	0.87
Carbon dioxide	CO <sub>2</sub>	n/a	1.30
Water	H <sub>2</sub> O	0.82	0.97
Sulfur hexafluoride	SF <sub>6</sub>	2.06	n/a
Ammonia	NH <sub>3</sub>	n/a	1.12
<b>Alkanes</b>			
Methane	CH <sub>4</sub>	n/a	1.62
Ethane	C <sub>2</sub> H <sub>6</sub>	n/a	2.84
Propane	C <sub>3</sub> H <sub>8</sub>	n/a	2.92
Butane	C <sub>4</sub> H <sub>10</sub>	n/a	4.46
Pentane	C <sub>5</sub> H <sub>12</sub>	n/a	5.21
Hexane	C <sub>6</sub> H <sub>14</sub>	6.20	5.90
Heptane	C <sub>7</sub> H <sub>16</sub>	n/a	6.94
Decane	C <sub>10</sub> H <sub>22</sub>	10.67	n/a
Cyclohexane	C <sub>6</sub> H <sub>12</sub>	5.39	5.39
Cyclodecane	C <sub>10</sub> H <sub>20</sub>	5.87	n/a
<b>Alkenes</b>			
Ethylene	C <sub>2</sub> H <sub>4</sub>	2.08	n/a
Hexene	C <sub>6</sub> H <sub>12</sub>	n/a	5.81
<b>Aromatic hydrocarbons</b>			
Benzene	C <sub>6</sub> H <sub>6</sub>	4.63	4.29
Naphthalene	C <sub>10</sub> H <sub>8</sub>	6.3	n/a
Anthracene	C <sub>14</sub> H <sub>10</sub>	8.5	n/a
Toluene	C <sub>6</sub> H <sub>5</sub> CH <sub>3</sub>	n/a	5.56
<i>o</i> -Xylene	C <sub>6</sub> H <sub>4</sub> (CH <sub>3</sub> ) <sub>2</sub>	5.85	5.43
<i>m</i> -Xylene	C <sub>6</sub> H <sub>4</sub> (CH <sub>3</sub> ) <sub>2</sub>	6.72	n/a
<i>p</i> -Xylene	C <sub>6</sub> H <sub>4</sub> (CH <sub>3</sub> ) <sub>2</sub>	6.54	n/a

Table A.1: (*Continued*).

Molecule	Formula	Measured $R$	$R$ from Ref. [10]
<b>Substituted alkanes</b>			
Carbon tetrafluoride	CF <sub>4</sub>	1.53	n/a
Perfluoropropane	C <sub>3</sub> F <sub>8</sub>	3.27	n/a
Perfluorohexane	C <sub>6</sub> F <sub>14</sub>	5.72	n/a
Perfluorooctane	C <sub>8</sub> F <sub>18</sub>	7.59	n/a
Carbon tetrachloride	CCl <sub>4</sub>	5.69	3.74
<b>Substituted benzenes</b>			
Fluorobenzene	C <sub>6</sub> H <sub>5</sub> F	4.46	n/a
1,4-Difluorobenzene	C <sub>6</sub> H <sub>4</sub> F <sub>2</sub>	5.21	n/a
Pentafluorobenzene	C <sub>6</sub> HF <sub>5</sub>	4.17	n/a
Hexafluorobenzene	C <sub>6</sub> F <sub>6</sub>	3.52	n/a
Chlorobenzene	C <sub>6</sub> H <sub>5</sub> Cl	n/a	4.88
Bromobenzene	C <sub>6</sub> H <sub>5</sub> Br	8.84	n/a
Nitrobenzene	C <sub>6</sub> H <sub>5</sub> NO <sub>2</sub>	4.53	n/a
Aniline	C <sub>6</sub> H <sub>5</sub> NH <sub>2</sub>	5.32	n/a
<b>Oxygen-containing molecules</b>			
Methanol	CH <sub>3</sub> OH	n/a	1.69
1-Propanol	C <sub>3</sub> H <sub>7</sub> OH	n/a	2.60
Acetone	CH <sub>3</sub> COCH <sub>3</sub>	n/a	2.50
Acetic acid	CH <sub>3</sub> COOH	n/a	1.54
Propionic acid	C <sub>2</sub> H <sub>5</sub> COOH	2.11	n/a
<b>Other molecule</b>			
Tetraethylsilane	Si(C <sub>2</sub> H <sub>5</sub> ) <sub>4</sub>	10.66	n/a





## Appendix B

# Table of physical parameters of atoms and molecules

Physical parameters of atoms and molecules studied are listed in Table B.1 for a reference purpose. The parameters include number of electrons  $Z$ , annihilation rate  $Z_{\text{eff}}$ ,  $\gamma$ -ray linewidth  $\Delta E$ , polarizability  $\alpha$ , dipole moment  $\mu_p$ , and ionization potential  $E_i$ . The sources of  $Z_{\text{eff}}$  can be found in Ch. 4.  $\gamma$ -ray linewidths are taken from Ref. [69], which is also the subject of Ch. 5. Atomic polarizabilities are taken from Ref. [10], while molecular polarizabilities are calculated using the empirical method described by Miller and Savchik [97]. Dipole moments are taken from Refs. [90, 104] and expressed in the units of debye, D. Ionization potentials are taken from Refs. [15, 40, 82, 119].

Table B.1: Physical parameters of molecules studied.

Molecule	Formula	$Z$	$Z_{\text{eff}}$	$\Delta E$ keV	$\alpha$ $\text{\AA}^3$	$\mu_p$ D	$E_i$ eV
<b>Noble gases</b>							
Helium	He	2	3.94	2.50	0.20	0	24.59
Neon	Ne	10	5.99	3.37	0.40	0	21.56
Argon	Ar	18	33.8	2.30	1.66	0	15.76
Krypton	Kr	36	90.1	2.10	2.54	0	14.00
Xenon	Xe	54	401	1.93	4.15	0	12.13
<b>Diatomic molecules (non-polar)</b>							
Hydrogen	H <sub>2</sub>	2	14.6	1.71	0.79	0	15.43
Deuterium	D <sub>2</sub>	2	14.7	n/a	0.79	0	15.46
Nitrogen	N <sub>2</sub>	14	30.5	2.32	1.94	0	15.58
Oxygen	O <sub>2</sub>	16	36.7	2.73	1.48	0	12.06
<b>Diatomic molecules (polar)</b>							
Carbon monoxide	CO	14	38.5	2.23	1.96	0.112	14.01
Nitric oxide	NO	15	34	n/a	1.70	0.153	9.25
<b>Polyatomic molecules (non-polar)</b>							
Carbon dioxide	CO <sub>2</sub>	22	54.7	2.63	2.66	0	13.77
Sulfur hexafluoride	SF <sub>6</sub>	70	86.2	3.07	4.45	0	15.29
<b>Polyatomic molecules (polar)</b>							
Water	H <sub>2</sub> O	10	319	2.59	1.47	1.85	12.61
Nitrous oxide	N <sub>2</sub> O	22	78	n/a	3.00	0.17	12.89
Nitrogen dioxide	NO <sub>2</sub>	23	1090	n/a	2.96	0.32	9.78
Ammonia	NH <sub>3</sub>	10	1600	2.27	2.26	1.47	10.19
<b>Alkanes</b>							
Methane	CH <sub>4</sub>	10	142	2.09	2.60	0	12.70
Ethane	C <sub>2</sub> H <sub>6</sub>	18	660	2.18	4.44	0	11.52
Propane	C <sub>3</sub> H <sub>8</sub>	26	3500	2.21	6.29	0.08	11.14
Butane	C <sub>4</sub> H <sub>10</sub>	34	11300	2.28	8.14	0	10.63
Pentane	C <sub>5</sub> H <sub>12</sub>	42	37800	2.24	9.98	0	10.35
Hexane	C <sub>6</sub> H <sub>14</sub>	50	120000	2.25	11.83	0	10.18
Heptane	C <sub>7</sub> H <sub>16</sub>	58	242000	n/a	13.68	0	9.90
Octane	C <sub>8</sub> H <sub>18</sub>	66	585000	n/a	15.52	0	10.03
Nonane	C <sub>9</sub> H <sub>20</sub>	74	643000	2.32	17.37	0	10.02
Decane	C <sub>10</sub> H <sub>22</sub>	82	507000	n/a	19.22	0	9.95
Dodecane	C <sub>12</sub> H <sub>26</sub>	98	1780000	2.29	22.91	0	9.93

Table B.1: (*Continued*).

Molecule	Formula	$Z$	$Z_{\text{eff}}$	$\Delta E$ keV	$\alpha$ $\text{\AA}^3$	$\mu_p$ D	$E_i$ eV
Hexadecane	$\text{C}_{16}\text{H}_{34}$	130	2 230 000	n/a	30.30	0	9.91
<b>Alkane Isomers</b>							
Isobutane	$\text{C}_4\text{H}_{10}$	34	14 400	n/a	8.14	0.13	10.63
Isopentane	$\text{C}_5\text{H}_{12}$	42	50 500	2.23	9.98	0.13	10.32
Neopentane	$\text{C}_5\text{H}_{12}$	42	21 100	2.23	9.98	0	10.35
<b>Ring alkanes</b>							
Cyclohexane	$\text{C}_6\text{H}_{12}$	48	20 000	2.31	11.08	0	9.88
Cyclodecane	$\text{C}_{10}\text{H}_{20}$	80	369 000	n/a	18.47	0	10.00
<b>Alkenes and alkyne</b>							
Ethylene	$\text{C}_2\text{H}_4$	16	1 200	2.10	4.23	0	10.51
Acetylene	$\text{C}_2\text{H}_2$	14	3 160	2.08	3.33	0	11.40
1-Hexene	$\text{C}_6\text{H}_{12}$	48	185 000	n/a	11.60	0.34	9.46
<i>trans</i> 3-Hexene	$\text{C}_6\text{H}_{12}$	48	196 000	n/a	11.60	0	8.94
1,3-Hexadiene	$\text{C}_6\text{H}_{10}$	46	389 000	n/a	11.38	n/a	8.53
<i>cis</i> 2, <i>trans</i> 4- Hexadiene	$\text{C}_6\text{H}_{10}$	46	413 000	n/a	11.38	0.36	8.26
<i>trans</i> 2, <i>trans</i> 4- Hexadiene	$\text{C}_6\text{H}_{10}$	46	388 000	n/a	11.38	0	8.09
1,3,5-Hexatriene	$\text{C}_6\text{H}_8$	44	414 000	n/a	11.16	0	8.29
<b>Aromatic hydrocarbons</b>							
Benzene	$\text{C}_6\text{H}_6$	42	15 000	2.23	10.40	0	9.25
Naphthalene	$\text{C}_{10}\text{H}_8$	68	494 000	2.29	16.59	0	8.15
Decahydronaphthalene	$\text{C}_{10}\text{H}_{18}$	78	389 000	n/a	17.73	0	9.35
Anthracene	$\text{C}_{14}\text{H}_{10}$	94	4 330 000	2.45	22.77	0	7.47
Toluene	$\text{C}_7\text{H}_8$	50	190 000	2.28	12.25	0.36	8.82
<i>o</i> -Xylene	$\text{C}_8\text{H}_{10}$	58	180 000	n/a	14.10	0.62	8.56
<i>m</i> -Xylene	$\text{C}_8\text{H}_{10}$	58	210 000	n/a	14.10	0.30	8.56
<i>p</i> -Xylene	$\text{C}_8\text{H}_{10}$	58	200 000	n/a	14.10	0	8.45
<b>Deuterated alkanes</b>							
d-Methane	$\text{CD}_4$	10	214	n/a	2.60	0	n/a
d-Hexane	$\text{C}_6\text{D}_{14}$	50	116 000	n/a	11.83	0	n/a
d-Heptane	$\text{C}_7\text{D}_{16}$	58	341 000	n/a	13.68	0	n/a
d-Octane	$\text{C}_8\text{D}_{18}$	66	408 000	n/a	15.52	0	n/a
d-Nonane	$\text{C}_9\text{D}_{20}$	74	641 000	n/a	17.37	0	n/a
d-Decane	$\text{C}_{10}\text{D}_{22}$	82	1 930 000	n/a	19.22	0	n/a

Table B.1: (*Continued*).

Molecule	Formula	$Z$	$Z_{\text{eff}}$	$\Delta E$ keV	$\alpha$ $\text{\AA}^3$	$\mu_p$ D	$E_i$ eV
<b>Deuterated benzenes</b>							
Benzene- <i>d</i>	$\text{C}_6\text{H}_5\text{D}$	42	36 900	n/a	10.40	0	9.44
Benzene-1,3,5- <i>d</i> <sub>3</sub>	$\text{C}_6\text{H}_3\text{D}_3$	42	43 800	n/a	10.40	0	n/a
Benzene- <i>d</i> <sub>6</sub>	$\text{C}_6\text{D}_6$	42	30 500	n/a	10.40	0	9.25
<b>Perfluorinated alkanes</b>							
Carbon tetrafluoride	$\text{CF}_4$	42	54.4	3.04	2.86	0	16.25
Hexafluoroethane	$\text{C}_2\text{F}_6$	66	149	3.04	4.76	0	14.60
Perfluoropropane	$\text{C}_3\text{F}_8$	90	152	3.05	6.67	n/a	n/a
Perfluorohexane	$\text{C}_6\text{F}_{14}$	162	535	3.09	12.40	0	12.75
Perfluorooctane	$\text{C}_8\text{F}_{18}$	210	1 064	n/a	16.22	0	12.55
<b>Perchlorinated alkanes</b>							
Carbon tetrachloride	$\text{CCl}_4$	74	9 530	2.29	10.31	0	11.28
Hexachloroethane	$\text{C}_2\text{Cl}_6$	114	68 600	n/a	16.02	0	11.22
<b>Perbrominated alkane</b>							
Carbon tetrabromide	$\text{CBr}_4$	146	39 800	2.09	15.26	0	10.31
<b>Periodited alkane</b>							
Carbon tetraiodide	$\text{CI}_4$	218	7 990	n/a	24.54	0	n/a
Methyl chloride	$\text{CH}_3\text{Cl}$	26	15 000	n/a	4.43	1.87	11.22
Dichloro- difluoromethane	$\text{CCl}_2\text{F}_2$	58	750	n/a	6.42	0.51	12.31
<b>Oxygen-containing molecules</b>							
Methanol	$\text{CH}_4\text{O}$	18	1 510	2.59	3.28	1.70	10.85
1-Propanol	$\text{C}_3\text{H}_8\text{O}$	34	19 900	n/a	6.95	1.68	10.20
Acetone	$\text{C}_3\text{H}_6\text{O}$	32	98 400	n/a	6.33	2.88	9.69
Acetic acid	$\text{C}_2\text{H}_4\text{O}_2$	32	5 880	n/a	5.26	1.74	10.35
Propionic acid	$\text{C}_3\text{H}_6\text{O}_2$	40	27 200	n/a	7.07	1.75	10.24
<b>Perfluorinated aromatics</b>							
Hexafluorobenzene	$\text{C}_6\text{F}_6$	90	1 200	2.95	9.79	0	9.90
Octafluorotoluene	$\text{C}_6\text{F}_5\text{CF}_3$	114	1 240	n/a	11.66	n/a	9.90
Octafluoronaphthalene	$\text{C}_{10}\text{F}_8$	132	3 080	n/a	15.54	0	8.85
<b>Substituted benzenes</b>							
Chlorobenzene	$\text{C}_6\text{H}_5\text{Cl}$	58	72 300	n/a	12.14	1.69	9.07
Bromobenzene	$\text{C}_6\text{H}_5\text{Br}$	76	172 000	n/a	13.00	1.70	8.98
Nitrobenzene	$\text{C}_6\text{H}_5\text{NO}_2$	64	430 000	2.47	12.14	4.22	9.92
Aniline	$\text{C}_6\text{H}_5\text{NH}_2$	50	400 000	n/a	11.49	1.53	7.69

Table B.1: (*Continued*).

Molecule	Formula	$Z$	$Z_{\text{eff}}$	$\Delta E$ keV	$\alpha$ $\text{\AA}^3$	$\mu_p$ D	$E_i$ eV
<b>Partially fluorinated hydrocarbons</b>							
Methyl fluoride	$\text{CH}_3\text{F}$	18	1 390	2.77	2.39	1.85	12.85
Difluoromethane	$\text{CH}_2\text{F}_2$	26	799	2.86	2.48	1.97	12.60
Trifluoromethane	$\text{CHF}_3$	34	247	2.85	2.65	1.65	14.80
Fluoroethane	$\text{C}_2\text{H}_5\text{F}$	26	3 030	2.62	4.17	1.94	12.43
1,1,1-Trifluoroethane	$\text{C}_2\text{H}_3\text{F}_3$	42	1 600	2.95	4.23	2.32	13.26
1,1,2-Trifluoroethane	$\text{C}_2\text{H}_3\text{F}_3$	42	1 510	2.91	4.23	1.58	n/a
1,1,1,2-Tetra- fluoroethane	$\text{C}_2\text{H}_2\text{F}_4$	50	1 110	3.00	4.38	n/a	n/a
1,1,2,2-Tetra- fluoroethane	$\text{C}_2\text{H}_2\text{F}_4$	50	467	2.97	4.38	n/a	n/a
2,2-Difluoropropane	$\text{C}_3\text{H}_6\text{F}_2$	42	8 130	2.78	5.88	n/a	11.42
1,1,1-Trifluoropropane	$\text{C}_3\text{H}_5\text{F}_3$	50	3 350	2.86	5.90	2.45	n/a
1-Fluorohexane	$\text{C}_6\text{H}_{13}\text{F}$	58	269 000	2.46	11.46	n/a	n/a
Fluorobenzene	$\text{C}_6\text{H}_5\text{F}$	50	45 100	2.43	10.01	1.60	9.20
1,2-Difluorobenzene	$\text{C}_6\text{H}_4\text{F}_2$	58	32 800	2.66	9.79	2.40	9.30
1,3-Difluorobenzene	$\text{C}_6\text{H}_4\text{F}_2$	58	13 100	2.52	9.79	1.58	9.35
1,4-Difluorobenzene	$\text{C}_6\text{H}_4\text{F}_2$	58	13 500	2.53	9.79	0	9.18
1,2,4-Trifluorobenzene	$\text{C}_6\text{H}_3\text{F}_3$	66	10 100	2.71	9.70	n/a	9.37
1,2,4,5-Tetra- fluorobenzene	$\text{C}_6\text{H}_2\text{F}_4$	74	2 760	2.77	9.68	0	9.36
Pentafluorobenzene	$\text{C}_6\text{HF}_5$	82	1 930	2.89	9.71	n/a	9.82
<b>Other molecules</b>							
Tetraethylsilane	$\text{Si}(\text{C}_2\text{H}_5)_4$	82	524 000	2.37	n/a	0	9.98
Glycerol	$\text{C}_3\text{H}_8\text{O}_3$	50	1 470 000	n/a	8.43	n/a	n/a
Sebacic acid dimethyl ester	$\text{C}_{12}\text{H}_{22}\text{O}_4$	126	7 560 000	n/a	24.39	n/a	n/a
Pyridine	$\text{C}_5\text{H}_5\text{N}$	42	85 400	2.34	9.47	2.19	9.25



## Appendix C

# Table of annihilation $\gamma$ -ray spectra from atoms and molecules

As discussed in Sec. 5.4, our measurements are precise enough to be able to study the line shapes of the spectra and not just their widths. While Gaussian line shapes are reasonable first approximations to the data, departures from a Gaussian line shape can be clearly distinguished. This can be seen from the values of  $\chi_r^2$  from fitting the Gaussian function Eq. (3.3) (e.g., see Table C.1). The values of  $\chi_r^2$ , which are expected to be an order of unity for a good model, are typically around 10 or higher for the Gaussian fit. We have attempted to find a general functional form to describe the measured line shapes. However, we were unsuccessful in obtaining a functional form that is unambiguous and has physical significance. Thus, in order to present our experimental data analytically in a quantitative way, we have fitted the observed spectra with a two-Gaussian function, which is described by

$$q(E) = \exp \left[ - \left( \frac{E - E_0}{a\Delta E_1} \right)^2 \right] + A_r \exp \left[ - \left( \frac{E - E_0}{a\Delta E_2} \right)^2 \right] \quad (\text{C.1})$$

convolved with the detector response as given in Eq. (5.5). The number of free parameters is 7:  $E_0$ ,  $\Delta E_1$ ,  $\Delta E_2$ ,  $A_r$ ,  $B_1$ ,  $B_2$ , and  $B_3$ . This fitting function has no physical significance of which we are aware. In addition, the Gaussian line widths,  $\Delta E_1$  and  $\Delta E_2$ , and the relative amplitude of the second Gaussian,  $A_r$ , are highly correlated. However, this fitting procedure yields good values of  $\chi_r^2$ , e.g.,  $\chi_r^2 = 1$ –3 (except for carbon monoxide and carbon tetrachloride), and this functional form serves the purpose of representing the experimentally measured

line shapes analytically with reasonable accuracy. The fitting parameters,  $\Delta E_1$ ,  $\Delta E_2$ , and  $A_r$ , are listed along with the values of  $\chi_r^2$  in Table C.1.



Table C.1:  $\gamma$ -ray line-shape parameters from fits to two Gaussians [Eq. (C.1)] for all atoms and molecules that we have studied.  $A_r$  is the relative amplitude of the second Gaussian.

Molecule	Formula	1 Gaussian fit		2 Gaussian fit			
		$\chi_r^2$	$\Delta E$	$\chi_r^2$	$\Delta E_1$	$\Delta E_2$	$A_r$
<b>Noble gases</b>							
Helium	He	4.6	2.50	0.8	2.15	3.90	0.177
Neon	Ne	14.8	3.37	1.7	3.14	6.12	0.060
Argon	Ar	19.8	2.30	2.9	2.25	7.27	0.010
Krypton	Kr	33.4	2.10	2.3	2.02	6.86	0.016
Xenon	Xe	7.1	1.93	0.9	1.80	5.03	0.033
<b>Inorganic molecules</b>							
Hydrogen	H <sub>2</sub>	14.9	1.71	2.0	1.50	2.65	0.153
Nitrogen	N <sub>2</sub>	27.5	2.32	2.8	2.04	3.76	0.126
Oxygen	O <sub>2</sub>	31.4	2.73	1.7	2.57	5.57	0.041
Carbon monoxide	CO	75.4	2.23	7.3	1.90	3.96	0.129
Carbon dioxide	CO <sub>2</sub>	13.0	2.63	1.3	2.52	5.99	0.026
Water	H <sub>2</sub> O	13.7	2.59	1.5	2.45	5.25	0.039
Sulfur hexafluoride	SF <sub>6</sub>	22.8	3.07	1.9	2.91	6.56	0.034
Ammonia	NH <sub>3</sub>	21.5	2.27	2.2	2.14	4.86	0.034
<b>Alkanes</b>							
Methane	CH <sub>4</sub>	12.1	2.09	1.9	2.05	6.58	0.008
Ethane	C <sub>2</sub> H <sub>6</sub>	12.7	2.18	2.6	2.14	7.28	0.006
Propane	C <sub>3</sub> H <sub>8</sub>	9.8	2.21	1.4	2.17	6.80	0.007
Butane	C <sub>4</sub> H <sub>10</sub>	17.5	2.28	3.7	2.24	8.40	0.011
Pentane	C <sub>5</sub> H <sub>12</sub>	9.7	2.24	1.5	2.21	7.32	0.006
Hexane	C <sub>6</sub> H <sub>14</sub>	9.9	2.25	1.4	2.22	7.36	0.006
Nonane	C <sub>9</sub> H <sub>20</sub>	11.2	2.32	1.8	2.28	8.92	0.009
Dodecane	C <sub>12</sub> H <sub>26</sub>	3.0	2.29	1.0	2.27	8.53	0.005
Cyclohexane	C <sub>6</sub> H <sub>12</sub>	7.3	2.31	1.2	2.27	8.39	0.009
<b>5-carbon alkane isomers</b>							
2-Methylbutane	C <sub>5</sub> H <sub>12</sub>	13.7	2.23	1.9	2.18	7.03	0.008
2,2-Dimethylpropane	C(CH <sub>3</sub> ) <sub>4</sub>	8.9	2.23	1.2	2.21	7.11	0.006
<b>2-carbon alkene and alkyne</b>							
Ethylene	C <sub>2</sub> H <sub>4</sub>	3.8	2.10	1.0	2.06	5.75	0.011
Acetylene	C <sub>2</sub> H <sub>2</sub>	7.0	2.08	1.3	2.00	5.11	0.021
<b>Aromatic hydrocarbons</b>							
Benzene	C <sub>6</sub> H <sub>6</sub>	15.5	2.23	2.0	2.18	6.21	0.011
Naphthalene	C <sub>10</sub> H <sub>8</sub>	12.3	2.29	1.9	2.25	6.62	0.011
Anthracene	C <sub>14</sub> H <sub>10</sub>	7.7	2.45	1.0	2.37	5.76	0.019
Toluene	C <sub>6</sub> H <sub>5</sub> CH <sub>3</sub>	8.3	2.28	1.2	2.23	7.35	0.012

Table C.1: (*Continued*).

Molecule	Formula	1 Gaussian fit		2 Gaussian fit			$A_r$
		$\chi_r^2$	$\Delta E$	$\chi_r^2$	$\Delta E_1$	$\Delta E_2$	
<b>Halocarbons</b>							
Carbon tetrafluoride	CF <sub>4</sub>	31.2	3.04	2.1	2.88	6.36	0.035
Carbon tetrachloride	CCl <sub>4</sub>	27.8	2.29	4.2	2.22	8.02	0.015
Carbon tetrabromide	CBr <sub>4</sub>	39.9	2.09	2.8	2.00	6.52	0.018
<b>Partially and fully fluorinated hydrocarbons</b>							
Methyl fluoride	CH <sub>3</sub> F	11.8	2.77	1.4	2.56	5.23	0.060
Difluoromethane	CH <sub>2</sub> F <sub>2</sub>	44.4	2.86	2.9	2.64	5.35	0.064
Trifluoromethane	CHF <sub>3</sub>	33.1	2.85	2.6	2.62	5.30	0.064
Fluoroethane	C <sub>2</sub> H <sub>5</sub> F	28.8	2.62	1.2	2.46	5.44	0.043
1,1,1-Trifluoroethane	CF <sub>3</sub> CH <sub>3</sub>	33.9	2.95	2.0	2.75	5.62	0.054
1,1,2-Trifluoroethane	CHF <sub>2</sub> CH <sub>2</sub> F	33.9	2.91	2.0	2.73	5.73	0.049
1,1,1,2-Tetrafluoroethane	CF <sub>3</sub> CH <sub>2</sub> F	29.4	3.00	1.4	2.82	6.03	0.044
1,1,2,2-Tetrafluoroethane	CHF <sub>2</sub> CHF <sub>2</sub>	38.6	2.97	1.7	2.80	6.25	0.039
Hexafluoroethane	C <sub>2</sub> F <sub>6</sub>	28.2	3.04	1.9	2.88	6.28	0.036
2,2-Difluoropropane	CH <sub>3</sub> CF <sub>2</sub> CH <sub>3</sub>	22.5	2.78	2.1	2.54	4.98	0.074
1,1,1-Trifluoropropane	CF <sub>3</sub> C <sub>2</sub> H <sub>5</sub>	28.6	2.86	2.3	2.66	5.58	0.052
Perfluoropropane	C <sub>3</sub> F <sub>8</sub>	20.9	3.05	1.4	2.90	6.21	0.036
1-Fluorohexane	CH <sub>2</sub> FC <sub>5</sub> H <sub>11</sub>	22.8	2.46	2.3	2.36	5.75	0.022
Perfluorohexane	C <sub>6</sub> F <sub>14</sub>	21.1	3.09	1.7	2.95	6.47	0.032
Fluorobenzene	C <sub>6</sub> H <sub>5</sub> F	21.5	2.43	1.4	2.31	5.47	0.027
1,2-Difluorobenzene	C <sub>6</sub> H <sub>4</sub> F <sub>2</sub>	27.8	2.66	1.6	2.50	5.44	0.042
1,3-Difluorobenzene	C <sub>6</sub> H <sub>4</sub> F <sub>2</sub>	30.6	2.52	1.8	2.37	5.15	0.044
1,4-Difluorobenzene	C <sub>6</sub> H <sub>4</sub> F <sub>2</sub>	20.0	2.53	1.1	2.38	5.31	0.038
1,2,4-Trifluorobenzene	C <sub>6</sub> H <sub>3</sub> F <sub>3</sub>	23.8	2.71	2.2	2.54	5.38	0.045
1,2,4,5-Tetrafluorobenzene	C <sub>6</sub> H <sub>2</sub> F <sub>4</sub>	19.7	2.77	1.4	2.62	5.63	0.040
Pentafluorobenzene	C <sub>6</sub> HF <sub>5</sub>	26.1	2.89	1.8	2.75	6.20	0.033
Hexafluorobenzene	C <sub>6</sub> F <sub>6</sub>	26.5	2.95	2.6	2.81	6.45	0.030
<b>Other organic molecules</b>							
Methanol	CH <sub>3</sub> OH	12.4	2.59	1.8	2.47	6.76	0.026
Tetraethylsilane	Si(C <sub>2</sub> H <sub>5</sub> ) <sub>4</sub>		2.37				
Nitrobenzene	C <sub>6</sub> H <sub>5</sub> NO <sub>2</sub>		2.47				
Pyridine	C <sub>5</sub> H <sub>5</sub> N	14.1	2.34	1.5	2.24	5.19	0.026

# References

- [1] See articles in *Canadian Journal of Physics*, 76:313-563, 1996.
- [2] L. J. Allamandola, A. G. G. M. Tielens, and J. R. Barker. Polycyclic aromatic hydrocarbons and the unidentified infrared emission bands: auto exhaust along the milky way! *Astrophysical Journal Letters*, 290:L25-28, 1985.
- [3] L. J. Allamandola, A. G. G. M. Tielens, and J. R. Barker. Interstellar polycyclic aromatic hydrocarbons: the infrared emission bands, the excitation/emission mechanism, and the astrophysical implications. *Astrophysical Journal Supplement*, 71:733-775, 1989.
- [4] C. D. Anderson. The apparent existence of easily deflectable positives. *Science*, 76:238-239, 1932.
- [5] C. D. Anderson. The positive electron. *Physical Review*, 43:491-494, 1933.
- [6] E. A. G. Armour. The theory of low-energy positron collisions with molecules. *Physics Reports*, 169:1-98, 1988.
- [7] E. A. G. Armour, D. J. Baker, and M. Plummer. The theoretical treatment of low-energy  $e^+$ -H<sub>2</sub> scattering using the kohn variational method. *Journal of Physics B*, 23:3057-3074, 1990.
- [8] E. A. G. Armour and J. W. Humberston. Methods and programs in collisions of positrons with atoms and molecules. *Physics Reports*, 204:165-251, 1991.
- [9] P. Asoka-Kumar, M. Alatalo, V. J. Ghosh, A. C. Kruseman, B. Nielsen, and K. G. Lynn. Increased elemental specificity of positron annihilation spectra. *Physical Review Letters*, 77:2097-2100, 1996.

- 
- [10] J. E. Bartmess and R. M. Georgiadis. Empirical methods for determination of ionization gauge relative sensitivities for different gases. *Vacuum*, 33:149–153, 1983.
- [11] S. Berko. Positron annihilation. In B. Williams, editor, *Compton Scattering*, pages 273–322. McGraw-Hill, London, UK, 1977.
- [12] S. Berko. Momentum density and Fermi-surface measurements in metals by positron annihilation. In W. Brandt, editor, *Proceedings of the international school of physics “Enrico Fermi” LXXXIII*, pages 64–145. North-Holland Pub. Co., Amsterdam, 1983.
- [13] C. V. Briscoe, S.-I. Choi, and A. T. Stewart. Zero-point bubbles in liquids. *Physical Review Letters*, 20:493–496, 1968.
- [14] B. L. Brown and M. Leventhal. Laboratory simulation of direct positron annihilation in a neutral-hydrogen galactic environment. *Physical Review Letters*, 57:1651–1654, 1986.
- [15] C. R. Brundle and A. D. Baker. *Electron spectroscopy: theory, techniques, and applications*. Academic, London, UK, 1977.
- [16] R. W. Bussard, R. Ramaty, and R. J. Drachman. The annihilation of galactic positrons. *Astrophysical Journal*, 228:928–934, 1979.
- [17] R. I. Campeanu and J. W. Humberston. The scattering of *s*-wave positrons by helium. *Journal of Physics B*, 10:L153–158, 1977.
- [18] M. Charlton. The attachment of positrons to molecules. *Comments on Atomic and Molecular Physics*, 24:53–64, 1990.
- [19] M. Charlton, J. Eades, D. Horvath, R. J. Hughes, and C. Zimmermann. Antihydrogen physics. *Physics Reports*, 241:65–117, 1994.
- [20] L. X. Cheng, M. Leventhal, D. M. Smith, W. R. Purcell, J. Tueller, A. Connors, D. Dixon, R. L. Kinzer, and J. G. Skibo. A maximum entropy map of the 511 keV positron annihilation line emission distribution near the galactic center. *Astrophysical Journal Letters*, 481:L43–46, 1997.
- [21] W. Cherry. PhD thesis, Princeton University, 1958.
- [22] L. G. Christophorou, K. S. Gant, and V. E. Anderson. Long-lived parent negative ions formed via nuclear-excited Feshbach resonances: part 5. *Journal of Chemical Society; Faraday Transaction II*, 73:804–811, 1977.

- [23] L. G. Christophorou, A. Hadjiantoniou, and J. G. Carter. Long-lived parent negative ions formed via nuclear-excited Feshbach resonances: part 3. *Journal of Chemical Society; Faraday Transaction II*, 69:1713–1722, 1973.
- [24] S. Y. Chuang and B. G. Hogg. Momentum distributions of two photon annihilating positron-electron pairs in hexane and decane. *Canadian Journal of Physics*, 45:3895–3900, 1967.
- [25] P. G. Coleman, T. C. Griffith, G. R. Heyland, and T. L. Killeen. Positron lifetime spectra for the noble gases. *Journal of Physics B*, 8:1734–1743, 1975.
- [26] P. G. Coleman, S. Rayner, F. M. Jacobsen, M. Charlton, and R. N. West. Angular correlation studies of positron annihilation in the noble gases. *Journal of Physics B*, 27:981–991, 1994.
- [27] D. G. Costello, D. E. Groce, D. F. Herring, and J. W. McGowan. Evidence for the negative work function associated with positrons in gold. *Physical Review B*, 5:1433–1439, 1972.
- [28] O. H. Crawford. Mechanism for fragmentation of molecules by positron annihilation. *Physical Review A*, 49:R3147–3150, 1994.
- [29] E. P. da Silva, J. S. E. Germane, and M. A. P. Lima. Annihilation dynamics of positrons in molecular environments: theoretical study of low-energy positron-C<sub>2</sub>H<sub>4</sub> scattering. *Physical Review Letters*, 77:1028–1031, 1996.
- [30] J. W. Darewych. Angular correlation of two-photon positron annihilation in hydrogen gas. *Canadian Journal of Physics*, 57:1027–1030, 1979.
- [31] J. W. Darewych. Elastic scattering and annihilation of low-energy positrons by molecular nitrogen. *Journal of Physics B*, 15:L415–419, 1982.
- [32] Yu. N. Demkov and V. N. Ostrovskii. *Zero-range potentials and their applications in atomic physics*. Plenum Press, New York, 1988.
- [33] C. D. Dermer and J. G. Skibo. Annihilation fountain in the galactic center region. *Astrophysical Journal Letters*, 487:L57–60, 1997.
- [34] M. Deutsch. Evidence for the formation of positronium in gases. *Physical Review*, 83:455–456, 1951.

- 
- [35] M. Deutsch. Three-quantum decay of positronium. *Physical Review*, 82:866–867, 1951.
- [36] P. A. M. Dirac. On the annihilation of electrons and protons. *Proceedings of the Cambridge Philosophical Society*, 26:361–375, 1930.
- [37] P. A. M. Dirac. A theory of electrons and protons. *Proceedings of the Royal Society of London*, 126:360–365, 1930.
- [38] R. J. Drachman. Addendum to “variational bounds in positron-atom scattering”. *Physical Review*, 179:237–239, 1969.
- [39] V. A. Dzuba, V. V. Flambaum, G. F. Gribakin, and W. A. King. Many-body calculations of positron scattering and annihilation from noble gas atoms. *Journal of Physics B*, 29:3151–3175, 1996.
- [40] J. L. Franklin, J. G. Dillard, and H. M. Rosenstock. *Ionization potentials, appearance potentials, and heats of formation of gaseous positive ions*, NBS Report No. NSRDS-NBS 26. U.S. Department of Commerce, Washington, DC, 1969.
- [41] Michael Frenklach and Eric D. Feigelson. Formation of polycyclic aromatic hydrocarbons in circumstellar envelopes. *Astrophysical Journal*, 341:372–384, 1989.
- [42] B. Ghaffari and R. S. Conti. Experimental evidence for chaotic transport in a positron trap. *Physical Review Letters*, 75:3118–3121, 1995.
- [43] A. S. Ghosh, T. Mukherjee, and J. W. Darewych. Angular correlation of two-photon positron annihilation in molecular hydrogen and nitrogen. *Hyperfine Interactions*, 89:319–324, 1994.
- [44] S. J. Gilbert, C. Kurz, R. G. Greaves, and C. M. Surko. Creation of a monoenergetic pulsed positron beam. *Applied Physics Letters*, 70:1944–1946, 1997.
- [45] G. L. Glish, R. G. Greaves, S. A. McLuckey, L. D. Hulett, C. M. Surko, J. Xu, and D. L. Donohue. Ion production by positron-molecule resonances. *Physical Review A*, 49:2389–2393, 1994.
- [46] R. J. Gould. Direct positron annihilation and positronium formation in thermal plasmas. *Astrophysical Journal*, 344:232–238, 1989.

- [47] E. Gramsch, J. Throwe, and K. G. Lynn. Development of transmission positron moderators. *Applied Physics Letters*, 51:1862–1864, 1987.
- [48] R. G. Greaves and C. M. Surko. unpublished.
- [49] R. G. Greaves and C. M. Surko. Solid neon moderator for positron trapping experiments. *Canadian Journal of Physics*, 51:445–448, 1996.
- [50] R. G. Greaves and C. M. Surko. Antimatter plasmas and antihydrogen. *Physics of Plasmas*, 4:1528–1543, 1997.
- [51] R. G. Greaves, M. D. Tinkle, and C. M. Surko. Creation and uses of positron plasmas. *Physics of Plasmas*, 1:1439–1446, 1994.
- [52] G. F. Gribakin. unpublished, 1996.
- [53] G. F. Gribakin. private communication, 1996.
- [54] G. F. Gribakin and W. A. King. The effect of virtual positronium formation on positron-atom scattering. *Journal of Physics B*, 27:2639–2645, 1994.
- [55] T. C. Griffith and G. R. Heyland. Experimental aspects of the study of the interaction of low-energy positrons with gases. *Physics Reports*, 39:169–277, 1978.
- [56] N. Guessoum, R. Ramaty, and R. E. Lingenfelter. Positron annihilation in the interstellar medium. *Astrophysical Journal*, 378:170–180, 1991.
- [57] L. Haarsma, K. Abdullah, and G. Gabrielse. Extremely cold positrons accumulated electronically for antihydrogen production. *Physical Review Letters*, 75:806–809, 1995.
- [58] J. B. Hasted and D. Mathur. Electron-molecule resonances. In L. G. Christophorou, editor, *Electron-Molecule interactions and their applications*, volume 1, pages 403–475. Academic, London, UK, 1983.
- [59] M. Heinberg and L. A. Page. Annihilation of positrons in gases. *Physical Review*, 107:1589–1600, 1957.
- [60] G. R. Heyland, M. Charlton, T. C. Griffith, and G. L. Wright. Positron lifetime spectra for gases. *Canadian Journal of Physics*, 60:503–516, 1982.
- [61] R. H. Howell, I. J. Rosenberg, and M. J. Fluss. Production and use of low-energy, monoenergetic positron beams from electron linacs. *Applied Physics A*, 43:247–255, 1987.

- [62] L. D. Hulett, Jr. Positron microscopy. *Materials Science Forum*, 175-178, pt:99-106, 1995.
- [63] L. D. Hulett, Jr., D. L. Donohue, J. Xu, T. A. Lewis, S. A. McLuckey, and G. L. Glish. Mass spectrometry studies of the ionization of organic molecules by low-energy positrons. *Chemical Physics Letters*, 216:236-240, 1993.
- [64] J. W. Humberston and J. B. G. Wallace. The elastic scattering of positrons by atomic hydrogen. *Journal of Physics B*, 5:1138-1148, 1972.
- [65] J. W. Humberston and P. Van Reeth. Annihilation in low energy positron-helium scattering. To be published in *Nuclear Instruments and Methods: Section B*, 1997.
- [66] K. Iwata, R. G. Greaves, T. J. Murphy, M. D. Tinkle, and C. M. Surko. Measurements of positron-annihilation rates on molecules. *Physical Review A*, 51:473-487, 1995.
- [67] K. Iwata, R. G. Greaves, and C. M. Surko. Annihilation rates of positrons on aromatic molecules. *Hyperfine Interactions*, 89:271-278, 1994.
- [68] K. Iwata, R. G. Greaves, and C. M. Surko. Positron annihilation in a simulated interstellar medium. *Canadian Journal of Physics*, 51:407-410, 1996.
- [69] Koji Iwata, R. G. Greaves, and C. M. Surko.  $\gamma$ -ray annihilation spectra from positron-molecule interactions. *Physical Review A*, 55:3586-3604, 1997.
- [70] Koji Iwata, G. F. Gribakin, R. G. Greaves, and C. M. Surko. Positron annihilation with inner-shell electrons in noble gas atoms. *Physical Review Letters*, 79:39-42, 1997.
- [71] A. Jain and D. G. Thompson. The scattering of slow positrons by  $\text{CH}_4$  and  $\text{NH}_3$ . *Journal of Physics B*, 16:1113-1123, 1983.
- [72] G. F. Knoll. *Radiation detection and measurement, Second Edition*. John Wiley and Sons, New York, 1989.
- [73] C. Kurz, R. G. Greaves, and C. M. Surko. unpublished.
- [74] C. Kurz, R. G. Greaves, and C. M. Surko. Temperature dependence of positron annihilation rates in noble gases. *Physical Review Letters*, 77:2929-2932, 1996.



- [75] L. D. Landau and E. M. Lifshitz. *Quantum mechanics*. Pergamon Press, Oxford, UK, third edition, 1977.
- [76] G. Laricchia, M. Charlton, C. D. Beling, and T. C. Griffith. Density dependence of positron annihilation and positronium formation in H<sub>2</sub> gas at temperatures between 77 and 297 K. *Journal of Physics B*, 20:1865–1874, 1987.
- [77] G. Laricchia and C. Wilkin. Semiempirical approach to positron annihilation in molecules. *Physical Review Letters*, 79:2241–2244, 1997.
- [78] A. Leger and J. L. Puget. Identification of the ‘unidentified’ ir emission features of interstellar dust? *Astronomy and Astrophysics*, 137:L5–8, 1984.
- [79] M. Leventhal, S. D. Barthelmy, N. Gehrels, B. J. Teegarden, J. Tueller, and L. M. Bartlett. Gris detections of the 511 keV line from the galactic center region in 1992. *Astrophysical Journal, Letters*, 405:L25–28, 1993.
- [80] M. Leventhal, C. J. MacCallum, and P. D. Stang. Detection of 511 keV positron annihilation radiation from the galactic center direction. *Astrophysical Journal Letters*, 225:L11–14, 1978.
- [81] M. Leventhal, A. Passner, and C. M. Surko. Positron-molecule bound states and positive ion production. In R. J. Drachman, editor, *Annihilation in Gases and Galaxies*, pages 272–283. National Aeronautics and Space Administration, Washington, DC, 1990.
- [82] D. Levin and G. Lias. *Ionization potential and appearance potential measurements, 1971-1981, NBS Report No. NSRDS-NBS 71*. U.S. Department of Commerce, Washington, DC, 1982.
- [83] R. E. Lingenfelter. private communication, 1997.
- [84] K. G. Lynn, J. R. MacDonald, R. A. Boie, L. C. Feldman, J. D. Gabbe, M. F. Robbins, E. Bonderup, and J. Golovchenko. Positron-annihilation momentum profiles in aluminium: Core contribution and the independent-particle model. *Physical Review Letters*, 38:241–244, 1977.
- [85] K. G. Lynn, B. Nielsen, and J. H. Quateman. Development and use of a thin-film transmission positron moderator. *Applied Physics Letters*, 47:239–240, 1985.

- [86] K.G. Lynn, M. Weber, L.O. Roellig, A.P. Mills, Jr, and A.R. Moodenbaugh. A high intensity positron beam at the Brookhaven reactor. In J.W. Humberston and E.A.G. Armour, editors, *Atomic physics with positrons*, pages 161–174. Plenum Press, New York, 1987.
- [87] J. H. Malmberg and C. F. Driscoll. Long-time containment of a pure electron plasma. *Physical Review Letters*, 44:654–657, 1980.
- [88] H. S. W. Massey. Slow positrons in gases. *Physics Today*, 29:42–51, 1976.
- [89] H.S.W. Massey, E.H.S. Burhop, and H.B. Gilbody. *Electronic and ionic impact phenomena*. Oxford University Press, Oxford, UK, 1974.
- [90] A. L. McClellan. *Tables of experimental dipole moments*. W. H. Freeman and Company, San Francisco, 1963.
- [91] R. P. McEachran, A. G. Ryman, and A. D. Stauffer. Positron scattering from neon. *Journal of Physics B*, 11:551–561, 1978.
- [92] R. P. McEachran, A. G. Ryman, and A. D. Stauffer. Positron scattering from argon. *Journal of Physics B*, 12:1031–1041, 1979.
- [93] R. P. McEachran, A. G. Ryman, A. D. Stauffer, and D. L. Morgan. Positron scattering from noble gases. *Journal of Physics B*, 10:663–677, 1977.
- [94] R. P. McEachran, A. D. Stauffer, and L. E. M. Campbell. Positron scattering from krypton and xenon. *Journal of Physics B*, 13:1281–1292, 1980.
- [95] J. D. McNutt, S. C. Sharma, and R. D. Brisbon. Positron annihilation in gaseous hydrogen and hydrogen-neon mixtures. i. low-energy positrons. *Physical Review A*, 20:347–356, 1979.
- [96] D. B. Miller, P. H. R. Orth, and G. Jones. Temperature dependence of the annihilation rate of positrons in argon gas. *Physics Letters*, 27A:649–650, 1968.
- [97] K. J. Miller and J. A. Savchik. A new empirical method to calculate average molecular polarizability. *Journal of the American Chemical Society*, 101:7206–7213, 1979.
- [98] A. P. Mills. Further improvements in the efficiency of low-energy positron moderators. *Applied Physics Letters*, 37:667–668, 1980.

- 
- [99] A. P. Mills, Jr. Surface analysis and atomic physics with slow positron beams. *Science*, 218:335–340, 1982.
- [100] A. P. Mills, Jr. and E. M. Gullikson. Solid neon moderator for producing slow positrons. *Applied Physics Letters*, 49:1121–1123, 1986.
- [101] T. J. Murphy and C. M. Surko. Annihilation of positrons in xenon gas. *Journal of Physics B*, 23:727–732, 1990.
- [102] T. J. Murphy and C. M. Surko. Annihilation of positrons on organic molecules. *Physical Review Letters*, 67:2954–2957, 1991.
- [103] T. J. Murphy and C. M. Surko. Positron trapping in an electrostatic well by inelastic collisions with nitrogen molecules. *Physical Review A*, 46:5696–5705, 1992.
- [104] R. D. Nelson, Jr., D. R. Lide, Jr., and A. A. Maryott. *Selected values of electric dipole moments for molecules in the gas phase, NBS Report No. NSRDS-NBS 10*. U.S. Department of Commerce, Washington, DC, 1967.
- [105] A. Omont. Physics and chemistry of interstellar polycyclic aromatic molecules. *Astronomy and Astrophysics*, 164:159–178, 1986.
- [106] J. R. Oppenheimer. Two notes on the probability of radiative transitions. *Physical Review*, 35:939–947, 1930.
- [107] P. H. R. Orth and G. Jones. Annihilation of positrons in argon I. experimental. *Physical Review*, 183:7–15, 1969.
- [108] P. E. Osmon. Positron lifetime spectra in molecular gases. *Physical Review*, 140:A8–11, 1965.
- [109] A. Passner, C. M. Surko, M. Leventhal, and A. P. Mills, Jr. Ion production by positron-molecule resonances. *Physical Review A*, 39:3706–3709, 1989.
- [110] D. A. L. Paul and L. Saint-Pierre. Rapid annihilation of positrons in polyatomic gases. *Physical Review Letters*, 11:493–496, 1963.
- [111] J. P. Peng, K. G. Lynn, P. Asoka-Kumar, and D. P. Becker. Study of the SiO<sub>2</sub>-Si interface using variable energy positron two-dimensional angular correlation of annihilation radiation. *Physical Review Letters*, 76:2157–2160, 1996.

- [112] J. L. Puget and A. Leger. A new component of the interstellar matter: Small grains and large aromatic molecules. *Annual Review of Astronomy and Astrophysics*, 27:161–198, 1989.
- [113] W. R. Purcell, L. X. Cheng, D. D. Dixon, R. L. Kinzer, J. D. Kurfess, M. Leventhal, M. A. Saunders, J. G. Skibo, D. M. Smith, and J. Tueller. OSSE mapping of galactic 511 keV positron annihilation line emission. To be published in *Astrophysical Journal*, 491, 1997.
- [114] W. R. Purcell, D. A. Grabelsky, M. P. Ulmer, W. N. Johnson, R. L. Kinzer, J. D. Kurfess, M. S. Strickman, and G. V. Jung. OSSE observations of galactic 511 keV positron annihilation radiation: initial phase 1 results. *Astrophysical Journal Letters*, 413:L85–88, 1993.
- [115] M. J. Puska and R. M. Nieminen. Theory of positrons in solids and on solid surfaces. *Reviews of Modern Physics*, 66:841–897, 1994.
- [116] W. Raith. Survey of recent experimental results on positron scattering in gases. part i: Total cross sections. In J. W. Humberston and M. R. C. McDowell, editors, *Positron Scattering in Gases*, pages 1–13. Plenum Press, New York, 1984.
- [117] R. Ramaty and R. E. Lingenfelter. Gamma ray line radiation. In J. Matthews, editor, *High Energy Astrophysics*, pages 32–68. World Scientific, New York, 1994.
- [118] A. Rich. Recent experimental advances in positronium research. *Reviews of Modern Physics*, 53:127–165, 1981.
- [119] M. B. Robin. *Higher excited states of polyatomic molecules*. Academic, New York, 1974.
- [120] P. J. Robinson and K. A. Holbrook. *Unimolecular reactions*. John Wiley and Sons, Bristol, UK, 1972.
- [121] D. M. Schrader, Finn M. Jacobsen, Niels-Peter Frandsen, and Ulrik Mikkelsen. Formation of positronium hydride. *Physical Review Letters*, 69:57–60, 1992.
- [122] D. M. Schrader and Y. C. Jean, editors. *Positron and positronium chemistry*. Elsevier, Amsterdam, The Netherlands, 1988.

- [123] D. M. Schrader and C. M. Wang. Approximate molecular orbital theory for positrons and positronium atoms bound to molecules. *Journal of Physical Chemistry*, 80:2507–2518, 1976.
- [124] P. J. Schultz and K. G. Lynn. Interaction of positrons beams with surfaces, thin films, and interfaces. *Reviews of Modern Physics*, 60:701–779, 1988.
- [125] S. C. Sharma and J. D. McNutt. Positron annihilation in gaseous nitrogen and nitrogen-neon mixture at 77 k. *Physical Review A*, 18:1426–1434, 1978.
- [126] K. Shizuma, M. Nishi, T. Fujita, and Y. Yoshizawa. Doppler broadening measurement of positron annihilation in rare gas. *Journal of the Physical Society of Japan; Letters*, 44:1757–1758, 1978.
- [127] B. M. Smirnov. *Negative ions*. McGraw-Hill, New York, 1982.
- [128] D. M. Smith, M. Leventhal, N. Gehrels, J. Tueller, W. N. Johnson, R. L. Kinzer, J. D. Kurfess, M. S. Strickman, D. A. Grabelsky, W. R. Purcell, and M. P. Ulmer. Search for Compton-backscattered annihilation radiation from the galactic center with the OSSE. *Astrophysical Journal*, 443:117–123, 1995.
- [129] P. M. Smith and D. A. L. Paul. Positron annihilation in methane gas. *Canadian Journal of Physics*, 48:2984–2990, 1970.
- [130] A. T. Stewart, C. V. Briscoe, and J. J. Steinbacher. Positron annihilation in simple condensed gases. *Canadian Journal of Physics*, 68:1362–1376, 1990.
- [131] C. M. Surko, R. G. Greaves, and M. Charlton. Stored positrons for anti-hydrogen production. *Hyperfine Interactions*, 109:181–188, 1997.
- [132] C. M. Surko, R. G. Greaves, and M. Leventhal. Use of traps to study positron annihilation in astrophysically relevant media. *Hyperfine Interactions*, 81:239–252, 1993.
- [133] C. M. Surko, M. Leventhal, and A. Passner. Positron plasma in the laboratory. *Physical Review Letters*, 62:901–904, 1989.
- [134] C. M. Surko, A. Passner, M. Leventhal, and F. J. Wysocki. Bound states of positrons and large molecules. *Physical Review Letters*, 61:1831–1834, 1988.

- [135] J. Szczepanski and M. Vala. Laboratory evidence for ionized polycyclic aromatic hydrocarbons in the interstellar medium. *Nature*, 363:699–701, 1993.
- [136] S. Tang, M. D. Tinkle, R. G. Greaves, and C. M. Surko. Annihilation gamma-ray spectra from positron-molecule interactions. *Physical Review Letters*, 68:3793–3796, 1992.
- [137] S. J. Tao. Annihilation of positrons in nitrogen. *Physical Review A*, 2:1669–1675, 1970.
- [138] M. D. Tinkle, R. G. Greaves, C. M. Surko, R. L. Spencer, and G. W. Mason. Low-order modes as diagnostics of spheroidal non-neutral plasmas. *Physical Review Letters*, 72:352–355, 1994.
- [139] M. Tuomisaari, K. Rytsölä, and R. Hautojärvi. Positron annihilation in xenon. *Journal of Physics B*, 21:3917–3928, 1988.
- [140] P. Van Reeth, J. W. Humberston, Koji Iwata, R. G. Greaves, and C. M. Surko. Annihilation in low-energy positron-helium scattering. *Journal of Physics B*, 29:L465–471, 1996.
- [141] P. Wallyn, P. Durouchoux, C. Chapuis, and M. Leventhal. The annihilation of positrons in the cold phase of the interstellar medium revisited. *Astrophysical Journal*, 422:610–615, 1994.
- [142] A. Weiss, R. Mayer, M. Jibaly, C. Lei, D. Mehl, and K. G. Lynn. Auger-electron emission resulting from the annihilation of core electrons with low-energy positrons. *Physical Review Letters*, 61:2245–2248, 1988.
- [143] R. N. West, J. Mayers, and P. A. Walters. A high-efficiency two-dimensional angular correlation spectrometer for positron studies. *Journal of Physics E*, 14:478–488, 1981.
- [144] C. L. Wilkins, A. K. Chowdhury, L. M. Nuwaysir, and M. L. Coates. Fourier transform mass spectrometry: Current status. *Mass Spectrometry Reviews*, 8:67–92, 1989.
- [145] C. Winkler, O. Pace, and S. Volonte. INTEGRAL - the international gamma-ray astrophysics laboratory. *ESA Journal*, 17:207–223, 1993.
- [146] G. L. Wright, M. Charlton, T. C. Griffith, and G. R. Heyland. The annihilation of positrons and positronium formation in gaseous Kr and Xe. *Journal of Physics B*, 18:4327–4347, 1985.

- 
- [147] J. Xu, L. D. Hulett, T. A. Lewis, D. L. Donohue, S. A. McLuckey, and O. H. Crawford. Internal energy deposition into molecules upon positron-electron annihilation. *Physical Review A*, 49:R3151–3154, 1994.
- [148] J. Xu, L. D. Hulett, Jr., T. A. Lewis, D. L. Donohue, S. A. McLuckey, and G. L. Glish. Positron-induced dissociation of organic molecules. *Physical Review A*, 47:1023–1030, 1993.
- [149] Jun Xu, L. D. Hulett, Jr., T. A. Lewis, and S. A. McLuckey. Chemical selectivity in the dissociative ionization of organic molecules by low-energy positrons. *Physical Review A*, 52:2088–2094, 1995.
- [150] N. Zafar, J. Chevallier, G. Laricchia, and M. Charlton. Single-crystal nickel foils as positron transmission-mode moderators. *Journal of Physics D*, 22:868–870, 1989.
- [151] S. Zhou, W. E. Kauppila, C. K. Kwan, and T. S. Stein. Measurements of total cross sections for positrons and electrons colliding with atomic hydrogen. *Physical Review Letters*, 72:1443–1446, 1994.
- [152] W. H. Zurek. Annihilation radiation from the galactic center: positrons in dust? *Astrophysical Journal*, 289:603–608, 1985.